Human retinal organoids- Exploration of a human induced pluripotent stem cell-derived *in vitro* model

Dissertation

zur Erlangung des Grades eines

Doktors der Naturwissenschaften

der Mathematisch-Naturwissenschaftlichen Fakultät

und

der Medizinischen Fakultät

der Eberhard-Karls-Universität Tübingen

vorgelegt

von

Kevin Achberger

aus Lindau am Bodensee, Deutschland

Mai 2018

Tag der mündlichen Prüfung: 19.3.19

Dekan der Math.-Nat. Fakultät: Prof. Dr. W. Rosenstiel

Dekan der Medizinischen Fakultät: Prof. Dr. I. B. Autenrieth

1. Berichterstatter: Prof. Dr. Stefan Liebau

2. Berichterstatter: Prof. Dr. Marius Ueffing

Prüfungskommission: Prof. Dr. Stefan Liebau

                           Prof. Dr. Marius Ueffing

                           Thomas Münch, PhD

                           PD Dr. Andrea Wizenmann

Erklärung / Declaration:

Ich erkläre, dass ich die zur Promotion eingereichte Arbeit mit dem Titel:

"Human retinal organoids- Exploration of a human induced pluripotent stem cell-derived *in vitro* model",

selbständig verfasst, nur die angegebenen Quellen und Hilfsmittel benutzt und wörtlich oder inhaltlich übernommene Stellen als solche gekennzeichnet habe. Ich versichere an Eides statt, dass diese Angaben wahr sind und dass ich nichts verschwiegen habe. Mir ist bekannt, dass die falsche Abgabe einer Versicherung an Eides statt mit Freiheitsstrafe bis zu drei Jahren oder mit Geldstrafe bestraft wird.

I hereby declare that I have produced the work entitled

"Human retinal organoids- Exploration of a human induced pluripotent stem cell-derived *in vitro* model",

submitted for the award of a doctorate, on my own (without external help), have used only the sources and aids indicated and have marked passages included from other works, whether verbatim or in content, as such. I swear upon oath that these statements are true and that I have not concealed anything. I am aware that making a false declaration under oath is punishable by a term of imprisonment of up to three years or by a fine.

Tübingen, den ....

             Datum / Date   Unterschrift /Signature

Statement of contributions

Stem cell-based Retina models

K. Achberger, J. C. Haderspeck, A. Kleger, and S. Liebau, "Stem cell-based retina models," Adv. Drug Deliv. Rev., May 2018.

A review about stem cell based *in vitro* retina models with a special focus on iPSC-derived retinal organoids. My contribution was to create the concept of the review and writing >40% of the manuscript. Figure 1 and Figure 3 were adapted from this publication.

Human Retina-on-a-Chip: Merging Organoid and Organ-on-a-Chip Technology to Generate Complex Multi-Layer Tissue Models (in preparation)

Kevin Achberger†, Christopher Probst†, Jasmin C. Haderspeck†, Julia Rogal, Johanna Chuchuy, Marina Nikolova, Virginia Cora, Wadood Haq, Sylvia Bolz, Nian Shen, Katja Schenke-Layland, Marius Ueffing, Stefan Liebau, Peter Loskill - †Shared Equally

My part of this project was the initial chip concept and design. I contributed to all performed experiments (see also Figure 26): Differentiation and co-culture of retinal organoids and RPE, phagocytosis assays, live cell imaging, immunofluorescence staining and microscopy. Method sections about transmission Electron microscopy (3.2.16), retina-on-a-chip production (3.2.23), chip assembly and culture (3.2.24) were adapted from this manuscript.

Diminished photoreceptor light sensitivity in retinal organoids from retinitis pigmentosa patients (in preparation)

Kevin Achberger†, Wadood Haq†, Sylvia Bolz, Jasmin C. Haderspeck, Marius Ueffing, Stefan Hauser, Stefan Liebau - †Shared Equally

I contributed to all performed experiments, all data analysis and writing >50% of the manuscript. The performed experiments are described in Figure 9-25. I reprogrammed keratinocytes from two patients suffering from retinitis pigmentosa to induced pluripotent stem cells and characterised these cells by immunofluorescence, mRNA

expression and germ layer differentiation. I differentiated control and patient iPS cells to retinal organoids and characterised both. I performed all cell culture experiments, all immunofluorescence experiments, all microscopic imaging, all mRNA expression analysis and image analyses. TEM experiments were performed by Sylvia Bolz (Institute for Ophthalmic Research Tübingen); Calcium imaging by Wadood Haq (Institute for Ophthalmic Research Tübingen). FACS was performed by Stefan Hauser (DZNE Tübingen).

Automated immunofluorescence image analysis in retinal organoids (in preparation)

Kevin Achberger†, Wadood Haq†, Sylvia Bolz, Jasmin C. Haderspeck, Marius Ueffing, Stefan Liebau - †Shared Equally

I contributed in developing and writing an image analysis routine, which allows for quantitative analysis of immunofluorescence images of retinal organoids. I wrote all computer codes and performed all analysis described in this thesis (Figure 7 and 27).

1. Table of contents

2. List of abbreviations

%	Percentage
°C	Degree Celsius
2D	Two-dimensional
3D	Three-dimensional
AA	Antibiotics- antimycotics
AC	Amacrine Cells
aPKC	Atypical protein kinase C
AMPA	α-amino-3-hydroxy-5-methyl-4-isoxazolepropionic acid
ARR3	Arrestin3
ATOH	Protein atonal homolog
BC	Bipolar Cells
BrdUs	Bromodeoxyuridine
Ca^{2+}	Calcium
CC	Connecting cilium
CDC42	Cell division control protein 42 homolog
CDL	Chemically defined lipid
cDNA	Complementary DNA
cGMP	Cyclic guanosine monophosphate
cKO	Conditioned knockout
CNG	Cyclic nucleotide gated channels
CO_2	Carbon dioxide
CRB	Crumbs
CRBn	Antibody directed against an immunogen in the N-terminal region of CRB1
CRB1c	Antibody directed against an immunogen in the central region of CRB1
d	Day
DAPI	4',6-diamidino-2-phenylindole
DMEM	Dulbecco's modified eagle medium
DNA	Deoxyribonucleic acid
dNTP	Deoxynucleotide

e.g.	Exempli gratia, for example
EB	Embryoid bodies
EDTA	Ethylenediaminetetraacetic acid
EGF	Epidermal growth factor
ESC	Embryonic stem cell
FACS	Fluorescence activated cell sorting
FBS	Fetal bovine serum
FGF	Fibroblast growth factor
g	Gravitational acceleration ~ 9.806 m/s^2
gDNA	Genomic DNA
GC	Ganglion cells
GFAP	Glial fibrillary acidic protein
GFP	Green fluorescent protein
GNAT	G Protein Subunit Alpha Transducin
h	Hour
HC	Horizontal cells
hESC	Human embryonic stem cells
hiPSC	Human induced pluripotent stem cells
HKGS	Human keratinocyte growth supplement kit
HMBS	Hydroxymethylbilane synthase
HSA	Human serum albumin
ICC	Immunocytochemistry
IF	Immunofluorescence
ILM	Inner limiting membrane
iPSC	induced pluripotent stem cells
IS	Inner segment
ISO	Isoform
ITS	Insulin-transferrin-selenium
k	Kilo
KO	Knockout
L-,S-,M- opsin	Long-wave sensitive opsin, short-wave sensitive opsin, middle-wave sensitive opsin
Lam G	Laminin globular domain

LCA	Leber's congenital amaurosis
LED	Light-emitting diode
LGN	lateral geniculate nucleus
LRP	Lipoprotein receptor-related protein
MC	Müller glial cells
MEF	Mouse embryonic fibroblasts
mESC	Mouse embryonic stem cells
MG	Matrigel
mGluR	Metabotropic glutamate receptor
min	Minutes
MITF	Microphthalmia-associated transcription factor
mJ	Milijoule
MPP	Membrane palmitoylated protein
mRNA	Messenger RNA
mTOR	Mechanistic Target of rapamycin
MUPP	Major urinary protein, pseudogene
NCID	Intracellular domain of the notch protein
NDS	Normal donkey serum
NE	Neuroepithelium
NEAA	Non-essential amino acids
nm, μm, mm	Nanometre, micrometre, millimetre
nM, μM, mM, M	Nanomolar, micromolar, millimolar
nl, μl, ml, l	Nanolitre, microlitre, millilitre, Litre
NR	Neural retina
O_2	Oxygen
OLM	Outer limiting membrane
ONL	Outer nuclear layer
OoC	Organ-on-a-chip
OPL	Outer plexiform layer
OS	Outer segment
PALS	Phenylalanine ammonia-lyase
pmol	Picomole
PAR	Human pseudoautosomal region

PATJ	Protein associated To tight junctions
PAX	Paired-box-gene
PBS -/-	Phosphate-buffered saline w/o magnesium and calcium
PCR	Polymerase chain reaction
PDE	Phosphodiesterase
PDMS	Polydimethylsiloxane
PEI	Polyethylenimine
PFA	Paraformaldehyde
pH	Potentia hydrogenii
PNA	Peanut
PRC	Photoreceptor cell
qRT-PCR	quantitative reverse transcription polymerase chain reaction
RA	Retinoic acid
REF	Rat embryonic fibroblasts
RNA	Ribonucleic acid
RO	Retinal organoid
ROM1	Rod outer segment membrane protein 1
RP	Retinitis pigmentosa
RPA	Patient A with CRB1 C948Y mutation
RPB	Patient B with CRB1 C948Y mutation
RPC	Retinal progenitor cells
RPE	Retinal pigmented epithelium
RT-PCR	Reverse transcription polymerase chain reaction
RX (RAX)	Retinal homeobox protein
s	second
S.E.M	Standard error of the mean
SR	Serum replacement
TGF	Transforming growth factor
TSC	Tuberous sclerosis
TUJ	β-(III)-Tubulin
TUNEL	TdT-mediated dUTP-biotin nick end labelling

w/o	Without
y	Year
YAP	Yes-associated protein 1

3. Summary/Zusammenfassung

Summary

The visual perception of our eyes is likely the most fundamental sensory input we have from the surrounding world. Therefore, the loss of the eyesight has a severe impact on the life quality of a human being. Several causes for blindness concern the ablation or dysfunction of the retina, for example in retinitis pigmentosa (RP) and Leber's congenital amaurosis (LCA). Here, the degenerative blindness is based on a progressive loss of photoreceptors caused by mutations in a various number of genes. Amongst the most frequent causative genes is *CRB1*, which is involved in photoreceptor and epithelial polarity among others. For developing future therapeutic approaches which could treat these diseases, it is necessary to elucidate the underlying pathomechanisms in suitable disease model systems. In that course, the discovery of self-forming and self-organising retinal organoids (RO) derived from induced pluripotent stem cells opens new possibilities for *in vitro* retina models. These retinal organoids contain all known retinal neural types including rod and cone photoreceptors and one type of glia. Even more astonishing, they present a correct layering, synaptic connections and light sensation.

In this thesis, I established the differentiation of induced pluripotent stem cell- derived retinal organoids according to previously published protocols based on a combination of adherent and suspension cell culture. To study the effect of retinitis pigmentosa caused by a *CRB1* mutation, iPSC lines from two patients (RPA, RPB) harbouring a single-amino acid exchange (C948Y) in the *CRB1* gene were created. Evaluation of 2 controls and 2 patient retinal organoids was held out by using immunocytochemistry (ICC), transcriptomic analysis using an array-based qRT-PCR system, electron microscopy and calcium imaging. For quantification of ICC staining signals, an ImageJ and R-based analysis procedure was designed in order to create profiles from individual ICC images allowing a position-dependent signal analysis.

Altogether, the main achievements of my work are I) the establishment of a valid retina *in vitro* model based on iPSC- derived retinal organoids and setting the hallmarks of differentiation using bona fide cell markers and transcriptomic analysis. II) The establishment of novel methods analysing the differentiation and the functionality of these RO including FACS-based single cell transcriptomics, electron microscopy and

calcium imaging. III) The usage of the RO model to model retinitis pigmentosa caused by a *CRB1* mutation showing a differential CRB1 expression pattern, alongside with potential changes in signalling and photoreceptor functionality. Still, I could not find any signs of photoreceptor degeneration even after one year of culture. Finally, IV) based on this work, a microfluidic chip was created allowing the interaction of adherent iPSC derived retinal pigmented epithelial cells and photoreceptor segments from three-dimensional retinal organoids.

This thesis sets the groundwork of for an analysis procedure, which could be used for any retina-related disease modelling, compound testing or mechanistic study *in vitro*. Moreover, it shed light on some of the pathomechanisms of retinitis pigmentosa caused by a *CRB1* mutation. In the future, the obtained results could contribute to a better understanding and treatment of the disease.

Zusammenfassung

Die Wahrnehmung von Lichtreizen durch unsere Augen ist vermutlich der fundamentalste Sinn, der einem Menschen zu Verfügung steht, um mit seiner Umwelt zu interagieren und diese zu erleben. Gerade deshalb ist der Verlust des Augenlichtes ein extremer Einschnitt in die Lebensqualität eines jeden Menschen. Zwei der häufigsten erblichen Erkrankungen, die zur Erblindung führen, sind Retinitis Pigmentosa (RP) und die Leber'sche Kongenitale Amaurose (LCA). Bei diesen degenerativen Retina-Erkrankungen führt das progressive Absterben von Photorezeptoren zu einem unaufhaltsamen Verlust der Lichtwahrnehmung. Einer der häufigsten genetischen Ursachen dafür sind Mutationen im *CRB1* Gen, welches vermutlich normalerweise an der Polarisierung und Stabilität von Epithelzellen und Photorezeptoren beteiligt ist. Um zukünftig Therapieformen zu entwickeln, die eine Linderung oder gar Heilung erreichen könnten, müssen die pathologischen Veränderungen, die mit der Krankheit einhergehen, genauestens studiert und verstanden werden.

Eine neue und vielversprechende Möglichkeit dies zu erreichen, ist die Entwicklung von selbstformierenden und selbstorganisierenden retinalen Organoiden (RO), die aus induziert pluripotenten Stammzellen (IPSZ) abgeleitet werden können. Diese retinalen Organoide beinhalten alle Zelltypen einer menschlichen Retina inklusive Stäbchen, Zapfen und retinalen Müller Glia Zellen. Darüber hinaus verfügen sie über eine fortgeschrittene Form der Organisation, die ähnlich einer menschlichen Retina in spezifischen Schichten angeordnet ist. Des Weiteren beinhalten die RO physiologisch relevante synaptische Verknüpfungen und können sogar auf Lichtreize reagieren.

In dieser Arbeit habe ich auf Basis publizierter Protokolle die Differenzierung von RO aus induziert pluripotenten Stammzellen etabliert, die auf einer Mischung aus Adhärenz- und Suspensionskultur basiert. Um die Effekte von Retinitis Pigmentosa mit zugrundeliegender *CRB1* Mutation zu untersuchen, kreierte ich iPS Zelllinien von zwei RP Patienten (RPA, RPB), die eine homozygote C948Y Mutation tragen. Die daraus generierten RO wurden mithilfe von Immunzytochemie (ICC), Transkriptom- Analysen mittels qRT-PCR sowie ultrastruktureller Bildgebung mittels Elektronenmikroskopie und funktioneller Evaluierung durch Calcium Imaging analysiert. Um ICC Färbungen effektiv und objektiv quantifizieren zu können, wurde ein Analyseverfahren entwickelt, das auf verschiedenen ImageJ und R-Macro Programmen basiert. Die wichtigsten

Resultate dieser Arbeit sind erstens die Etablierung eines validen iPSZ-basiertes *in vitro* Retina Modells und zugleich die Analyse der wichtigsten Differenzierungsschritte mithilfe von bekannten Zellmarkern und transkriptomischen Analysen. Zweitens, die Entwicklung einer neuartigen Methodik um Fluoreszenzbilder von retinalen Organoiden einfach und objektiv zu quantifizieren. Drittens, die Nutzung der RO für das Modellieren von Retinitis Pigmentosa, verursacht durch *CRB1* Mutationen. Hierbei konnte ich vor allem ein verändertes CRB1 Expressionsmuster feststellen, sowie deutliche Hinweise auf veränderte Signalwege und darüber hinaus eine verminderte Lichtaktivität von retinalen Photorezeptoren. Dennoch war es selbst nach einem Jahr Kultur nicht möglich, deutliche Zeichen von Photorezeptordegeneration zu beobachten. Aufgrund dieser Limitierungen und um das Modellieren von Retinaerkrankungen in Zukunft möglicherweise zu verbessern, kreierte ich, aus den im Rahmen dieser Arbeit entstandenen Daten, ein Organ-on-a-chip System, welches eine bisher nicht kontrolliert mögliche Interaktion zwischen Photorezeptor und retinaler Pigmentepithelzelle erlaubt. Zusammen mit dem hier präsentierten Krankheitsmodell möchte ich damit in Zukunft zum besseren Verständnis von degenerativen Retinaerkrankungen beitragen und darüber hinaus eine Verbesserung von *in vitro* Retinamodellen erzielen.

4. Introduction

4.1. The eye

For man, the eye is the most important sensory organ for providing information about our surrounding environment.

What we sense as vision is based on the detection of light waves by a specialised tissue at the back of the eye called retina (Figure 1). The retina is the innermost layer of the eye and in addition, the mammalian eye has two more layers: the external layer is made of the sclera and the cornea, the intermediate layer makes up the iris, the ciliary bodies and the choroid. The cornea is the outermost epithelium, which connects with the outside world. Together with the lens, which is variable in shape, it refracts the light to focus on a specialised structure of the retina, the area centralis (fovea centralis in humans) (1).
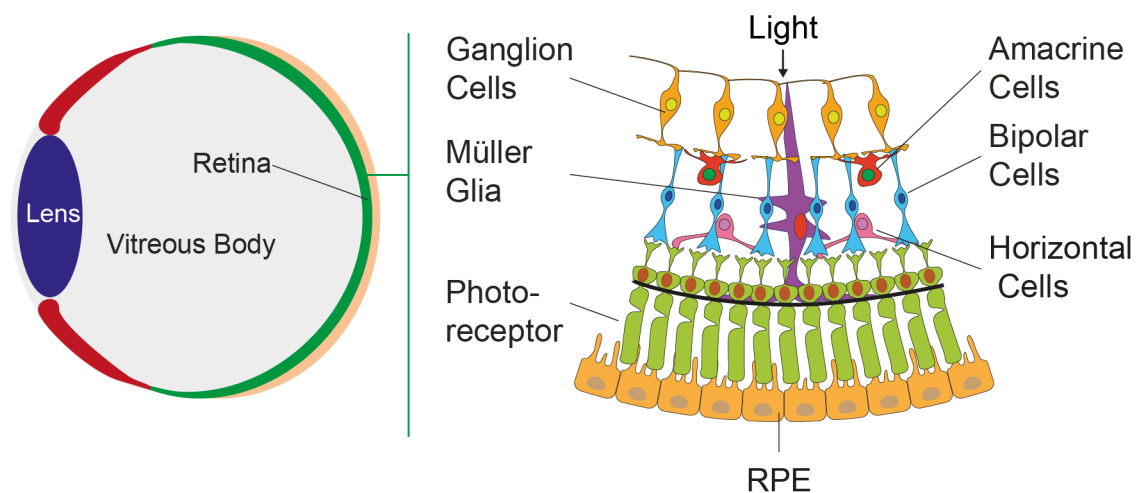
Figure 1- The mammalian retina

In mammalians, the retina is situated at the back of the eye (left image, green) behind the vitreous body (grey). The retina displays a highly organised layering (right image) with the retinal pigmented epithelia (RPE) in the outermost layer, followed by photoreceptors with inner and outer segments, retinal interneurons (bipolar cells, horizontal cells, amacrine cells), ganglion cells and the retina-specific type of glia (Müller glia), spanning the whole retina. For the light sensation by the photoreceptor outer segments, the light has to travel through all retinal layers (except for the RPE). Adapted from Achberger *et al.* 2018 (2).

4.2. The vertebrate retina

4.2.1. Composition

The retina is a circular plane sheet coating the back of the eye. It reaches from the centre, the area centralis to the rim transition zone, the ora serrata. The circular retina sheet has a diameter of 30-40 mm and the retina itself is approximately 0.5 mm thick (3). Based on the embryonic development, it can be divided into an inner neural retina containing the retinal neurons and glia and the outermost epithelia layer of cells containing pigmented melanosomes, which are therefore called retinal pigmented epithelia (RPE) cells (4).

The neural retina (NR) is built of six major types of retinal neurons with a variety of subtypes and glia cells, mainly represented by the Müller glia, and can be further subdivided into distinct layers (3,5). A depiction of the retinal composition is shown in Figure 1. Since the NR is inversed in composition, the light has to pass the whole retina until two types of photoreceptors (PRCs), the rods and cones, in the outermost layer, finally detect it. Their cell bodies lie in the outer nuclear layer (ONL), whereas their apical processes, the inner and outer segments, are located in a separated segment layer. A tight junction belt, the outer limiting membrane (OLM), divides both layers. In the layer below the ONL, the synapse containing outer plexiform layer (OPL), the PRCs form synapses with interneurons, which are situated in the inner nuclear layer. These neurons namely bipolar cells (BCs), horizontal cells (HCs) and amacrine cells (ACs) are responsible for early processing of the light induced signals. The bipolar cells are finally passing on the processed information to ganglion cells (GCs). The correlating synapses between BCs and GCs are located in an inner plexiform layer, whereas the nuclear bodies of GCs form a separate ganglion layer. Then, the axons of the ganglion cells, which are located in the innermost layer of the retina, are condensed to the optic nerve, which ultimately project to the visual cortex in the brain. The already mentioned OLM and the inner limiting membrane (ILM) separating the GC axons from the vitreous body are, at least to current knowledge, produced by the Müller glia.

4.2.2. Photoreceptors

4.2.2.1. Rods and cones
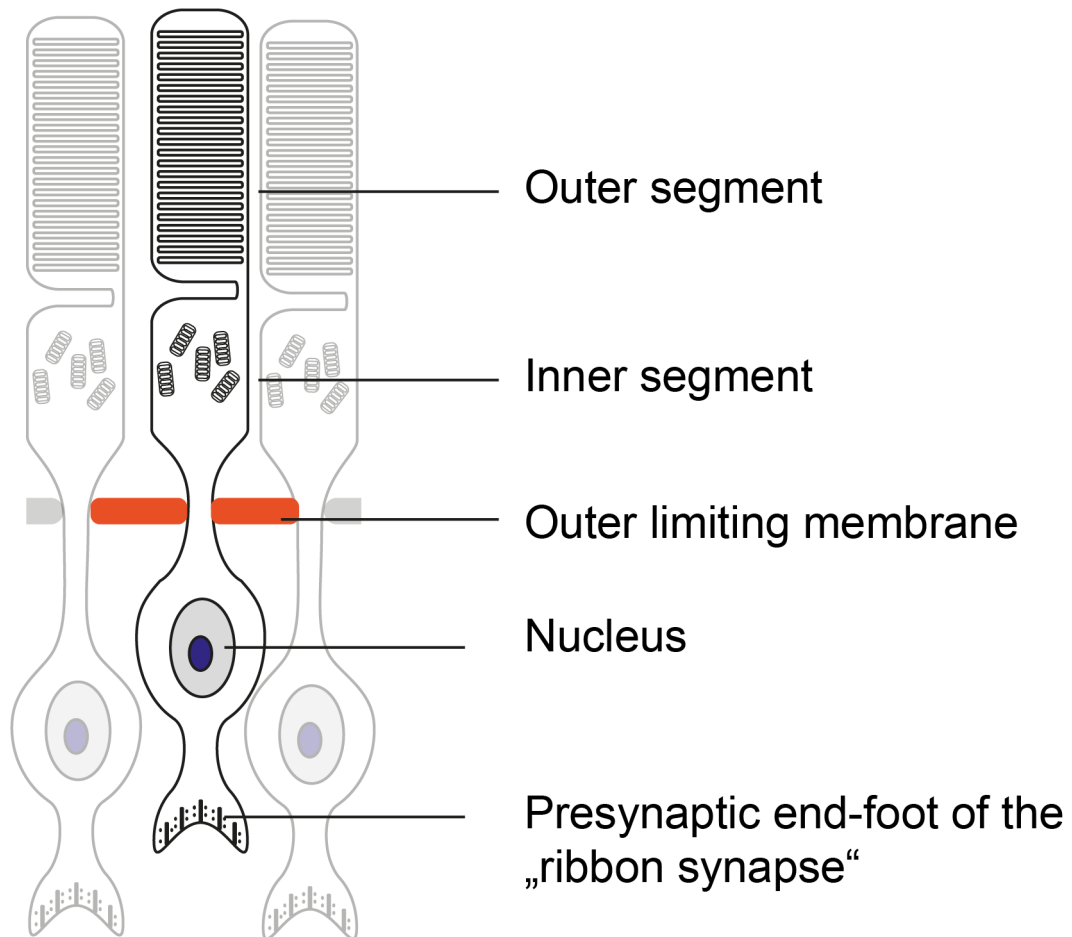
Figure 2- Photoreceptor cells

The principle makeup of a photoreceptor. The soma and nuclei of PRCs are found in the outer plexiform layer, whereas the inner and outer segments are located in the segment layers. The outer limiting membrane separates both layers. The outer segment contains membrane disks, which harbour the chromophores rhodopsin and opsin and, amongst others, the proteins of the phototransduction cascade. The inner segment is filled with apically oriented mitochondria. Inner and outer segments are connected by a cilium (connecting cilium). The end-feet of rod and cone photoreceptors form the presynaptic compartment of the ribbon synapses and connect the PRCs with the ON- and OFF-bipolar cells as well as horizontal cells.

The average human retina harbours around 92 million rods and 4.6 million cone photoreceptors (6). Their distribution pattern is strictly determined with a domination of

rods in the periphery and a tight packing of cones mainly in the centre of the retina. Here, a specialised structure can be found, the fovea centralis, which is exclusively made up by cones. Due to a more than one-to-one connection to bipolar cells and being the focus of the refracted light, it represents the field of the highest resolution (1,7).

The photoreceptor cells can be subdivided into four different cell types: one type of rod cells (black/white, for low light conditions) and three different cone cells, detecting light of different colour wave lengths (8). Both rods and cones share a common basic makeup (Figure 2): Their cell bodies are located in the ONL, both have an inner and outer segment with a connecting cilium (CC) (9) and both have a distal end-foot making up the terminal synapse connecting the PRC to the interneurons (10). However, in detail they exhibit some major differences: The rods photoreceptors are, as the name indicates, long and rod shaped and react maximally on 500 nm light waves due to the expression of the light-sensitive pigment rhodopsin (9,11). The rod cell is highly sensitive to a low amount of photons and therefore important for vision in dark-dim conditions (12,13). In contrast to that, the cones are shorter and have a conical segment. By their ability to detect a certain light spectrum, they can be divided in three different types: short wave (s)-cones, which detect blue light with a maximum of 420 nm, middle wave (m)-cones detecting green light (530 nm) and long wave (l) cones for red light (560 nm) (11). The difference in light wave detection is coupled to the expression of specialised opsins (S-,M-,L-opsin) and enables colour vision and discrimination (14). Nevertheless, cones are less sensitive to light (15). Still, their high concentration in the fovea centralis and their higher temporal resolution make them the dominant photoreceptor type under bright light conditions (16).

4.2.2.2. Inner and outer segments

The makeup of both rod and cone inner and outer segment (IS, OS) is quite comparable. The inner segments of both PRC types harbour a high amount of endoplasmic reticulum, ribosomes, Golgi apparatus and high numbers of mitochondria directly adjacent to the OS (9,17). The inner segment is separated by a connecting cilium (CC) from the outer segment. The outer segments are, independent of their either conical or rod shaped form, constructed of stacked disks of membranes that

4

contain the chromophores rhodopsin in rods and L/M/S- opsins in the three cone types (18). At the base, near to the CC, disks are produced as protrusions of the OS membrane, whereas at the apex, they are shed off and phagocytosed by RPE cells (19) allowing for a continuous regeneration of outer segment disks (20). Both processes take place throughout life resulting in a constant length of the segments (21).

4.2.2.3. Phototransduction in Rods and Cones

The activation of photoreceptors by photons is the base for vision in all animals. In mammals, the molecule which is responsible for the light detection is 11-cis retinal (22). Depending on the photoreceptor type, it is covalently bound to either rhodopsin or one of the opsin forms. This interaction changes the original absorption maximum of 11-cis-retinal to the respective maximum sensitivity of each photoreceptor type (23). Upon the presence of light, the 11-cis retinal converts to all-trans retinal changing the conformation of the opsins, finally triggering the release of retinal and the activation of the G-protein transducin (24,25). In the following, transducin activates the cGMP phosphodiesterase (PDE) which in turn hydrolyses cGMP and therefore decreases its intracellular concentration (25–27). Ultimately, this leads to the closing of cGMP dependent inward rectifying cation channels (CNG channels), causing a hyperpolarisation (28). This is somewhat different from other neurons, since photoreceptors are depolarised and therefore most active under dark conditions, causing a so-called "dark current" (29). This dark current is triggering a constant glutamate release at the PRC synapse, which decreases during light activation causing a response of the subsequent bipolar and horizontal cells (25).

After light activation, each of the participating molecules needs to recover and their proteolytic functionality needs to be terminated. A number of proteins such as Arrestin and Recoverin are involved in this process (30,31).

4.2.3. Signal transduction from photoreceptors to the ganglion cells

The distal processes of the photoreceptors form large synapses to the succeeding bipolar and horizontal cells, which can be found exclusively in the outer plexiform layer

(32). Both rod and cone synapses show an ultrastructurally visible specialisation called ribbons. These ribbons are located close to the active zone and are packed with calcium bound vesicles. These high numbers of vesicles correlate to the constant activity of photoreceptors in the dark and therefore to the high demand of glutamate vesicle release (33). Each photoreceptor synapse is interacting with a minimum of one bipolar cell as well as with horizontal cells (32,34).

The human retina contains a variety of different bipolar cell types. Ten of them are involved in cone pathways and only one is responsible for signal transduction of rods (35,36). In the central parafoveal area, rod bipolar cells make contact to around 15-20 rods, whereas in periphery they contact around 40-50 (32,37). Specialised bipolar cell types in the fovea such as the midget bipolar cells and the blue cone connecting types display one-to-one contacts (38).

Bipolar cells are further classified by their response to the light induced reduction of glutamate release at the synapse. Bipolar cells which respond with a hyperpolarisation and no spiking action potential during the light stimulus are called OFF-centre, whereas depolarising cells responding with spiking are called ON-centre (39). This mechanism is implemented by two different types of glutamate receptors: ON-centre BCs contain a G-protein coupled metabotropic Glutamate receptor type (mGluR6) which decreases the membrane potential and therefore the level of activation upon glutamate binding (40). Consequently, the BC depolarises upon reduced glutamate binding during light stimulation. The OFF-centre type contains ionotropic AMPA glutamate receptors, which are activated during dark phases (40). Of note, all rod bipolar cells are of the ON- centre type (41).

In the inner plexiform layer, the OFF- and ON- cone bipolar cells project to respective OFF- and ON- ganglion cells. The synapses formed here are from ribbon and normal type (42). However, only the ionotropic type of glutamate receptors is present(43). The rod bipolar cells are not directly wired to the ganglion cells, but form synapses with the amacrine cell type AII, where the signal is modulated and passed onto ON- ganglion cells of the cone pathway (44). Because of the converging nature of the signalling, each ganglion cell possesses a receptive field with the information of a distinct retinal area(45). The ganglion cells form the optic nerve, projecting to the lateral geniculate

nucleus (LGN) in the thalamus. The residing LGN neurons finally transmit the information to the visual cortex(46).

4.2.4. The modulating retinal neurons - horizontal cells and amacrine cells

The horizontal cells and amacrine cells are both responsible for the lateral signal transduction within the retina and therefore modulate the vertical transduction between PRCs, BCs and GCs. Their functions and mechanisms are highly complex and shall be described here only briefly. The horizontal cells are involved in the photoreceptor-bipolar synapse where they modulate the signal transduction. In humans, three types (HI, HII, HIII) of horizontal cells can be distinguished, mainly varying in dendritic field size and the photoreceptor type they connect to (47). All horizontal cells of the same type are connected by gap junctions, forming a large network which enables a variety of pre-processing mechanisms (48). In addition, they fulfil important feedback functions by modulating the pH within the synaptic cleft or changing the membrane potential at the cone pedicle (49). Recently, it has been shown that they even form backward directed synapses with cones (50).

The dendrites and axons of the amacrine cells are directed into the inner plexiform layer where they modulate the cone bipolar-ganglion cell synapse or in case of the rod bipolar-ganglion cell synapse, they are involved in the direct signal transduction (48). A rising number of at least 2 different amacrine types can be differentiated in mammalians, which are categorised by cell body size, dendritic tree size, the level of branching and especially the layer within the IPL they are projecting to (51,52).

4.2.5. Müller glia

As the main glial cell type in the retina, Müller glia span the whole width of the retina with their nuclei exclusively located in the INL (53). Their apical and distal processes are building the inner and outer limiting membrane, where they form junctions with adjacent Müller cells (53). Therefore, one of their main function is to delimitate them distally from the vitreous body and blood vessels and apically from the RPE cells, where they form interdigitating villi (54). Apart from their barrier function they are crucial for the metabolism of the retinal neurons, producing *e.g.* 11-cis-retinol (55).

4.2.6. Astrocytes and microglia in the retina

Both astrocytes and microglia are regularly found within the retina. Nuclei and processes of astrocytes, which are from ectodermal origin, are almost entirely found within the GC- nerve fibre layer (56). They are strongly stained by GFAP antibodies (57). Their main function is believed to be the covering of ganglion cells axons and the participation in the blood-brain barrier (58). In contrast, microglia were recently found to originate from yolk sac mesoderm (59,60). Both types are found in all retinal layers and are stimulated by injury and trauma. Thereafter, they fulfil macrophagic functions by *e.g.* phagocytosis of dying retinal neurons (61).

4.2.7. Retinal pigmented epithelium

The retinal pigmented epithelium (RPE) is located in the outermost layer of the retina forming a part of the blood-retina barrier (62). In addition, the apical processes of the RPE cells are in direct contact to the photoreceptor outer segments. The RPE layer consists of a single row of pigmented hexagonally ("cobble-stone") shaped cells which are packed by tight junctions (63). Some of their main functions are the phagocytosis and digestion of sheared off photoreceptor outer segments (64) and the secretion and absorption of substances for the photoreceptors such as *e.g.* the provision of 11-cis retinal for the opsins (65). Furthermore, they play a role in the homeostasis of ions in the retina (66,67). Their pigmentation enables them to absorb light reducing the occurrence of reactive oxygen species (68).

4.3. Eye development
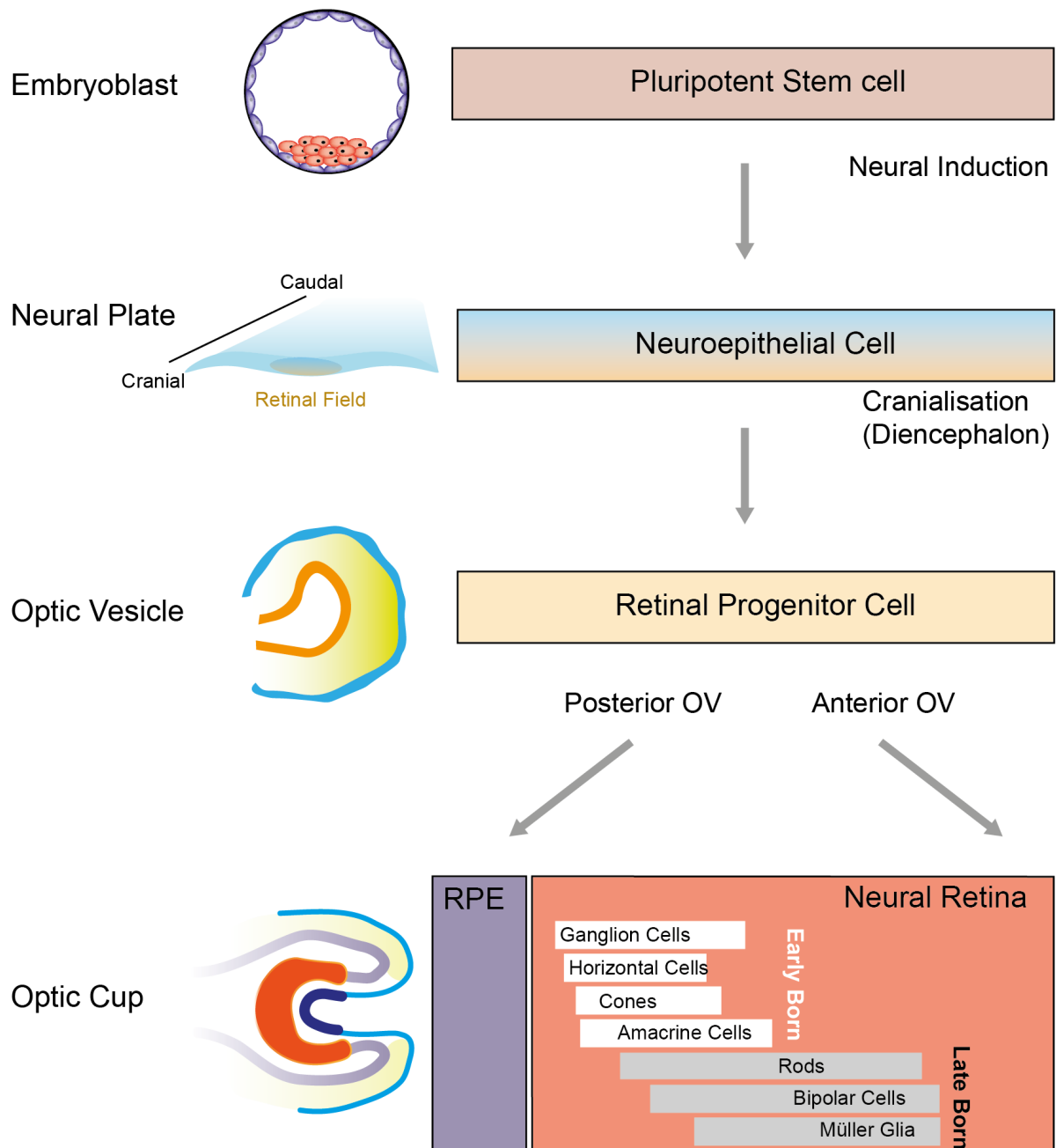
Figure 3- Retinal Development

Depiction of the retinal development (modified from (2)). Briefly, pluripotent stem cells of the embryoblast develop into the three germ layers: ectoderm, mesoderm and endoderm. The neuroectodermal cells of the diencephalic neural plate specialise into eye field cells. Here, the first retinal progenitor cells (RPC) can be found forming two evaginating structures called optic vesicles. After an optic vesicle makes contact with the surface ectodermal lens progenitors, it infolds forming an optic cup. Here, the RPC subdivides into RPE progenitors and neural retinal progenitor cells. The neural retina gives rise to all retinal neurons and one type of glial cells in a concerted order and organisation. Depending on the time point of their first emergence, the cells are divided into early and late born retinal cells.

In vertebrates, the eye structures are arising from three different origins: the retina, RPE cells and the margin iris epithelium are derived from neuroectoderm, the lens from the lens placode and extraocular mesenchyme is produced by neural crest cells and mesoderm (4). An overview on the eye development is depicted in Figure 3.

The development of the eye starts with the formation of two eye fields bilaterally evaginating from the neural plate/tube forming the so called optic vesicles (4). The process of eye formation is driven by a coordinated change in cell shape and behaviour and is controlled by transcription factors such as Pax6 and Rax (69,70). The optic stalk which connects the optic vesicles to the neural tube will later form the optic fissures (4). In parallel to the optic vesicle, evagination of the adjacent surface ectoderm is initiating the lens placode. In a second step, this lens placode is invaginating into the direction of the optic vesicle. In response to that, the central part of the optic vesicle itself starts invaginating forming an optic cup (71). At this stage, the retinal progenitors in the dorsal part of the vesicle commit to the fate of RPE cells (72). The ventral progenitors form the neural retina, which will later give rise to all the retinal neurons and glial cells (72).

The crucial factors initiating these commitments are Vsx2 (Chx10) and Mitf (72,73). In mouse, Mitf is initially expressed in all retina progenitors and downregulated by the expression of Vsx2 (73). Vsx+ progenitors then commit to a neural retina fate whereas the remaining Mitf+ cells form the RPE (73). Later, Mitf is crucially involved in the upregulation of terminal RPE differentiation and pigmentation genes such as Dct, Trp-1 and Tyrosinase (74). The cellular mechanism of the optic cup infolding are not well understood, however, contractile filopodia might provide a mechanical force driving the process (75).

4.3.1. From the retinal progenitors to retinal neurons

All cells of the retina are derived from one common multipotent progenitor. As previously described, the earliest fate decision occurs between the neural retina and the RPE. After the neural retinal progenitors are established, they give rise to all post-mitotic retinal neurons and Müller glia in a predetermined time course and number (76,77). Cells which arise early such as retinal ganglion cells, a subset of amacrine

cells, horizontal cells and cones are called early born, whereas the late born cells (rods, bipolar cells, rest of the amacrine cells and Müller glia cells) arise later (see also Figure 3).

Several studies had shown that a network of transcription factors expressed by the retinal progenitors greatly influences cell fate. Among these factors are *e.g.* Pax6, Rax and Otx2 (78–80). If Pax6 for example is artificially inactivated in the NR of mice, the progenitors only give rise to amacrine cells (78,81). Nevertheless, most of the cell fate influencing transcription factors are of a permitting rather than decisive nature. For example, Atoh7 is required for the ganglion cell fate in mice and zebrafish (82,83), however not all Atoh7- expressing cells will become ganglion cells (84,85).

In zebrafish, it was observed that transcription factor expression dynamics changes hierarchically. In early progenitors, vsx2 is expressed, downregulating vsx1 and atoh7 (86). When vsx2 expression wears off, two distinct populations of vsx1 and atoh7 arise which are more limited in the cell types they can produce (86). In mammalians, similar limited progenitor populations have been found: Ascl1+ and Neurog2+ (87,88). However, these two populations only vary in the number of ganglion cells they can generate.

In general, it is still unknown how this determined programme is implemented. Currently, there are three models, which might explain major aspects (77,89). The first model states that at certain times a progenitor has only certain "competences" to differentiate into specific cell types. The second model states that the competence of differentiation is progressively restricted. Consequently, early progenitors can produce all retinal cells, whereas later cells are more restricted to certain cell types most likely by the influence if already generated daughter cells. The third model claims that the arising of cell types is a stochastic process with changing probabilities that a certain cell type can arise. This however does not mean that it is not influenced by the expression of certain determining genes, which might favour a certain cell type at a certain time.

4.3.2. The differentiation of photoreceptors

The birth of photoreceptors from progenitors is taking place over a long period during retina development. When the fate of a certain photoreceptor is implemented, it still needs to mature for weeks to months depending on the species (90,91).

According to Swaroop *et al*. (90), the whole process can therefore be divided into several steps: first, as already described, the proliferation of retinal progenitors takes place, with a dynamic change in competence or likelihood for certain cell types to arise. Second, photoreceptor precursors are implemented which are still able to become all four known photoreceptor cell types. After a certain set of photoreceptor genes is expressed, cells are irreversibly heading for their fate. This is followed by axonal growth, synapse and inner/outer segment formation. In humans, all photoreceptors are produced prenatally, with first rods and cones arising at week 10 and 8, respectively (90,92,93). At birth, the PRCs are still immature and continue to mature postnatally. S-opsin mRNA can be found starting from week 12, rhodopsin from week 15 (92).

The influencing factors of photoreceptor fate determination are reasonably well understood. The establishment of photoreceptor precursors is influenced by notch signalling (94,95) and transcription factors such as Otx2 (80,96) and Crx (97,98). Observations in mice indicate that S- cone is the "default" photoreceptor type (90). However, if expression of the transcription factor Nrl is induced, the fate changes to rod cells (99,100). If the thyroid receptor tr2ß is expressed, it changes to M/L- cones (101). The subsequent decisive step between M and L- cones is not clear yet. Mouse studies including artificially expressed L- Opsin indicate that it might be a stochastic process (102).

4.4. Retinitis pigmentosa and Leber's congenital amaurosis

Retinitis pigmentosa (RP) and Leber's congenital amaurosis (LCA) are two forms of inherited retinal dystrophies leading to blindness. Both diseases are characterised by a progressive loss of photoreceptors and the emergence of pigment deposits (103). The main differential criteria is the onset of the disease: In LCA, visual impairments are usually present already at birth or within the first 5 years of life and develop rapidly. Visual impairments in retinitis pigmentosa emerge later and usually are milder

developing over several decades. The onset time point of the first notable symptoms allows discrimination between early (within first years of life) and late onset forms of RP (beginning or after midlife). The cut-off point between LCA and RP is however arbitrary and ambiguous (103). The prevalence for LCA is around three per 100,000 births, for RP it is one in 4,000 births (103–106). LCA and RP usually start with night blindness due to an initial loss of rods and are therefore characterised as rod-cone diseases. However, for some mutations also cone-rod degeneration can be observed (103,107).

Currently, both for LCA and for RP, there is no therapy or cure that could restore or even stop vision loss. Some measures are suitable to slow down the vision decay such as the avoidance of light by *e.g.* using sunglasses or therapies with vitamin based-medications (103,108).

Until today, around 45 causative genes for RP and 14 genes for LCA were identified (103,109). The affected genes fulfil crucial functions in photoreceptors (especially genes involved in the visual cycle and transduction such as rhodopsin and opsin), RPE cells and other retinal cells (103,109). The mode of inheritance of LCA and RP can be dominant or recessive and either autosomal and X-linked, respectively (103,109). Amongst the most common causative genes for LCA and RP is the human crumbs analogue *CRB1* (110).

4.4.1. RP/LCA caused by *CRB1* mutations

10-15 % of all LCA cases and around 4 % of RP cases are caused by mutations within the *CRB1* gene (111,112). Until now, over 150 mutation variants have been found causing missense or null mutations (110). Although the mode of inheritance is believed to be autosomal recessive, only in approximately 70 % of the CRB1 RP or LCA patients, both alleles display potentially pathogenic mutations (110). This indicates that in these cases, either a second unknown gene is affected or the mutations might be situated intronically. The most common mutation C948Y is caused by a single base pair exchange (guanine to adenine) in exon 8 at position 2,843 of the mRNA (110,113). It leads to the replacement of the 948th amino acid from cysteine to tyrosine affecting an EGF-like domain.

Besides the common RP and LCA features of photoreceptor loss and pigment deposits, many, but not all *CRB1* mutated retinae show a preservation of para-arteriolar RPE (114,115) and the occurrence of a retinal telangiectasia (115,116). The latter is characterised by abnormally permeable blood vessels with exudations that can also lead to retinal detachment.

Until today, it was not possible to find a clear correlation between *CRB1* mutations and the presented pathological phenotype of a patient. Although null mutations were seen to cause LCA more likely, most other mutations can lead to LCA, early and late forms of RP with both presence or absence of the above described unique features (110). Of note, CRB1-LCA and RP patients present a thickened retina instead of the usually much thinner retina due to the photoreceptor loss (117).

4.5. Crumbs

CRB1 is a human protein that is expressed in the retina and the brain (118). The gene of *CRB1* is located on chromosome 1q31 containing 12 exons. The protein contains 19 epidermal growth factor (EGF)-like domains and 3 laminin globular (Lam G)-like domains. Several splice variants of *CRB1* have been described so far, the longest consisting of 4,218 bps encoding 1,406 aa (114,119) (V1, see Figure 4). Of the suggested splice variants, 3 have been confirmed in human retina (*V1*, *V2*, *VSec* (120), marked with * in Figure 4). The splice variant *VSec* is altered at the 3' end only encoding 1,376 aa. The longest isoform also contains a transmembrane and cytoplasmic domain harbouring FERM and PDZ- binding motifs. Consequently, the transmembrane variant can be found at the cell membrane whereas a shorter version (*VSec*) is a non-transmembrane version and most likely secreted by the cell (114).

In mice, Crb1 was found in epithelial cells, but especially in Müller glia and in photoreceptor inner segments concentrating adjacent to the outer limiting membrane (121,122). In fact, Crb1 is part of a crumbs complex which is localised at the subapical region apically to the zonula adherens (121,123). The crumbs complex contains, apart from Crb1, also Crb2 and Crb3 which show high similarity to Crb1 concerning structure and function (124,125). Crb2 for example is believed to have overlapping functions with aberrant expression patterns (126). In the mouse retina, Crb1 is only expressed

in Müller glia, while Crb2 is expressed also in photoreceptors (121,127,128). Crb3, on the other hand, is much shorter, lacks most of the Crb1/2 regions and is expressed in more cell types of the mouse retina (120,125,127). In humans, it was suggested that the expression patterns of Crb1 and Crb2 are reversed (127).

Further proteins of the crumbs complex are bound by the intracellular domains of crumbs proteins: Mpp5/Pals1, Patj, Mupp1, Mpp3 and Mpp4 (129). In close connection to that lies the Partitioning defective (PAR) complex harbouring the proteins Par3, Par6, atypical protein C (aPKC) and cell division control 42 (Cdc42) (130).

All the crumbs and Par complex proteins are believed to play a role in the establishment of cell polarity and might be involved in signalling processes (131,132). The putative roles shall be elucidated in the following section.
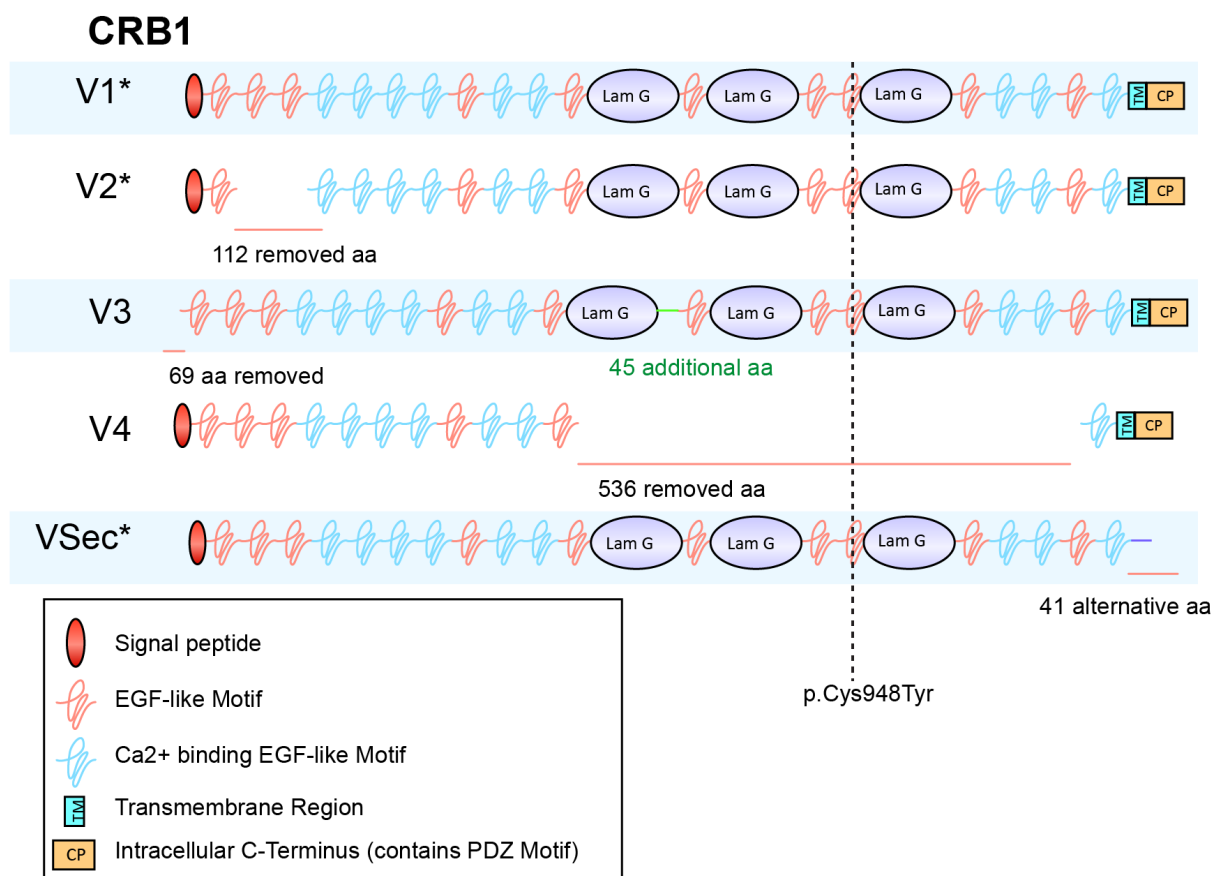
Figure 4- CRB1 variants and mutations

(A) Overview of CRB1 regions and motifs are depicted. V1-4 and VSec are all described splice variants in humans. Note that the patient cells studied in this thesis contain a single exchange of cysteine with

tyrosine at position 948 (Cys948Tyr). *Splice variants, which have been verified for human retina. The figure was adapted from Bujakowska *et al*. 2012 (110). Lam G= Laminin G lobular domain.

4.5.1. Putative roles and pathways influenced by crumbs protein

Originally, the crumbs protein has been described in drosophila where crumbs is responsible for the establishment and maintenance of polarity of epithelial cells (133,134). Moreover, the crumbs associated PAR complex was found to be involved in polarisation of epithelial and neural cells as well as axon myelination, oriented cell migration and asymmetric cell division (135). In retina and other neural tissues, Crb plays a role in the integrity of apical domains or in the case of the photoreceptors, the stability of the inner and outer segments by connecting the inner segments to the Müller glia cells forming the outer limiting membrane (123,136).

Recently, Crb was also recognised to play a role in cell signalling, especially tissue growth, proliferation and retinal differentiation pathways. The suspected roles in retinal development comprising several pathways are summarised in the next section (also reviewed in (131)).

4.5.1.1. Wnt

Wnt signalling is one of the key regulating signalling pathways in retinal development (137). It is crucial for *e.g.* the establishment of the retinal field and the maintenance of retinal progenitors during development (138,139). The key component of the canonical wnt pathway is ß-catenin, which is degraded by a destruction complex in the absence of wnt ligands. Upon binding of wnt molecules to its receptor frizzled and to the co-receptor Lrp5/6, the destruction complex is disassembled and ß-catenin can translocate to the nucleus and interact with transcription factors, which regulate the expression of cell cycle and cell fate genes. In mice, numerous knockout models of wnt components lead to defects in retinal development (140,141). Crb1 and the crumbs complex might be one of the regulating components due to its importance in correct location of ß-catenin and p120-catenin at the adherence junction (142,143).

4.5.1.2. Notch

Notch signalling can be implemented by the four notch (1-4) receptors, which can bind 5 ligands (Delta- like 1, -3, -4, Jagged 1 and 2). Upon binding, the intracellular part of notch receptor (NICD) is cleaved off by γ- secretase, and translocates to the nucleus. There, it binds to the transcription factor Rbp- J regulating the expression of *e.g. HES* (hair and enhancer of split) and *HEY* genes (144).

Notch signalling is crucial for retinal development and especially the cell fate and maintenance of retinal progenitors (145,146). In the condition of inactivated Dll1, a ligand for notch receptors, a decrease of early retinal progenitors and a change in ganglion cell number was observed (147). CRB1 and CRB2 in humans and crumbs in drosophila were seen to inhibit γ- secretase activity (148,149). Moreover, in zebrafish, crb could bind the notch receptor extracellularly inhibiting the binding of ligands (150). In drosophila, a notch- dependent over -proliferation of progenitors has been observed (151).

4.5.1.3. Hippo

The hippo pathway regulates *e.g.* cell proliferation, apoptosis and is involved in determining proper organ size (152). External signals lead to an activation of Lats1/2 (warts in drosophila) by Mst1/2 (hippo). Lats in term inhibits Yap that consequently leads to enhanced proliferation and less apoptosis by regulation of *e.g.* Cyclin genes.

In drosophila, crb can bind the hippo-regulating gene expanded (153). This leads to a mislocalisation of the components causing tissue overgrowth. In mammalians, another hippo regulating protein Amot is associated with the crumbs complex proteins Patj, Pals1, Mupp1 and Par3 (154). In mice, a Crb1/2 conditional knockout in retinal progenitors exhibited a dysregulation of yap/hippo protein (143).

4.5.1.4. mTOR

Nutrients, growth factors and cellular energy- related proteins activate the mTOR pathway in mammals (155). It consists of two different complexes: mTorc1, which is sensitive to nutrients and Mtorc2, which is involved in cytoskeletal reorganisation and

cell survival. Tsc1/2 heterodimers which are involved in regulation of the Mtorc1 complex can bind through the crumbs complex protein Patj via its PDZ domain (156). However, not much is known about the role of mTOR in retinogenesis. The stimulation of the mTOR component Akt leads to a degeneration of photoreceptors, which suggests a role of the pathway in homeostasis of photoreceptors (157).

4.6. Animal models of retinitis pigmentosa caused by Crb mutations

The effects of Crb1, Crb2 or crumbs loss have been studied extensively in drosophila flies and mice. In flies, the crumbs knockout leads to a shortening of rhapdomers, which are equivalent to photoreceptor outer segments of mammals. Ultimately, they display a loss of photoreceptors and retinal degeneration (123).

In mice, different models have been studied. First, the natural occurring rd8 mouse, which harbours a 1 bp deletion in *Crb1* leading to a premature stop codon (136). The produced protein lacks a transmembrane and intracellular region. The retina of these animals is largely disorganised with the appearance of retinal folds and loss of photoreceptor cells. In addition, adherence junctions are partly absent. However, the integrity of photoreceptors is still largely maintained, allowing for an almost normal retinal function. Interestingly, the phenotype of the rd8 mouse is supressed on a C57BL/6J genetic background.

The first Crb1 mouse knockout was created in 2004 (121). The deletion was achieved by removal of the promoter region and the first exon. Surprisingly, the animal displayed an almost normal vision with retinal pathology just present in the inferior quadrant. There, photoreceptors were displaced and half rosettes appeared. In addition, the OLM integrity was lost. Continuous light exposure lead to a strengthening of the phenotype but it was still limited to the inferior quadrant. Again, on a C57BL/6J genetic background this phenotype was suppressed.

The knockout of Crb2 in mice was seen to be embryonically lethal (158). To study retinogenesis, a conditional knockout of Crb2 in early retinal progenitors was generated (126). The retina of these mice showed abnormal lamination with a change in number of late born progenitors, rods and Müller glia. Degeneration was present in all quadrants with thinning of the photoreceptor layer and shortening of cone outer

segments. One month after birth, impairment of retinal functionality could be observed which could not be suppressed by the C57BL/6J genetic background.

In the following, a combined knockout of Crb1 and conditional Crb2 in retinal progenitors was generated causing a much more severe phenotype of degeneration (143). In these retinas, no separate photoreceptor layer was formed and photoreceptor nuclei were displaced. Again, late born cells (rods, Müller glia, and bipolar cells) were increased, whereas early born numbers remained unaffected. One month after birth, a severe loss of photoreceptors was noted and after three months, no retinal activity could be monitored anymore.

4.7. Human embryonic stem cells (ESCs) and human induced pluripotent cells (iPSCs)

Embryonic stem cells (ESCs) are pluripotent stem cells obtained from the inner cell mass of preimplantation embryos. The term "pluripotent" refers to their potency to differentiate into all types of the three germ layers. To overcome the obvious ethical difficulties that arise with the use of human embryos, other methods to obtain pluripotent stem cells had to be found. Consequently, the finding of Yamanaka and his group (159) that somatic cells can be reprogrammed to so called induced pluripotent stem cells was a ground-breaking step. Virtually all somatic cells of the body (fibroblasts, keratinocytes, neural stem cells (NSCs), human blood *etc.*) (159–163) can be used for reprogramming. The reprogramming is achieved by forced expression of the four so-called Yamanaka factors (Klf4, Sox2, Oct3/4 and C-Myc). These factors can be delivered *e.g.* by lentiviral (164), episomal vectors (165) or mRNA (166). The differentiation into various cell types such as hepatocytes, cardiovascular progenitors, cardiomyocytes and all kinds of neuronal cells has been established over the last few years (167–169). At present, the neuronal differentiation of human ESCs and iPSCs to dopaminergic neurons, motoneurons as well as astrocytes and oligodendrocytes or even to whole so-called brain organoids is possible (170–173). In this study, we focused on the differentiation of keratinocyte-derived iPSCs into retinal cells by making use of self-organised three-dimensional tissues called retinal organoids.

4.8. Generation of retinal cells and retinal organoids

The opportunity to culture mouse (174,175) and human embryonic stem cells (hESCs) *in vitro* (176) and the discovery of iPSCs (159) in the 2000s years opened up the possibility to generate and differentiate neural tissues including retinal cells. The first neural differentiation protocols enabled the emergence of retinal cells in a mixed unorganised fashion (177–180). Especially the arising of photoreceptors and RPE could be achieved by different approaches and were validated by respective marker expression and in case of the photoreceptors by the presence of (Rhod)opsins (177,181). However, all these adherent protocols lacked proper organisation, interaction of cell types and purity of retinal cells.

In 2011, Eiraku and colleagues (182) achieved the establishment of three-dimensional spheroids called organoids from mouse ESCs which not only showed marker gene expression of retinal progenitors and cell types but they could also display a proper organisation and development closely resembling the embryonic retina. They found that these organoids were able to form an optic vesicle and subsequently an optic cup in a self-organising manner without the influence of an external structure. The optic cups from mESCs and later also from hESCs harboured neural retinal progenitors as well as RPE cells of the correct orientation (182,183). When retinal organoids from hESCs, mESCs or human iPSCs were differentiated into optic vesicles, also the arising of the neural retinal neurons could be observed. All retinal cell types as discussed in the respective section were present as well as inner and outer limiting membranes. In addition, these organoids displayed a primitive but correct layering with an exclusive photoreceptor nuclei layer (resembling the outer nuclei layer), an inner layer harbouring interneurons, and an inner ganglion cell layer.

The protocol used in a study of Nakano *et al*. 2012 (183) was based on a solely three-dimensional culture of embryoid bodies, which were under pro-neural, neural tube inducing conditions and in the presence of growth factor-reduced Matrigel- primed in an anterior forebrain direction. This was achieved by an inhibition of wnt signalling and subsequent hedgehog activation. Another strategy used by Zhong *et al*. for generating hiPSC- derived optic vesicles was the use a sequential 3D and 2D cell culture and an undirected neural differentiation (184). They found that neural induced iPSCs had the tendency to form forebrain and especially the diencephalon derived retinal progenitors.

When the retinal progenitors were allowed to form three-dimensional spheroids they formed the very same organoids as described in Nakano *et al*. Both organoids are virtually indistinguishable in their ability to form retinal neurons, photosensitive rod and cone photoreceptors as well as proper layering and photoreceptor ribbon synapses (183–185). An overview on the most common human retinal organoid protocol is given in Figure 5. Based on these protocols, many groups found that photoreceptors of retinal organoids could form proper inner segments, but mostly even after a long time lacked mature outer segments (184,185). Nevertheless, retinal organoids show incredible features *in vitro* and allow for disease modelling in a retina-like structure closing in more and more to the physiological situation and might be a valid tool for drug screening and safety studies as well as a promising source for cell replacement therapy approaches.

a **3D- Protocols**

Nakano *et al*. 2012

iPSC

EB — G-MEM
20% KSR
Pyruvate
+IWR1e (3d)

+10%FBS
+Matrigel

+CHIR99021
+SAG

Optic Cup
(NR+RPE)

DMEM/F12
N2

Zhong *et al*. 2014

iPSC

EB

DMEM/F12
N2

NE — d16

DMEM/F12
B27

NR — d28

DMEM/F12
B27

Long-Term
+ 10% FBS
+ Taurine
+ RA

b **Nakano *et al*. 2012**

Day 0

Day 12

Day 18-24

Day 24+

c **Zhong *et al*. 2014**

Day 0

Day 7

Day 28

Day 28+

Suspension

Adherent
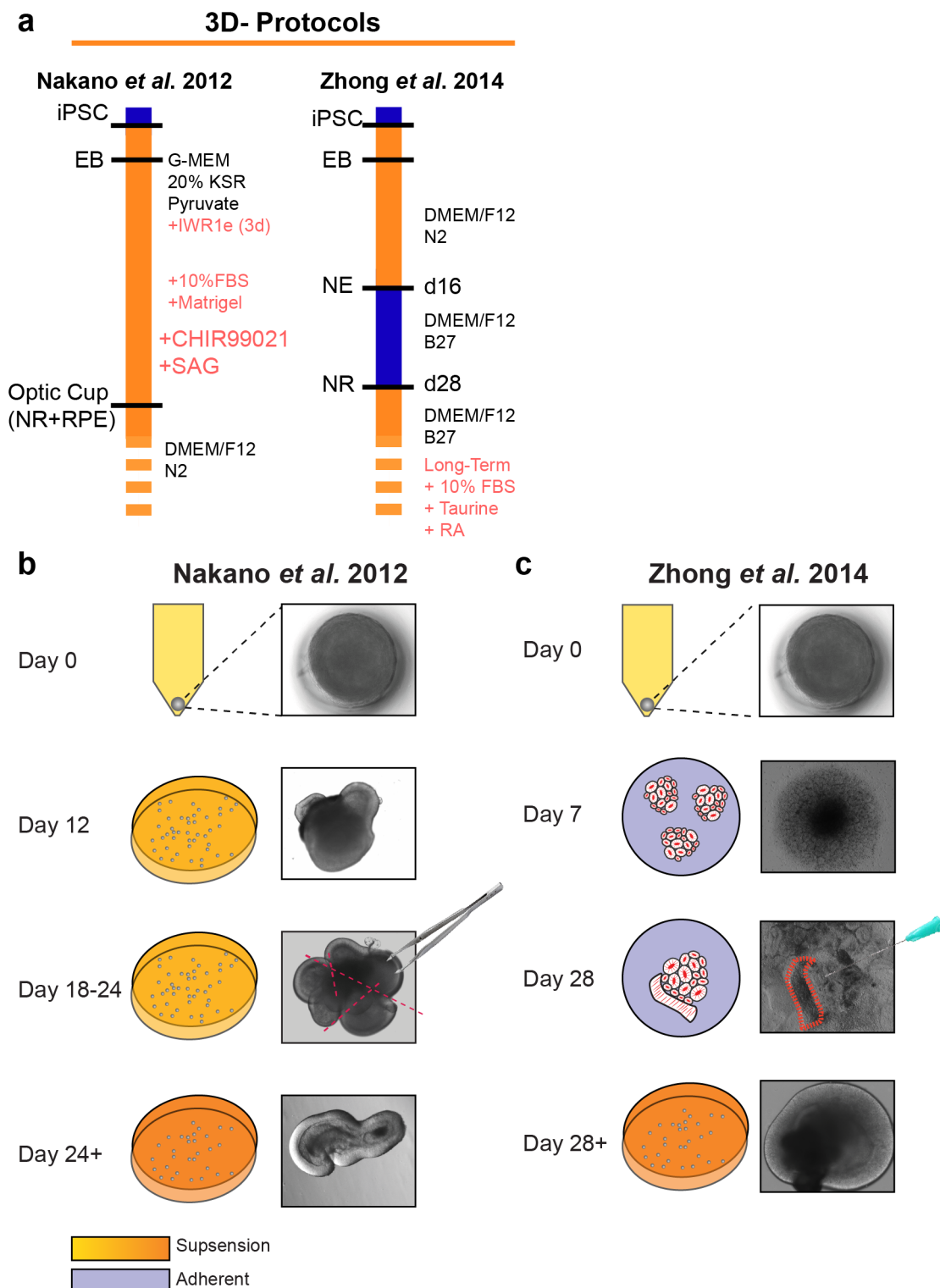
Figure 5- Comparison of retinal organoid protocols

(A) Overview of most important retinal organoid protocols published in the last years. Important factors and steps are marked. Orange bars indicate suspension culture; blue bars indicate adherent culture steps. (B) Illustration of the Nakano *et al*. 2012 (183) protocol. At day 0, embryoid bodies are produced in non-adherent 96 V-bottom well plates. After 12 days, EBs show outgrowing retinal structures.

Between day 18 and 24, the outgrowing retinal areas were excised and kept in suspension culture. (C) Illustration of the Zhong *et al*. 2014 (184) protocol. At day 0, EBs are produced in non-adherent 96 V-bottom well plates. At day 7, EBs are plated on Matrigel-coated well plates and at day 24-28, retinal field areas are manually picked and cultured in suspension afterwards.

4.9. Microfluidic organ-on-a-chip systems

In the endeavour to create cellular systems that can even more closely mimic the human physiology, the organ-on-a-chip (OoC) technology was developed. OoC comprises a class of microfluidic devices, which can harbour one or several cell types and bring them a) in a physiological interaction and context and b) supply a closely natural environment. Furthermore, OoC devices supply constant perfusion via microfluidic channels. This not only reduces the required media but also supplies constantly fresh medium while removing old cellular waste. The goal of OoC is the modelling of an organ system *in vitro* by using the smallest functional unit of it. They can then be used for mechanistic studies concerning development of functional adult tissue or for drug screening or safety testing. In combination with the iPS cell technology, virtually all cell types can be cultured inside an OoC. In addition, the microfluidic devices can supply a physiological niche by *e.g.* reducing or increasing mechanical shear stress, implementing movements, supplying suitable surfaces or in combination with three-dimensional gels (*e.g.* hydrogels) supply a proper extracellular matrix. A famous example for OoC system is the lung-on-a-chip system (186), which harbours two types of lung cells and an alveolus-like movement of the device. Until now, several organs have been modelled in this way, such as liver on a chip (187) or kidney on a chip (188).

4.10. Aim of the thesis

This thesis was designed to establish the differentiation and culture of iPSC-derived retinal organoid to model retina development and retina-associated diseases based on previously published protocols. In a second step, I generated iPS cells from two siblings suffering from the inherited degenerative retina disease retinitis pigmentosa caused by a mutation in the *CRB1* gene. Subsequently, I used these cells to generate retinal organoids and study them for developmental aberrations and degenerative

pathology. Additionally, I developed a package of software tools to quantify protein expression and morphological evaluation using immunofluorescence. Further analysis involved transcriptomic evaluation on the RNA level and electron microscopic ultrastructural imaging. Furthermore, I used an organoid calcium imaging approach to study the light response in control and patient organoids. Inspired by the results of these experiments, I finally developed an improved *in vitro* model using organ-on-a-chip technology called retina-on-a-chip. In summary, this thesis exploits the usability of iPS cell-derived retinal organoids for disease modelling and gives future directions of an improved form of organoid culture.

5. Material and Methods

5.1. Material

5.1.1. Biological materials

Table 1: List of biological materials

Cell type	Supplier
Lenti-X™ Cells	Takara Bio, Kusatsu, Japan
Mouse embryonic fibroblasts	Obtained as described earlier (160)
Rat embryonic fibroblasts	Obtained as described earlier (160)

5.1.2. Laboratory equipment

Table 2: List of laboratory equipment

Equipment	Company
BioMark™ HD, Fluidigm	Fluidigm, South San Francisco, CA, USA
Centrifuges (Heraeus™ Megafuge™ 16 Centrifuge, Heraeus™ Fresco 17 Centrifuge)	Thermo Fischer Scientific, Waltham, MA, USA
Cryostat, Microm HM 560	Thermo Fischer Scientific, Waltham, MA, USA
Evos FL	Thermo Fischer Scientific, Waltham, MA, USA
Freezer (-20°C)	Liebherr, Biberach, Germany
Freezer (-80°C)	Thermo Fischer Scientific, Waltham, MA, USA
Fridge 4°C	Liebherr, Biberach, Germany
Gel electrophoresis SubCell® GT	BioRad, Hercules, CA, USA
Ice machine, AF103	Scotsman, Great Blakenham, UK
Incubator 37 °C, Heracell™ 240i	Thermo Fischer Scientific, Waltham, MA, USA

LED (Thomsen LED-5-14000W/75°)	Conrad, Hirschau, Germany
Legato™ 210 pump	KD Scientific, Holliston, MA, USA
Microscope (Axioskop 2 mot plus, Primo Vert)	Zeiss, Oberkochen, Germany
NanoPhotometer P330	Implen, München, Germany
Nitrogen Tank, CryoPlus™ 2	Thermo Fischer Scientific, Waltham, MA, USA
PCR Thermocycler, peqStar	Peqlab Biotechnologie, Erlangen, Germany
Reichert Ultracut S	Leica, Wetzlar, Germany
Sony SH800 cell sorter	Biotechnology
StepOnePlus real-time PCR systems	Thermo Fischer Scientific, Waltham, MA, USA
Sterile Bench, MSC-Advantage	Thermo Fischer Scientific, Waltham, MA, USA
SU-8 developer	Micro Resist Technology, Berlin, Germany
Upright fluorescence microscope (BX50WI)	Olympus, Tokio, Japan
UV developer Quantum ST4	Vilber Lourmat, Eberhardzell, Germany
Vacuum Pump, Integra Vacusafe	Integra Biosciences, Biebertal, Germany
Vortexer	Bender+ Hobein, Zürich, Switzerland
Water bath, Lab Line waterbath	Thermo Fischer Scientific, Waltham, MA, USA
Zeiss EM 900 transmission electron microscope	Zeiss, Jena, Germany

5.1.3. Plastic wares and tools

Table 3: List of plastic wares and tools

Material	Company
6-, 12, 24- well-plates (Tissue treated, Non treated)	Becton Dickinson, New York, NY, USA
96.96 Dynamic Array™ IFC	Fluidigm, South San Francisco, CA, USA
96 Well-V-shaped culture plates	Sarstedt, Nümbrecht, Germany
Cell scraper	Thermo Fischer Scientific, Waltham, MA, USA
Cell strainer 70µm	Becton Dickinson, New York, NY, USA
Coverslips, Menzel (24 mm x 24 mm, 24 mm x 40 mm)	Thermo Fischer Scientific, Waltham, MA, USA
Dako pen	Dako, Hamburg, Germany
Gloves Peha-Soft® nitrile	Hartmann, Heidenheim, Germany
PET membranes	Sabeu, Northeim, Germany
Petri dishes (10cm, 6cm)	Greiner Bio-One, Frickenhausen, Germany
Pipette tips (10µl, 100µl, 200µl, 1 ml, 5ml)	Eppendorf, Hamburg, Germany
Pipettes, Eppendorf Research® Plus (10µl, 100 µl, 200µl, 1000 µl, 5ml)	Eppendorf, Hamburg, Germany
QiaShredder™	Qiagen, Hilden, Germany
Reaction tubes (15 ml, 50 ml)	Becton Dickinson, New York, NY, USA
Reaction tubes small (0,5 ml, 1,5 ml, 2,0 ml)	Sarstedt, Nümbrecht, Germany
Sterile filters (0.22 µm, 0.45µm)	Merck Millipore, Darmstadt, Germany

Super Frost® Plus object slides	R. Langenbrinck, Emmendingen, Germany
T25-flasks (Culture treated)	Greiner Bio-One, Frickenhausen, Germany
Tissue-Tek® Cryomold® (10 mm x 10 mm x 5mm)	Sakura Finetek, Alphen aan den Rijn, NL
Ultra-Fine-Clipper-Scissors-II	Fine Science Tools, Heidelberg, Germany

5.1.4. Cell culture media

Table 4: List of cell culture media

Medium	**Company**
Antibiotic-antimycotic 100 x liquid	Thermo Fischer Scientific, Waltham, MA, USA
CryoStem™	Biological Industries, Beit Haemek, Israel
DMEM, high glucose	Thermo Fischer Scientific, Waltham, MA, USA
DMEM/F12 + GlutaMAX™	Thermo Fischer Scientific, Waltham, MA, USA
Epilife® + HKGS supplement	Thermo Fischer Scientific, Waltham, MA, USA
Fetal bovine serum (FBS)	Thermo Fischer Scientific, Waltham, MA, USA
GlutaMax™ 100 x liquid	Thermo Fischer Scientific, Waltham, MA, USA
KnockOut™-DMEM	Thermo Fischer Scientific, Waltham, MA, USA
KnockOut™-serum replacement	Thermo Fischer Scientific, Waltham, MA, USA

Non-essential amino acids	Thermo Fischer Scientific, Waltham, MA, USA
Normal donkey serum(NDS)	Sigma-Aldrich, St. Louis, MO, USA
OptiMEM™	Thermo Fischer Scientific, Waltham, MA, USA
PeproGrow™ hESC embryonic stem cell media	PeproTech, Hamburg, Germany
Phosphate-buffered saline (PBS) w/o magnesium and calcium	Thermo Fischer Scientific, Waltham, MA, USA
Synth-A-Freeze® cryopreservation medium	Thermo Fischer Scientific, Waltham, MA, USA

5.1.5. Chemicals and supplements

Table 5: List of all chemicals and supplements

Chemicals and Supplements	Company
9-cis-retinal	Sigma-Aldrich, St. Louis, MO, USA
Activin A	Cell Guidance Systems LLC, St. Louis, MO, USA
Agarose	AppliChem, Darmstadt, Germany
all-trans-retinoic acid	Sigma-Aldrich, St. Louis, MO, USA
Apotransferrin	Serologicals, Atlanta, GA, USA
Araldite® resin	Serva, Heidelberg, Germany
B-27™ without vitamin A	Thermo Fischer Scientific, Waltham, MA, USA
Bis-[3-trimethoxysilypropyl]amine	Sigma-Aldrich, St. Louis, MO, USA
(-)- Blebbistatin	Sigma-Aldrich, St. Louis, MO, USA

Boric acid	Sigma-Aldrich, St. Louis, MO, USA
Bovine insulin	Sigma-Aldrich, St. Louis, MO, USA
Bromodeoxyuridine (BrDU)	Roche, Basel, Switzerland
Chemically defined lipid (CDL) concentrate	Thermo Fischer Scientific, Waltham, MA, USA
Chlorotrimethylsilane	Sigma-Aldrich, St. Louis, MO, USA
Dorsomorphin dihydrochloride	Tocris Bio-Techne, Wiesbaden-Nordenstadt, Germany
EDTA	Sigma-Aldrich, St. Louis, MO, USA
Ethanol	Serva, Heidelberg, Germany
Fura-2-AM	Thermo Fischer Scientific, Waltham, MA, USA
Glutaraldehyde	Electron Microscopy Sciences, Munich, Germany
Heparin sodium salt	Sigma-Aldrich, St. Louis, MO, USA
Human recombinant EGF	Cell Guidance Systems LLC, St. Louis, MO, USA
Human recombinant FGF-2	Cell Guidance Systems LLC, St. Louis, MO, USA
Human serum albumin (HSA)	Biological Industries, Cromwell, CT, USA
HyStem®-C- hydrogel	EsiBio, Alameda, CA, USA
Isopropanol	VWR, Radnor, PA, USA
ITS	BD Bioscience, San Jose, CA, USA

L-Ascorbic acid	Sigma-Aldrich, St. Louis, MO, USA
Lenti-X™ concentrator	Takara Bio, Kusatsu, Japan
MassRuler Express Forward DNA Ladder Mix	Thermo Fischer Scientific, Waltham, MA, USA
Mitomycin C	Biomol GmbH, Hamburg, Germany
Osmium tetroxide	Electron Microscopy Sciences, Munich, Germany
Paraformaldehyd	Roth, Karlsruhe, Germany
Pluronic™ F-127	Thermo Fischer Scientific, Waltham, MA, USA
Polybrene® (Hexadimethrine bromide)	Sigma-Aldrich, St. Louis, MO, USA
Polydimethylsiloxane (PDMS) Sylgard 184	Dow Corning, Midland, MI, USA
Polyethylenimine	Polysciences, Warrington, PA, USA
Progesteron	Sigma-Aldrich, St. Louis, MO, USA
ProLong™ gold antifade mountant with DAPI	Thermo Fischer Scientific, Waltham, MA, USA
Proplyene oxide	Serva, Heidelberg, Germany
Putrescine dihydrochlorid	Sigma-Aldrich, St. Louis, MO, USA
RedSafe™ nucleic acid staining solution	ABC Scientific, Glendale, CA, USA
Rock-inhibitor Y-27632	Ascent Scientific, Avonmouth, UK
Sodium cacodylate buffer, pH 7.4	Electron Microscopy Sciences, Munich, Germany

SU8-50 photoresist	MicroChem, Westborough, MA, USA
Sucrose	Roth, Karlsruhe, Germany
Taurine	Sigma-Aldrich, St. Louis, MO, USA
TGFβ1	Cell Guidance Systems LLC, St. Louis, MO, USA
Tissue-Tek® O.C.T.™ compound	Sakura, Alphen aan den Rijn, NL
TRIS Base	Roth, Karlsruhe, Germany
Triton® X-100	Roth, Karlsruhe, Germany
Uranyl acetate	Serva, Heidelberg, Germany
β-Mercaptoethanol	Thermo Fischer Scientific, Waltham, MA, USA

5.1.6. Coatings

Table 6: List of all coatings

Coatings	Company
Collagen IV	Sigma-Aldrich, St. Louis, MO, USA
Laminin	Roche, Basel, Switzerland
Matrigel®	Corning, New York, NY, USA
Matrigel®, hESC-Qualified	Corning, New York, NY, USA
Matrigel®, Growth factor reduced	Corning, New York, NY, USA
Poly-L-ornithine	Sigma-Aldrich, St. Louis, MO, USA

5.1.7. Enzymes

Table 7: List of all enzymes

Enzymes	Company
Accumax™	Sigma-Aldrich, St. Louis, MO, USA
Dispase	Stem Cell Technologies, Vancouver, Canada
PrimeStar® GXL DNA polymerase	Takara Bio, Kusatsu, Japan
TrypLE™ Express	Thermo Fischer Scientific, Waltham, MA, USA

5.1.8. Primers

Human primers, which were used for qRT-PCR, are given in Table 8.

Table 8: List of human primers used for qRT-PCR

Gene Name	Source/Company	Forward	Reverse
CRB1 V2	(120)	TCTGTCCCCACAATTATTCTGGATA	TCTCTGAGGACAGCTCCACACAT
CRB1 VSec	(120)	GTAAGCAGCCTCTCCTTTTATGTCTCT	CAACAACTGGCTCGTCATTCATAC
CRB1 V1/2	(120)	CCTCTGTGATGTTGCCTTTGC	GTGGTGAAAATGTCGGAGATCAA
CRB1 V1/3/Sec	(120)	GCCTCTTTGTTGGTCAAAACCTT	GTGTATCCAGGCCAGCAGTGA
CRB1 V1/2/Sec	(120)	ACCCCAGGAGAAAGGAGCTTT	CTTGCCACAGGAACCAATGG
CRB1 N-Terminal	Qiagen, Hilden, Germany		

OCT	Qiagen, Hilden, Germany		
NANOG	Qiagen, Hilden, Germany		
FOXA2	Qiagen, Hilden, Germany		
AFP	Qiagen, Hilden, Germany		
MYH6	Qiagen, Hilden, Germany		
T	Qiagen, Hilden, Germany		
SOX1	Qiagen, Hilden, Germany		
TUBB3	Qiagen, Hilden, Germany		

5.1.9. Taqman™ probes

All Taqman™ probes were obtained from Thermo Fisher Scientific, Waltham, USA

Table 9- List of all Taqman™ probes

Gene name	Article No.
ANXA4	Hs00154040_m1
APC	Hs01568269_m1
APH1A	Hs01046142_g1
ARR3	Hs01020134_m1
ATOH7	Hs00376955_s1
CCND1	Hs00765553_m1
CCNE1	Hs01026536_m1
CDC42	Hs00918044_g1

CRB2	Hs00543624_m1
CRB3	Hs00373616_m1
CRX	Hs00230899_m1
CTGF	Hs01026927_g1
CTNNB	Hs00355049_m1
CTNND1	Hs00609738_g1
DKK1	Hs00183740_m1
DKK3	Hs00951307_m1
DVL1	Hs00182896_m1
ESCO1	Hs00405607_m1
GLI2	Hs01119974_m1
GLUL	Hs00365928_g1
GNAT1	Hs00181100_m1
GNAT2	Hs00292542_m1
GSK3B	Hs01047719_m1
HIST3H2BB	Hs01592663_s1
HES5	Hs01387463_g1
HEY1	Hs01114113_m1
INADL	Hs00195106_m1
LEF1	Hs01547250_m1
LRP6	Hs00233945_m1
MPP5	Hs00223885_m1
MTOR	Hs00234522_m1
MYC	Hs00153408_m1
MYCN	Hs00232074_m1
NCSTN	Hs00299716_m1
NEUROD2	Hs00272055_s1
NOTCH1	Hs01062014_m1
NRL	Hs00172997_m1
OPN1MW	Hs04194752_g1
OPN1SW	Hs00181790_m1

PDE6B	Hs01557860_m1
PEN2	Hs00708570_s1
PKCA	Hs00925193_m1
POU4F2	Hs00960964_g1
PRKCI	Hs00995854_g1
PROX1	Hs00896294_m1
PSEN1	Hs00997789_m1
PTTG1	Hs01921016_gH
PTTG2	Hs00747713_sH
RHO	Hs00892431_m1
RX	Hs00429459_m1
SMO	Hs01090242_m1
TSC1	Hs01060648_m1
TSC2	Hs01020387_m1
TUBB3	Hs00801390_s1
VSX2	Hs01584047_m1
WNT5A	Hs00998537_m1

5.1.10. Antibodies

5.1.10.1. Primary

Table 10: List of primary antibodies

Antibody	Company	Dilution
Afp	Abcam, Cambridge, UK	1:500
Ap2α	Santa-Cruz, Santa-Cruz, CA, USA	1:200
Arrestin3 (ARR3)	Santa-Cruz, Santa-Cruz, CA, USA	1:100
BrDU	Serotech	1:200
Brn3B	Santa-Cruz, Santa-Cruz, CA, USA	1:50
Calbindin	Swant, Marly Innovation Center, Schweiz	1:500
Cdc42	Abcam, Cambridge, UK	1:200
Chx10(Vsx2)	Santa-Cruz, Santa-Cruz, CA, USA	1:200

Cngb3	Sigma-Aldrich, St. Louis, MO, USA	1:200
Cralbp	Abcam, Cambridge, UK	1:250
Crb1c	Thermo Fischer Scientific, Waltham, USA	1:200
Crb1n	Novus Biologicals, Littleton, CO, USA	1:200
Ctbp2(Ribeye)	Becton Dickinson, New York, NY, USA	1:200
Desmin	Dako, Hamburg, Germany	1:500
G0α	Merck Millipore, Darmstadt, Germany	1:400
Glutamine Synthetase (Glul)	Merck Millipore, Darmstadt, Germany	1:500
Ki67	Cell Signaling	1:400
L/M-Opsin	Merck Millipore, Darmstadt, Germany	1:200
Na^+/K^+ ATPase $α3$	Abcam, Cambridge, UK	1:100
Pals1	Novus Biologicals, Littleton, CO, USA	1:200
Pde6b	Thermo Fischer Scientific, Waltham, USA	1:400
PKCα	Santa-Cruz, Santa-Cruz, CA, USA	1:500
Recoverin	Merck Millipore, Darmstadt, Germany	1:1000
Rhodopsin	Santa-Cruz, Santa-Cruz, CA, USA	1:200
Rod Transducin	Santa-Cruz, Santa-Cruz, CA, USA	1:500
ROM1	Proteintech, Chicago, USA	1:200
S-Opsin	Merck Millipore, Darmstadt, Germany	1:200
ZO-1	Thermo Fischer Scientific, Waltham, USA	1:100

5.1.10.2. Secondary

Table 11: List of secondary antibodies

Antibody	Type	Company	Dilution
Alexa Fluor™ 488	Donkey anti mouse IgG	Abcam, Cambridge, UK	1:1000

Alexa Fluor™ 488	Donkey anti rabbit IgG	Abcam, Cambridge, UK	1:1000
Alexa Fluor™ 488	Donkey anti goat IgG	Abcam, Cambridge, UK	1:1000
Alexa Fluor™ 488	Donkey anti chicken IgG	Abcam, Cambridge, UK	1:1000
Alexa Fluor™ 568	Donkey anti mouse IgG	Abcam, Cambridge, UK	1:1000
Alexa Fluor™ 568	Donkey anti rabbit IgG	Abcam, Cambridge, UK	1:1000
Alexa Fluor™ 568	Donkey anti goat IgG	Abcam, Cambridge, UK	1:1000
Alexa Fluor™ 647	Donkey anti mouse IgG	Abcam, Cambridge, UK	1:1000
Alexa Fluor™ 647	Donkey anti rabbit IgG	Abcam, Cambridge, UK	1:1000
Alexa Fluor™ 647	Donkey anti goat IgG	Abcam, Cambridge, UK	1:1000

5.1.11. Fluorescence- coupled proteins

Table 12: List of fluoresence-coupled proteins

Substance	Details	Company	Dilution
Lectin PNA Alexa Fluor™ 488, 568, 647	Arachis hypogaea (peanut), Alexa Fluor™ 488 or 568 or 647 Conjugate	Sigma-Aldrich, St. Louis, MO, USA	1:1000

5.1.12. Kits & assays

Table 13: List of kits and assays used

Kits/Assays	Company
Click-iT™ TUNEL Alexa Fluor™ 488 Imaging Assay	Thermo Fischer Scientific, Waltham, USA
PreAmp Master Mix	Fluidigm, South San Francisco, CA, USA
JetQuick™, gel extraction kit	Genomed, Leesburg, Finland
QIAamp® DNA Mini Kit	Qiagen, Hilden, Germany
QuantiFast SYBR™ Green RT-PCR Kit	Qiagen, Hilden, Germany
RNeasy® Mini Kit/RNeasy® Micro Kit	Qiagen, Hilden, Germany

5.1.13. Lentiviral vectors

Table 14: List of lentiviral vectors

Antibody	Company	Dilution
pJG-IRPB-eGFP	Lentiviral expression vector expressing eGFP under the IRBP promoter	Gift from Deepak Lamba & Thomas Reh [32]
pRRL.PPT.SF.hOKSMco.idTom.preFRT	Lentiviral expression vector carrying human OCT4, KLF4, SOX2, C-MYC and dTomato	(189)

5.1.14. Software

Table 15: List of software

Software	Company, Website
Fluidigm Real-Time PCR Analysis Software v.3.0.2.	Fluidigm, South San Francisco, CA, USA
Graph Pad (Prism)	Graphpad Software, La Jolla, CA, SUA
Microsoft Office Excel 2016	Microsoft, Redmond, WA, USA
VisiView® software	Visitron Systems, Puchheim, Germany
GATC Viewer	GATC, Konstanz, Germany
ImageJ v1.51w	https://imagej.nih.gov/
AxioVision 4.8.1	Zeiss, Oberkochen, Germany
R 3.5 and RStudio Desktop	https://cran.r-project.org/bin/windows/base/ https://www.rstudio.com/
SH800 software	Sony Biotechnology, Weybrige, UK

5.2. Methods

5.2.1. Cell culture

Cell culture was performed under sterile conditions under a sterile bench and the incubation took place in an incubator at 37 °C in a water-saturated atmosphere of 5 % CO_2 and 20 % (ROs) or 5 % O_2 (hiPSC, Keratinocytes)), respectively. All used media had been warmed up using 37°C water bath.

The use of human material was approved by the ethical committee of the Tübingen University (No. 841/2016BO2) and in compliance with the guidelines of the Federal Government of Germany and the Declaration of Helsinki concerning Ethical Principles for Medical Research Involving Human Subjects. Both patients, which are part of the study, were informed according to predesigned information sheets and provided written consent to the use of the collected hair material for subsequent generation of iPS cells and analysis.

5.2.2. Culture of hair keratinocytes

Keratinocytes for iPSC reprogramming were obtained from plucked hair from healthy donors and from two brothers suffering from retinitis pigmentosa. Both carry a homozygous C948Y mutation in the *CRB1* gene. In this thesis, control lines (CTRL) are k3 (male) and k5 (male) as well as RP patients: RPA for older sibling (male) and RPB for the younger sibling (male).

Briefly, for keratinocytes outgrowth, plucked hairs including the root and the outer root sheath containing the keratinocytes were cut small and platted on a Matrigel-coated T25 culture treated flask. Coating was done for 1 hour at 37 °C with a 1:10 dilution of Matrigel in Epilife-HKGS. For proper fixation, the hair was covered with a drop of 1:5 Matrigel in Epilife-HKGS and incubated for 2 hours at 37°C. Afterwards, flaks were filled with 1 ml conditioned-MEF medium (conditioned for one day on MEF cells and sterile filtered (0.22 μm filter) subsequently) + 10 ng/ml FGF2 + 10 μM Y-27632 (ROCK- inhibitor). After initial outgrowing of keratinocytes (after 2- 5 days), medium was changed to Epilife + HKGS. Medium was changed daily until 80-90 % confluency was reached. Cells were then either replated on collagen IV (20 μg/ml)- coated dishes (1 h at 37 °C) or frozen in Synth-A-Freeze® cryopreservation medium. For freezing, keratinocytes were detached with dispase, collected and centrifuged at 300 g , 2 min. Cells were then resuspended in Synth-A-Freeze® medium, distributed onto 5 cryovials/T25 flaks and long-term stored in a nitrogen tank. For thawing, cryovials were warmed-up quickly in the water bath and cells were centrifuged at 300 g for 2 min. Thereafter, supernatant was discarded, cells were resuspended in Epilife + HKGS medium and seeded on collagen IV (20 μg/ml)-coated well plates.

REF/MEF Medium

- DMEM, high glucose
- 15% FBS
- 1x Antibiotic- antimycotic (100x)
- 1x Nonessential amino acids (100x)

5.2.3. Reprogramming of keratinocytes to human iPSC

For reprogramming of keratinocytes, cells were cultured in Epilife + HKGS on 6-well plates until they reached ~50-70 % confluency. On the first day of the protocol, cells were transduced in Epilife+ HKGS medium with 5×10^8 particles of a polycistronic virus containing the four Yamanaka factors (OCT4, KLF4, SOX2, C-MYC) and dTomato (189). To increase transfection efficiency, 8 µg/ml Polybrene® (Hexadimethrine bromide) was added to the cocktail. On the second day, medium was discarded, replaced by new Epilife + HKGS and transduction was repeated. On the third day, transduced keratinocytes were lifted with TrypLE™, centrifuged at 300 g for 2 min and reseeded in a ratio 1:4 in reprogramming medium on 6- wells, which were preseeded with growth-inactivated rat embryonic fibroblasts (REF)-feeder cells 2 days before (150.000 cells/6- well). After the seeding of transduced keratinocytes on the feeder cells, medium was changed daily. First colonies appeared after ~ 10- 15 days. After 25 days, colonies were big enough to be lifted with a pipette tip and reseeded onto hESC-qualified matrigel- coated dishes. Matrigel- coating was performed at 37 °C for 1 hour.

REF were isolated from day E14 Sprague Dawley rat embryos as described earlier (160) and cultured in REF/MEF medium. Cells were mitotically inactivated using 7.5 µg/ml mitomycin C per 90-100 % confluent 10 cm petri dish (around 6-10 mio cells) for 2.5 hours. Afterwards cells were detached using TrypLE™.

Reprogramming medium

- KnockOut™ DMEM
- 20 % Serum Replacement
- 2 mM GlutaMAX™
- 1x Nonessential amino acids (100x)
- 1x Antibiotic- antimycotic (100x)
- 100 µM β-mercaptoethanol

- 50 µg/ml L-ascorbic acid
- 10 ng/ml FGF-2
- 10 mM Y27632 (ROCK- inhibitor)

5.2.4. Cultivation of human iPSC

The cells were cultivated in FTDA medium at 5 % O_2 and 5 % CO_2 in 6- or 12 well plates coated with hESC-qualified matrigel. For coating the plates, 500 µl Matrigel®/well was incubated for 1 h at 37 °C. Medium was changed daily. The cells were passaged at 80- 90% confluency. For this purpose, old medium was removed, cells were washed 1x with DMEM/F12 and then detached carefully by dispase (1mg/ml) digestion (1min) at 37 °C. After removing the dispase solution, two additional washings were performed with PBS -/- Afterwards, colonies were detached carefully in 1 ml FTDA with a cell scraper and collected in a 15 ml reaction tube. An adequate volume of medium was added, so cell colonies could be distributed to desired number of wells (usually in a 1:6 ratio). HiPSCs were cultured up to 40 passages. Cells with unwanted morphology and differentiated cells were scratched off mechanically.

5.2.5. Freezing and thawing of hiPSCs

The freezing of hiPSCs was performed similarly to the splitting protocol except that cells were collected in FTDA medium, centrifuged at 300g, 2 min and then the medium was discarded. Cells were then resuspended in 0.8 ml/well CryoStem™ and transferred to cryovials. The vials were cooled down to -80°C in a cryo- container filled with isopropanol overnight. The next days, the tubes were stored in liquid nitrogen at -196 °C.

Thawing of the iPSCs was prepared by coating a 6-well with hESC- matrigel for 1 hour at 37 °C. The cryovials were taken from the liquid nitrogen tank and were rapidly thawed in a 37 °C water bath. When the liquid was completely thawed, it was pipetted into a 15 ml reaction tube and 1 ml of DMEM/F12 was added. Cells

were then centrifuged for 2 min at 300g. The supernatant was carefully replaced by an appropriate volume of FTDA medium and seeded onto the coated 6-well.

FTDA

- DMEM/F12+ GlutaMAX™
- 1:1000 ITS
- 1:100 Human serum albumin (HSA)
- 1:100 Chemically defined lipids (CDL)
- 10 ng/ml FGF2
- 0.5 ng/ml TGFβ1
- 50 nM Dorsomorphin
- 5 ng/ml Activin A
- 1x Antibiotic-Antimycotic (100x)

5.2.6. Germ layer differentiation

For germ layer experiments, 2.88×10^6 hiPS cells were detached on day 0 using TrypLE™ and dissociated to single cells. Then, they were mixed with PeproGrow™ medium, 10 µM Y-27632 and 10 µM blebbistatin and distributed on 96 untreated v-bottom 96-wells. For EB formation and reaggregation, the plate was centrifuged at 400g for 4 min. On day 1, 80 % of the medium was removed and replaced by hESC differentiation medium. On day 4, EBs were reseeded onto growth-factor-reduced matrigel coated (1 hour, 37 °C) 6- or 12- well plates or glass cover slips. On day21, cells were either fixed with 4 % PFA for 20 min for immunofluorescence staining or harvested for RNA purification (see respective sections).

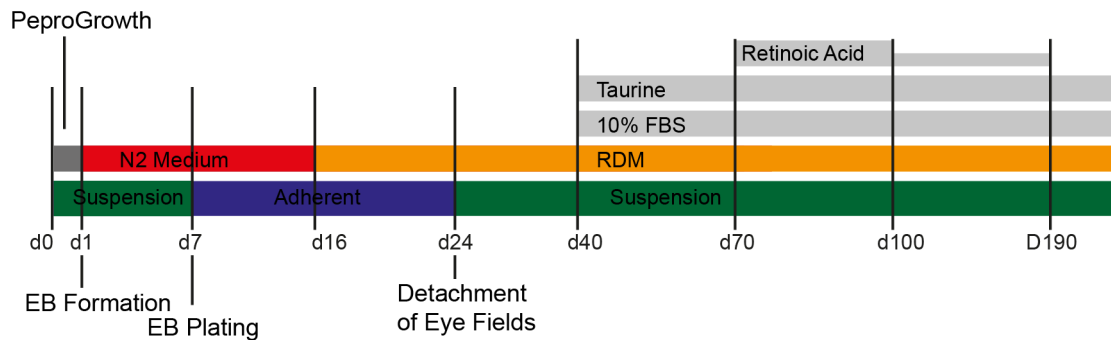### 5.2.7. Differentiation of retinal organoids

Figure 6- Retinal organoid protocol based on Zhong *et al* 2014 (184).

Scheme of the differentiation protocol from hiPSC (d0) to retinal organoids (d24-X). Important manual steps are labelled. Lowest bar shows culture method: green= suspension culture, blue= adherent culture Upper bars represent medium and supplement use in the respective time frames.

Human iPSC- derived retinal organoids were differentiated based on a protocol by Zhong *et al*. 2014 (184) with some modifications (overview see Figure 6). Briefly, for EB formation, 2.88×10^6 hiPSCs were detached on day 0 using TrypLE™ and dissociated to single cells. They were then mixed with PeproGrow™ medium, 10 µM Y-27632 and 10 µM blebbistatin and distributed on 96 untreated v-bottom 96-wells. For reaggregation, the plate was centrifuged at 400 g for 4 min. On day 1, 80% of the medium was removed and replaced by N2 medium. Medium was changed again at day 4. On day 7, EBs were plated on growth-factor-reduced matrigel- coated 6 wells (coating 1 h at 37 °C) at a density of 32 EBs/well and thereafter medium was changed daily. On day 16, medium was switched to RDM medium. On day 24, retinal fields were detached using 10 µl tips and collected in 10 cm bacterial dishes, adding 10 µM Y-27632 for one day. Afterwards, medium was changed twice a week. After completed formation, retinal organoids (RO) were selected and if necessary detached from non-retinal spheres using Ultra-Fine-Clipper-Scissors-II. Starting from day 40, RO were supplemented with 10 % FBS and 100 µM taurine. During day 70- 100 1 µM retinoic acid was added, reduced to 0.5 µM during day 100- 190 and removed afterwards.

N2 Medium

- DMEM/F12 (1:1)+ GlutaMAX™
- 24 nM Sodium selenite
- 16 nM Progesterone
- 80 µg/ml Human apotransferrin
- 20 µg/ml Human recombinant insulin
- 88 µM Putrescin
- 1x Nonessential amino acids (100x)
- 1x Antibiotic-Antimycotic (100x)

RDM Medium

- DMEM/F12 (1:1)+ GlutaMAX™: DMEM, high glucose (1:1)
- 1x B-27™ (w/o vitamin A)
- 1x Nonessential amino acids (100x)
- 1x Antibiotic-antimycotic (100x)

5.2.8. Differentiation of retinal pigmented epithelia cells

Retinal pigmented epithelia cells (RPE) were derived as a side product from RO differentiation according to Zhong *et al*. 2014 (184). For this purpose, pigmented areas or spheres were removed from RO using microscissors under an inverted cell culture microscope. RPE clusters were collected in 1.5 ml reaction tubes and washed with PBS -/-. For disassociation, RPE cells were treated with Accumax™ for 90 minutes at 37 °C. Thereafter, the reaction was stopped by adding RDM+ 10% FBS, followed by centrifugation at 1500 rpm for 2 minutes. Plates for RPE culture were pre-coated with 0.01 % Poly poly-L-ornithine for 30 minutes, followed by 20 µg /ml laminin for 4 hours at 37 °C. Cells were cultured in RDM + 10 % FBS + 20 µg/ml EGF, 20 µg/ml FGF2, 2 µg/ml heparin and 10 µM ROCK-inhibitor. After 24 hours, FBS was removed and after the cell reached confluency, medium was replaced to pure RDM.

5.2.9. Lentivirus production

Lentiviral production was performed using Lenti-X™ cells (Takara). In that course, Lenti-X™ were seeded on 10cm culture-treated dishes in DMEM+ 10% FBS. When cells reached around 80 % of confluency, a mixture of transfection mix was prepared as followed:

Per 10cm dish:

- 400µl Opti-MEM™
- 12 µg Target vector
- 5.5 µg pSPAX2 (gift from Didier Trono (Addgene plasmid # 12260))
- 2 µg pMD2.G (gift from Didier Trono (Addgene plasmid # 12259))
- 70 µg Polyethylenimine

After the mix had been incubated 10 min at room temperature, 1 ml of pure DMEM was added to the cocktail. Medium from the Lenti-X™ cells was replaced by 6.5 ml pure DMEM (without FBS) and the cocktail was added dropwise to the cells. After 4 hours of incubation at 37 °C, medium was again removed, cells were carefully washed once with PBS -/- and 8 ml fresh DMEM + 10 % FBS medium was added. Two and four days after transfection, supernatant from individual plates was collected in a single 50 ml reaction tube and stored at 4 °C. The first time, medium was replaced with fresh medium. After both collection steps, medium was centrifuged at 400 g, 2 min and filtered using a 0.45 µm sterile filter. Afterwards, Lenti-X™ concentrator was added in a ratio of 1:3 and incubated at 4 °C overnight. The next day, the mixture was centrifuged (45 min, 4 °C, 1500 g), the supernatant was discarded and the remaining virus particles were resuspended in DMEM/F12 or Epilife (1 ml per 10 cm plate). Portions of 100 µl were aliquoted and stored at -80 °C until further use.

5.2.10. Lentiviral transduction of RPE cells

iPSC-RPE lines were incubated with lentiviral particles generated from pJG-IRPB-eGFP plasmids in RDM + 10 % FBS for one day, washed three times with PBS -/- and further cultivated in RDM + 10% FBS.

5.2.11. Labelling of hiPSC-retinal organoids for live cell experiments

For labelling RO photoreceptor segments, ROs were incubated for 30 min in culture medium containing 20 μg/ml PNA lectin-Alexa Fluor™ 568 and washed 4 times with medium afterwards.

5.2.12. Fluorescence activated cell sorting (FACS)

For FACS experiments, up to 3 RO/sample were selected at the chosen time point and washed once with PBS -/- in a 1.5 ml reaction tube. Afterwards, 500 μl undiluted Accumax™ + 2 mM EDTA was added to the cells and they were incubated for around 60 min at 37 °C. Every 10- 15 min, the ROs were pipetted up and down several times in order to break down the RO. After no RO pieces were visible anymore, cells were centrifuged down at 500 g, 2 min and supernatant was discarded. Thereafter, cells were washed once in 50- 100 μl ice-cold FACS Buffer, centrifuged at 500 g, 2 min and supernatant was again removed. Finally, cells were kept in 50 μl FACS Buffer and within 4 hours, FACS experiments were performed at the Sony SH800 Cell Sorter at the DZNE Institute, Tübingen (with Dr. Stefan Hauser). GFP threshold was set according to a negative control using untransfected ROs. For cell population sorting (all IRBP-GFP+ above threshold), cells were sorted inside 1.5 ml reaction tubes directly in 350 μl RLT Buffer from Qiagen RNeasy® Kit (+ 1:100 β-mercaptoethanol). Afterwards, samples were directly frozen on dry ice and RNA extraction was performed later as described (see RNA extraction).

FACS Buffer:

- PBS -/-
- 10 % FBS
- 2mM EDTA

5.2.13. BrdU proliferation assay

For BrdU proliferation assay, BrdU was added to fresh RDM medium (+ 10 % FBS+ 100µM taurine). At d79 of differentiation, ROs were selected and cultured in non- adherent 6- well plates in presence of BrdU. After 24 hours, cells were collected, washed once with PBS -/- and fixed for cryosectioning as described (see Fixation and cryosectioning of organoids). For BrdU detection, a BrdU detecting antibody was used (see Table 10).

5.2.14. Fixation and cryosectioning of organoids

Fixation of suspension-cultured ROs was done after one time washing with PBS -/- in a 1.5 ml reaction tube for 20 min in a 4 % PFA/ 20 % sucrose solution. Afterwards, cells were washed twice with PBS -/- and incubated in 30 % sucrose overnight at 4 °C. Within the next 3 days, organoids were placed and embedded in Tissue Tek® O.C.T.™ in 1 cm^2 cryomolds. Freezing was executed with a precooled -80 °C metal block and storage in a -80 °C freezer. Cryosectioning was performed at the cryostat, Microm HM 560 at -20 °C sample temperature and -20 °C blade temperature. Slice thickness was set at 14 µm in all experiments. Samples were aligned in a way that CTRL and RP patient samples could be stained simultaneously on the same slide.

5.2.15. Immunocytochemistry

For immunocytochemistry, cells were either plated and cultured on coated glass plates or cryosectioned as described in the previous section. Adherent cells were washed with PBS -/- and fixed with 4% PFA/20% sucrose for 20 min at room temperature. Two additional washing steps with PBS -/- were carried out. Samples were blocked with 10 % normal donkey serum + 0.2 % Triton®-X in PBS -/- for 1 hour at room temperature. Primary antibodies were applied in blocking buffer solution overnight at 4 °C. Afterwards, 3x 3min PBS -/- washing steps were performed and secondary antibodies were applied in 1:1 diluted blocking buffer (in PBS -/-) for 1 hour at room temperature. Both primary and secondary

antibodies were applied in concentrations listed in Table 1 and Table 2. Removal of the secondary antibodies was followed by 3x3 min PBS -/- washings with subsequent mounting in Prolong™ antifade reagents containing DAPI. Microscopy was performed using an Axiokope 2 mot plus microscope.

5.2.16.   Transmission electron microscopy

Electron microscopy was performed by Kevin Achberger and Sylvia Bolz (Institute for Ophthalmic Research, Tübingen). Briefly, at day 125 or d190, organoids dedicated for electron microscopic evaluation were fixed in Karnovsky buffer (2.5 % glutaraldehyde, 2 % paraformaldehyde, 0.1 M sodium cacodylate buffer, pH 7.4) overnight at 4 °C. After fixation, the samples were rinsed three times in 0.1 M sodium cacodylate buffer (pH 7.4) for a total of 30 min, and postfixed in 1 % OsO_4 for 1.5 hours at room temperature. After three additional washings in cacodylate buffer and dehydration with 50 % ethanol, tissues were counterstained with 6 % uranyl acetate dissolved in 70 % ethanol followed by graded ethanol concentrations (80 % and 96 % ethanol 30 min each, 100 % for 3 times 10 min). The dehydrated samples were incubated in a 2:1 and 1:1 mixture of propylene oxide and Araldite® resin for 1 hour each, on a shaker. Finally, organoids were infiltrated with pure Araldite® and polymerised by overnight incubation at 60 °C. Araldite®- containing organoids were embedded in a fresh resin in block molds and cured 12 hours at 60 °C followed by 2 hours at 90 °C. Ultrathin sections (50 nm) were cut on a Reichert Ultracut S, collected on copper grids and counterstained with Reynolds lead citrate. Sections were analysed with a Zeiss EM 900 transmission electron microscope equipped with a 2k x 2k CCD camera.

5.2.17.   Calcium imaging

Calcium imaging was performed by K. Achberger and Dr. Wadood Haq. Briefly, ROs were loaded with the calcium indicator Fura-2-AM (0.27 μM) and incubated for 35 min at 37 °C. After washing (DMEM/F12+ GlutaMAX™), ROs were inserted into a microscope recording chamber. Recording was performed using an upright fluorescence microscope. During the calcium-imaging recording, stacks (single-

plane two-channel) of the Fura-2-AM fluorescence at the focal plane of the photoreceptors were acquired at 10 Hz (λ_{exc}= 340 and 380 nm; 30 ms exposure time, 8-pixel binning) using the VisiView software. The light stimulation was applied by an LED (Thomsen LED-5-14000W/75°) guided through a light path to the RO. The parameters of the stimulation were white light, full field, luminous intensity of 5.3 candela (measured by USB400-UV-VIS-ES, OceanOptics, Germany) and duration of 5 seconds (5 stimuli, 120 s per stimulus control recording, 60 s stimulation interval). The light stimulation protocol was executed and the trigger-events were recorded by I/O-box of the Multi-Channel Systems. The calcium-imaging ratio-stacks were generated by dividing the fluorescence images recorded at the excitation wavelengths of F340 and F380 (ImageJ, RatioPlus, https://imagej.nih.gov/).

Activity detection

The calcium-imaging recording plane (170 X 128 pixel) was divided into 10 X 10 pixel-bins, obtaining 192 "cells", each of ~ 10 X 10 µm size. For each cell, the calcium traces (X_1, …, X_m, through the ratio-stack) were calculated and the stimulus triggered response-intensity (Resp $(stim)_i$) was detected: the difference of the calcium-intensity ($X_n - X_{n-3}$) during the light stimulation and one second after the light stimulation. A cell was considered as light dependent responsive, if one of the Resp $(stim)_i$ exceeded the threshold (Thr = mean ($X_c - X_{c-1}$)) obtained from the control recording. As a reliability-control, also the control-recording (pre-stimuli) was evaluated, and the Resp$(ctr)_i$ for 5 distinctive time points (equally distributed) during the control-recording were calculated. Also here, a cell was considered as active, if one of the Resp$(ctr)_i$ exceeded the Thr.

Data representation

The heat-map represents the cell activity as count of Resp$(all)_i \geq$ Thr(all), there by Resp$(all)_i = (X_n - X_{n-3})$ and Thr(all) = mean ($X_n - X_{n-1}$) are calculated for the calcium-trace of each cell. For statistical measures, the relative number of cell responses per recording (percentage, 192 cells per recording plane) are

evaluated and presented as average of 5 light stimuli and 5 control time-points (see activity detection).

5.2.18. Genotyping of *CRB1* mutation

DNA extraction for *CRB1* C948Y genotyping was conducted with the QIAamp® DNA Mini kit. In course of the extraction, a quarter of a full iPSC 6-well was harvested and pelleted by centrifugation. After the extraction, DNA concentration was assessed with a NanoPhotometer. 5 ng of DNA was used as template for amplification via polymerase chain reaction (PCR).

PCR reaction was performed with PrimeStar® GXL DNA Polymerase Kit. Reaction mix was as followed:

- 10 µl 5x PrimeStar® Buffer
- 4 µl dNTP (2,5 mM stock)
- 1,5 µl Forward primer (from 1:10 working solution from 100 pmol/µl stock)
- 1,5 µl Reverse primer (from 1:10 working solution from 100 pmol/µl stock)
- 1µl PrimerStar® GXL DNA Polymerase
- 5-10 ng Template (gDNA)
- Filled up to 50 µl with H_2O

Forward and reverse primers for detecting *CRB1* mutation:

- Forward: TCAGAAGCCAGACTCCACTGTTAAT
- Reverse: GTACTTAGACACCCTTGCAGGC

PCR program was set as followed:

- 98 °C   2 min
- 30 cycles:
    - 98 °C   10 s
    - 60 °C   15 s

- o 68 °C   1 min
- 68 °C   5 min
- 8 °C   hold

Afterwards, PCR products were separated using gel electrophoresis. Gel was prepared with 1% agarose solved in TBE buffer.

TBE buffer (1x)

- 89 mM TRIS base
- 89 mM boric acid
- 2 mM EDTA (pH 8.0)
- In H_2O

Gel was visualised using Quantum ST UV Chamber and PCR band was excised using a scalpel. DNA from PCR fragments was extracted using Agarose Gel Extraction Kit. Finally, sequencing was performed by GATC Biotech (Konstanz, Germany). Sequencing primer was CCAGACTCCACTGTTAAT. Results were visualised using GATC Viewer.

5.2.19.   RNA purification

RNA purification was carried out with the RNeasy® Mini Kit or Micro Kit. Purification was performed according to the enclosed instructions. The RNeasy® Mini Kit allows extraction of up to 35 µg total RNA from mammalian cells. All samples used for RNA purification were washed 2x in PBS -/- and resuspended and lysed in 350 µl RLT Buffer. This was followed by homogenisation carried out with shredder columns (QiaShredder). Subsequently, RNA was bound to a column by ethanol addition. Several washing steps in order to get rid of contaminating substances (such as proteins) followed. RNA was finally eluted with RNAse- free water in 1.5 ml reaction tubes.

5.2.20. Quantitative real- time PCR (qRT-PCR)

PCR was performed as previously described (190) on a StepOne instrument using QuantiFast SYBR Green RT-PCR Kit according to the manufacturer's protocol. Relative gene expression was calculated as a ratio of target gene expression level to the level of the housekeeping gene *GAPDH* or *HMBS* as indicated in the respective figures.

5.2.21. Fluidigm array

For high-throughput gene expression analysis, the BioMark™ HD was used. Experiments were performed as previously described (190). Data analysis was performed using Office Excel 2016.

5.2.22. Retina-on-a-chip production and culture

The retina-on-a-chip production was performed by the Fraunhofer IGB, Stuttgart. The retina-on-a-chip consists of two polydimethylsiloxane (PDMS) layers and a porous PET membrane in between, bonded to a thin glass slide (170 µm). First, PDMS master molds were fabricated. For the media channel mold, SU8-50 photoresist was spin-coated onto a previously cleaned 4" silicon wafer to obtain a height of 100 µm. To create the desired structure, the substrate was exposed to 350 mJ/cm^2 of UV light, followed by development in SU-8 developer for 6 minutes. Finally, the wafer was rinsed with isopropanol and blow-dried using nitrogen. The second wafer for RO and RPE culture was fabricated in two steps. Initially, a base layer of 25 µm for the membrane insert was fabricated by spin coating a first layer of photoresist SU8-. The exposure to UV light in this case was 200 mJ/cm2. Subsequently, the wafer was developed in SU-8 developer for 4 minutes, rinsed in isopropanol and blow-dried with nitrogen. Next, the wafer was coated with a second layer of SU8-3025 to fabricate the tissue channels with a height of 40 µm. The wafer was exposed to UV light at 250 mJ/cm2 for 10 seconds and developed for 4 minutes. Afterwards, both master molds were silanised with chlorotrimethylsilane. Subsequently, Sylgard 184 PDMS was

mixed at a 10:1 ratio of prepolymer to curing agent and molded by using the wafers as negative master mold. The layer for the media supply was made by exclusion molding followed by curing overnight at 60 °C. The RO/RPE culture layer was fabricated by pouring 25 g of the PDMS mixture onto the master mold and curing it overnight at 60 °C. Next, the PDMS slabs were peeled off the wafers and the media-supply layers were bonded to a glass slide previously cleaned by a 30-second exposure to oxygen plasma at 50 Watts. Inlets and outlets were punched using a biopsy puncher with a diameter of 0.75 mm. To culture the cells and organoids, four chambers were punched out of the PDMS with a biopsy puncher of 2 mm diameter. Semipermeable membranes with a diameter of 20 mm, made from PET with a pore diameter of 3 μm and a thickness of 10- 20 μm, were functionalised using bis-[3-trimethoxysilypropyl]amine. Before assembly, both PDMS layers were cleaned with isopropanol and Scotch tape to remove dust particles. Afterwards, both layers were treated with an oxygen plasma at 50 W for 30 s. Then, the membrane was placed into the inlay of the RO/RPE culture layer. Finally, both layers were aligned to each other using a stereo microscope and baked overnight at 60°C to stabilise bonding.

5.2.23.   Chip assembly and culture

For chip culture experiments, PDMS retina-on-a-chips were prepared in two steps: on the first day, RPE was loaded inside the chip. For that, PET membranes inside the chip were coated for four hours with laminin (50 μg/ml), and washed with PBS -/- thereafter. Then, RPE was dissociated from adherent well culture as described above. Single-cell RPE cells were then counted and an amount of 27 000 cells per well was loaded in RDM + 10 % FBS from above inside the chamber. After the cell adhered on the second day, organoids were placed on top of the RPE cells. For that cause, medium inside the wells was removed, and 8 μl of HyStem®-C hydrogel was poured in the wells. HyStem®-C preparation was performed according to the manufacturer's recommendation. Afterwards, organoids were pipetted inside the well and manoeuvred in the middle of the well. For hydrogel solidification, the chip was incubated for 30 min at 37 °C and then

RDM + 10 % FBS medium was placed on top of the chip. For pump medium supply, the chips were connected by plastic tubes medium-containing syringe. Automatic medium supply was performed by a Legato™210 pump at a speed of 20 µl/hours for 3 days.

5.2.24. Fluorescence data analysis via ImageJ/R programme Slope Approach

Fluorescence images from cryosections were quantified and analysed with a set of self-developed and programmed ImageJ macros and R analysis software. The source code of each tool was made available online. In the following, the input, function and output of each tool shall be described briefly.

5.2.24.1. Slope Approach (ImageJ)

Input:

ZVI files (Zeiss), multichannel fluorescence images or cryosections (as described in the respective sections). All images of an analysis group, I stained i) on the very same slide with the same antibody dilutions, ii) recorded with the same exposure durations, iii) drew a visible zero-line (the "OLM" line)

Function:

The programme will open a folder of *.ZVI one by one and ask the user for input. First, the user has to tilt the image (OLM straight from left to right; organoid on the bottom). Second, the user needs to draw the zero-line ("OLM"–line). Third, the user defines the slope for start and stop condition (slope = the orientation of the layers in respect to the zero line, see Figure 7a). Then, the programme will produce profile plots for all positions of the chosen ranged with a slope ranging between the start and stop slope.

Output:

Output-data are pixel intensity values for each line and each position, corrected from a round basis shape to a rectangular image.
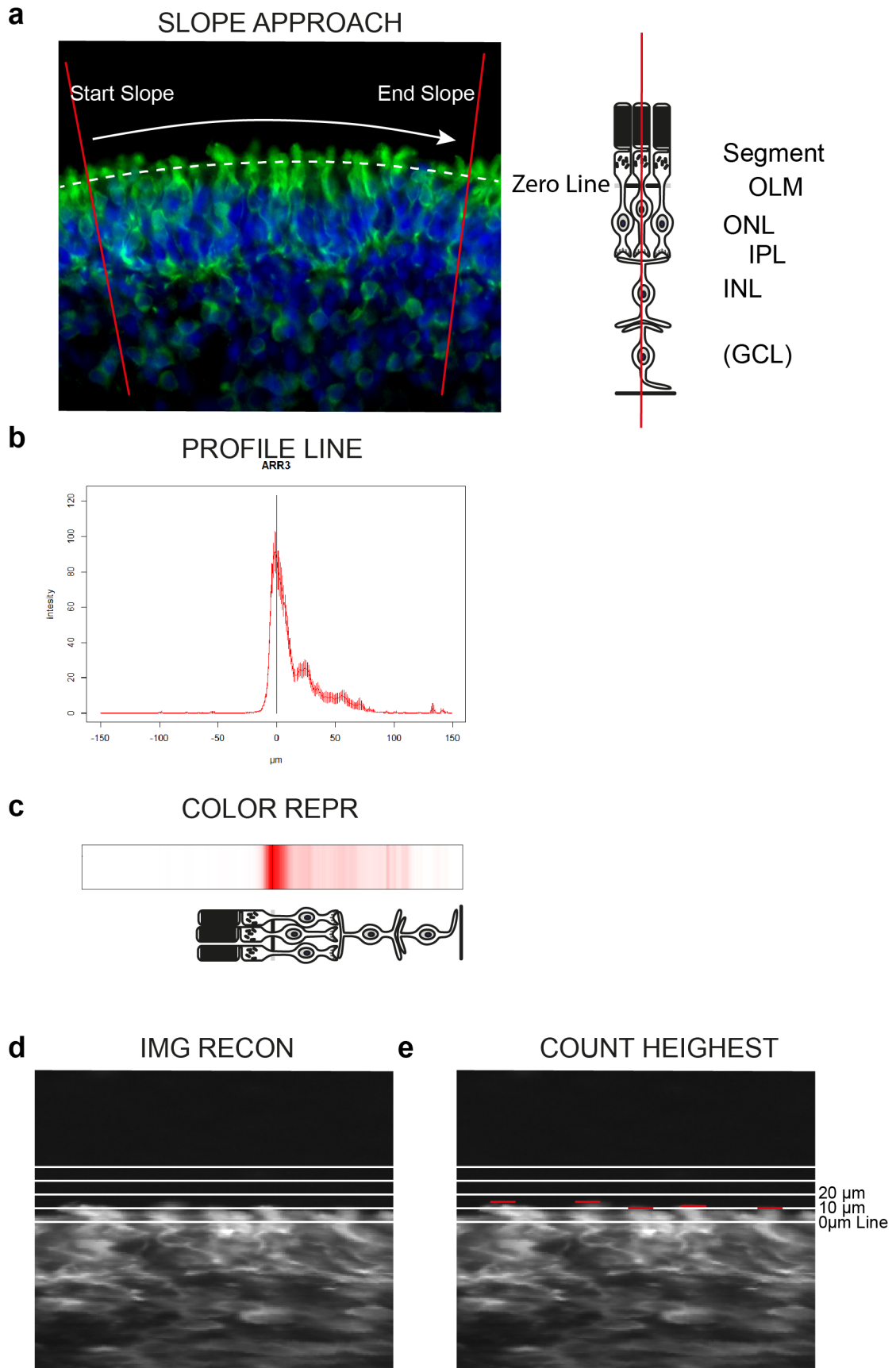
a

SLOPE APPROACH

Start Slope

End Slope

Zero Line

Segment
OLM

ONL
IPL

INL

(GCL)

b

PROFILE LINE

ARR3

intesity

µm

c

COLOR REPR

d

IMG RECON

e

COUNT HEIGHEST

20 µm
10 µm
0µm Line

Figure 7- Overview of ImageJ/R tools

Examples for slope tool set applications (a) slope approach. Left image: representative image of d365 RO stained for ARR3 (green). White dotted line shows zero line defined by the user set on the OLM. Red lines show start and end slope defined by the user. Arrow indicates the direction of the profile line running from left to right. Right image: Scheme of the retinal organoid cell types vertically cut by the profile line (red). (b) Profile Line. Representative merged profile of control images (d365, ARR3). X-axis: 0 is zero line. Negative range: outside the organoid. Positive range: inside the organoid. Threshold was subtracted from values. Values below threshold were set as 0. 1 unit equals 1.25 µm. (c) Corresponding colour ramp (white = 0, red = Max) of the profile line shown in (b). Retinal organoid cell types scheme is shown for comparison. (d) Reconstruction of image in (a) recorded with slope approach tool. White lines were added for better visualisation (lowest line = 0, distance between lines= 10 µm). (e) Representative reconstructed images showing the principle of the counting highest tool. Red bars are exemplary highest points of PRC segments as selected by the user. DAPI = blue.

5.2.24.2. Horizontal profiling (R)

Input:

Pixel-values from Slope Approach macro in *.txt format

Function:

Programme will merge all profiles of one image to one stereotypic profile plot per image and channel. It can remove the background using either background intensity values set by the user or using an algorithm, which will find the "object slide background". Note that the organoid background usually differs from the object slide background.

Optionally, it can merge images of one condition (*e.g.* control) to one profile. Further, the programme can calculate the summed pixel value for a range on the profile plot line (*e.g.* between the zero line and 10 µm outside the organoid).

Output:

Profile plots of single images or merged for one condition (Example, see Figure 7b)

Tables containing the summed values for each set range and each image.

5.2.24.3. ImageRecon (ImageJ)

Input:

Pixel-values from Slope Approach macro in *.txt format

Function:

The programme will produce an image based on the pixel intensity values. This results in a straightened image. Optionally, lines can be displayed in certain positions (*e.g.* the zero-line, or the 10 µm line).

Output:

TIFF files, containing the straightened images (see Figure 7d).

5.2.24.4. CountingHighest (ImageJ)

Input:

TIFF files from Image Recon

Function:

The programme will show each image individually to the user and ask him to count the number of features (see Figure 7e). The programme will save numbers and the y-coordinates of the selections, which enables *e.g.* position information of segments (*e.g.* for calculation of the distance between zero line and the feature)

Output:

Table containing number of features per image, length of the image (zero-line) and the y-coordinate of each selected point

5.2.24.5. MeasuringHighest (R)

Input:

Table from CountingHighest

Function:

This tool calculates the mean number of features per length for each individual condition and if coordinates were given, it calculates the mean length between the zero-line and the y-coordinate of the selection.

Output:

Table containing number of selection/length (and the mean) and the mean distances between zero line and the selections per image or merged per condition.

5.2.24.6. ColourRepresentation (R):

Input:

ProfilePlots from Slope Approach

Function:

The tool will make a colour representation of each merged profile plot. This can be used to visualise the signal location of fluorescence signal tested (example see Figure 7c).

Output:

Tiff images containing colour representation of the signal distribution.

5.2.25. Statistical tests

Statistical analyses were performed using student's t-test using Microsoft Excel 2016. Results are provided as mean values ± standard error of the mean (S.E.M.). Statistical significance was represented as follows:

$p < 0.05$ = * ; $p < 0.01$ = ** ; $p < 0.001$ = ***.

6. Results

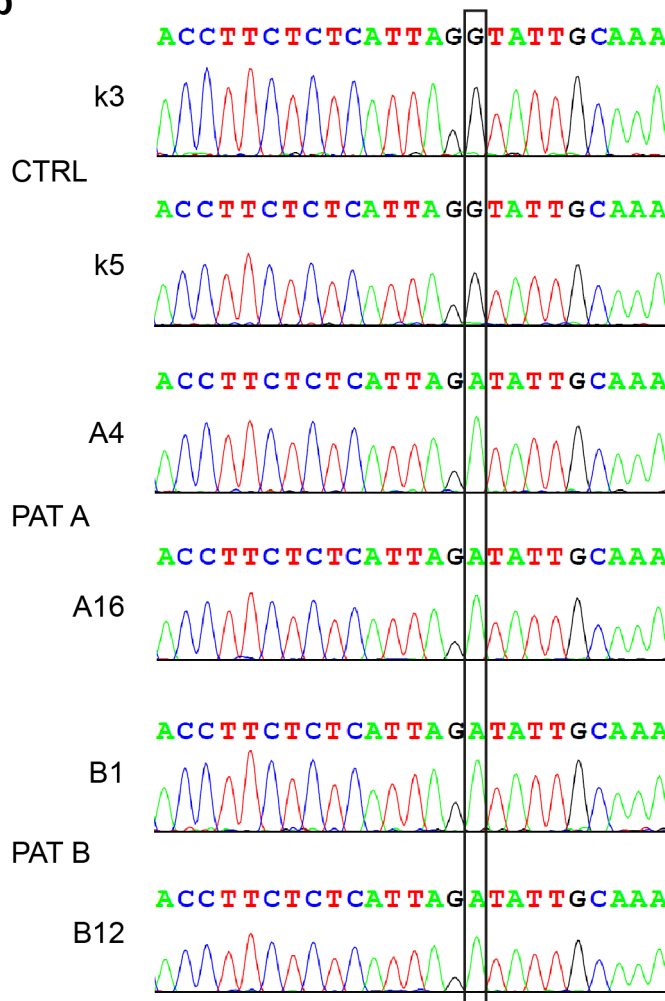### 6.1. Patients suffering from retinitis pigmentosa caused by a homozygous C948Y *CRB1* mutation

For this study, two patients suffering from a diagnosed form of retinitis pigmentosa were selected. Both were diagnosed with early-onset retinitis pigmentosa. The selected patients are brothers, 19 and 22 years old at the time of hair sample collection (Figure 8a). Hereafter, the older brother will be called RPAx (short Ax), the younger brother RPBx (short Bx). X standing for the yielded clonal iPS cell line.

From hair samples of the patients, keratinocytes were obtained and the presence of the one base pair missense mutation was assessed in the resulting iPS cell lines (RPA4, RPÀ16, RPB1, RPB12) via PCR followed by sequencing (Figure 8b). In contrast to a control person, both patients had an exchange of guanine to adenine leading to an amino acid exchange of cysteine to tyrosine (Figure 8b). The exchange affects the 3-dimensional structure of an EGF-binding region, which is usually established by a disulphide bridge of two cysteines (Figure 8c).

a

| Patient	Age at the time of iPSC generation	Status	Diagnostics	Mutation	Family
RPA	22	Blind	Early-Onset RP	Homozygous CRB1 C948Y	Brother of RPB Father: Heterozygous for CRB1 C948Y Mother: Unknown genetics
RPB	19	Progressed RP with central aspects	Early-Onset RP	Homozygous CRB1 C948Y	Brother of RPA Father: Heterozygous for CRB1 C948Y Mother: Unknown genetics

b

c

C948Y (Cysteine to Tyrosine)
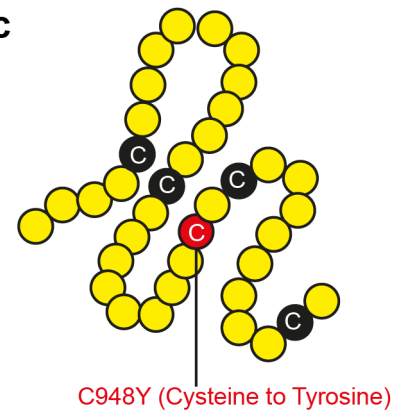
Figure 8- Patients suffering from retinitis pigmentosa caused by a homozygous C948Y *CRB1* mutation

(a) Status and phenotypic comparison of the two retinitis pigmentosa patients (b) Comparison of the *CRB1* sequence in range of the C948Y mutation for control (k3, k8) and patient lines (A4, A16, B1, B12). Displayed is position 94745- 94769 of *CRB1* gene (according to NCBI NG_008483.2). Black square highlights the mutation side of the retinitis pigmentosa patients (guanine changed to adenine) at position 2843 of the mRNA (transcript variant 1). (c) Schematic

representation of the *CRB1* C948Y mutation side in the EGF-like region on the protein level. Yellow circles represent amino acids. Black circles labelled with C are cysteines.

6.2. Generation and characterisation of iPSC lines from patients RPA and RPB

As already described, hair were taken from two brothers suffering from retinitis pigmentosa. When plated on matrigel, these hairs gave rise to keratinocytes, which were successfully reprogrammed to iPS cell lines. Figure 9a shows this process exemplarily. In course of the reprogramming, keratinocytes were transduced with a lentiviral expression vector containing the four so- called Yamanaka factors (OCT4, KLF4, SOX2 and C-MYC) and a dTomato fluorophore (see Figure 9a and section 5.1.13). Plated on REF feeder cells and cultured in hiPS-medium, keratinocytes could be reprogrammed to iPS cell colonies within four weeks (Figure 9a). For each patient, several clonal lines arising from single reprogrammed cells were produced. For this study, the clonal lines RPA4, RPA16, RPB1 and RPB12 were used.

Subsequently, these lines were tested for pluripotency markers. First, lines were checked for the immunofluorescence staining of the pluripotency markers OCT4, SOX2, NANOG and SSEA4 (Figure 9b). Second, mRNA expression of *OCT4* and *NANOG* was assessed in comparison to the housekeeping gene *HMBS* (Figure 9c).
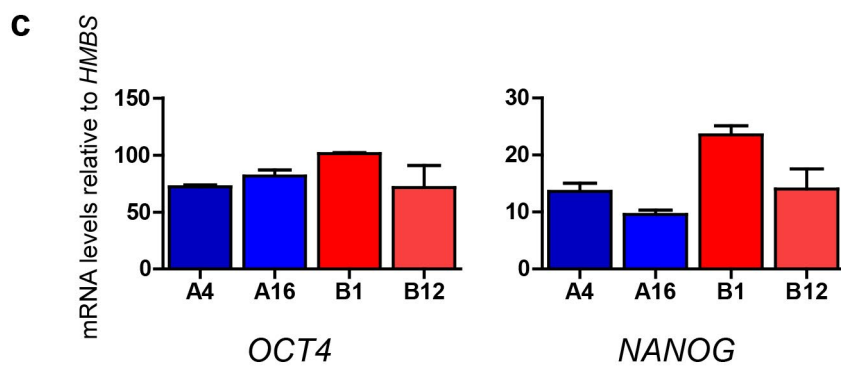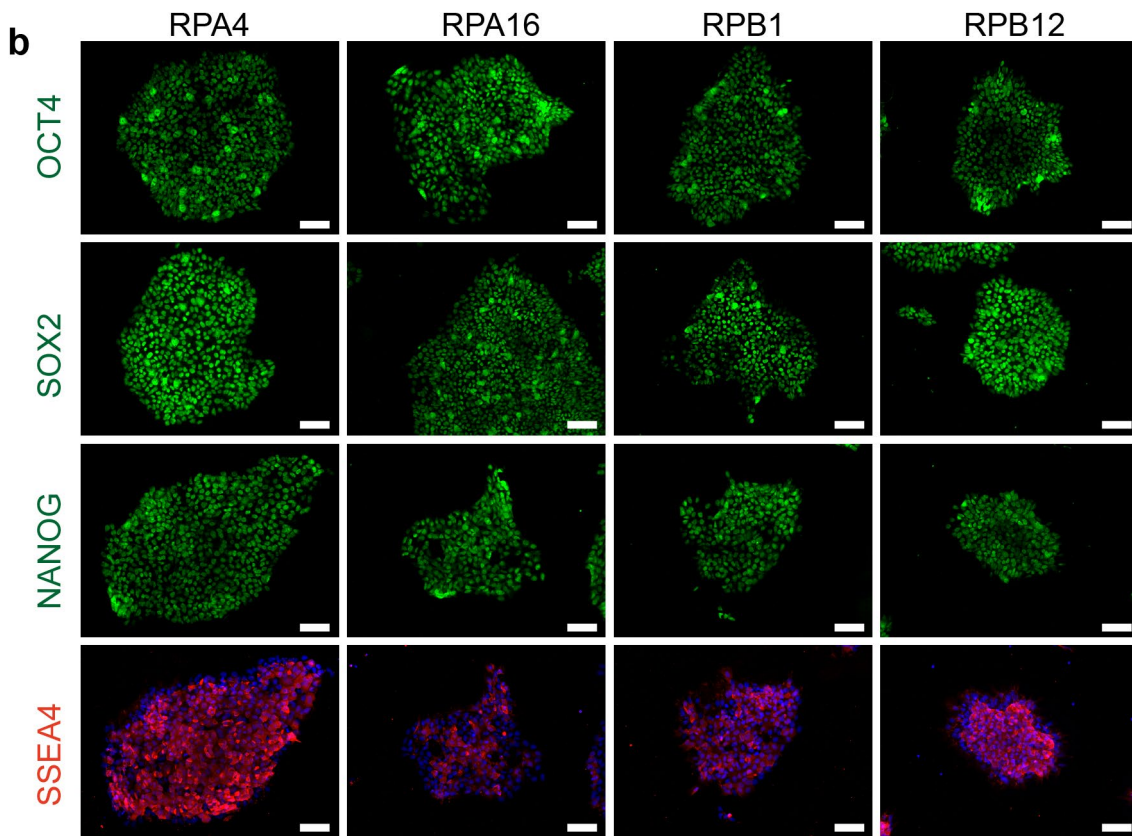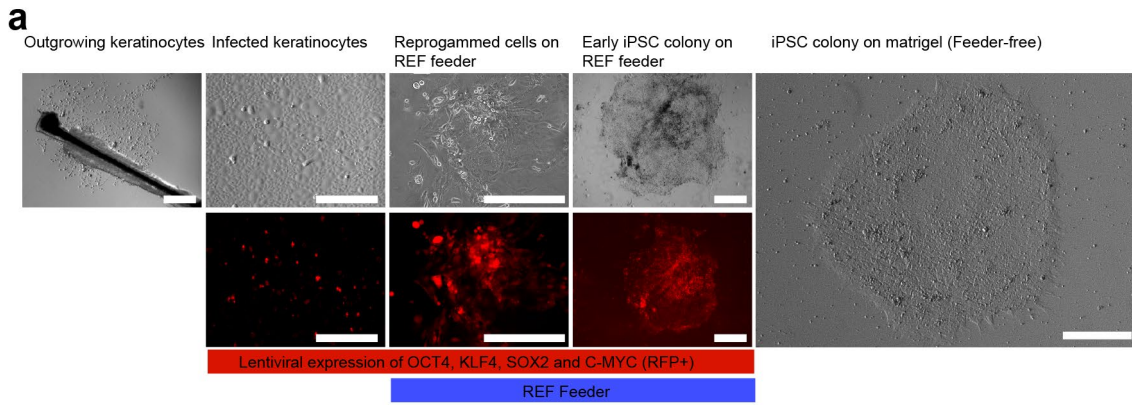
a

Outgrowing keratinocytes | Infected keratinocytes | Reprogammed cells on REF feeder | Early iPSC colony on REF feeder | iPSC colony on matrigel (Feeder-free)

Lentiviral expression of OCT4, KLF4, SOX2 and C-MYC (RFP+)

REF Feeder

b

RPA4　RPA16　RPB1　RPB12

OCT4

SOX2

NANOG

SSEA4

c

OCT4

NANOG

mRNA levels relative to *HMBS*

A4　A16　B1　B12

Figure 9- Generation and characterisation of iPSC lines from patients RPA and RPB

(a) Scheme of the iPSC reprogramming process: keratinocytes grow out of plated hair (first column) and are transduced with a lentiviral vector containing the four Yamanaka factors OCT4, KLF4, SOX2 and C-MYC and a red fluorophore (dTomato) (second column, top showing brightfield image and bottom row showing RFP signal). Afterwards, cells are replated onto inactivated rat embryonic fibroblasts (REF) until iPSC colonies arise (third and fourth column). Thereafter, single colonies are picked and expanded feeder-free on matrigel- coated wells (last column). (b) Pluripotency markers of generated RP iPS cell lines. The clonal lines RPA4, RPA16, RPB1 and RPB12 were stained for OCT4, SOX2, NANOG (all green) and SSEA4 (red). (c) Gene expression of the pluripotency genes *OCT4* (*POUF51*) and *NANOG* from iPS cell lines RPA4, RPA16, RPB1 and RPB12 (n= 3). DAPI = blue. Error bars: S.E.M. Scale bars: (a) 500 µm (b) 100 µm.

6.3. Germ layer differentiation of retinitis pigmentosa patient iPS cell lines

One of the primary properties of pluripotent stem cells is the ability to generate cells from all three germ layer: endoderm, mesoderm and ectoderm. In order to proof this ability, an undirected germ layer differentiation was performed for the iPS cell lines from retinitis pigmentosa patients (Figure 10). From all tested iPSC lines, cells from all germ layers could be identified by using specific markers: AFP for endoderm, DESMIN for mesoderm, and TUJ for ectoderm (Figure 10a). These results were verified by mRNA expression analysis, where an increase of marker genes (*FOXA2* and *AFP* for endoderm, *MYH6* and *T* for mesoderm, *SOX1* and *TUBB3* for ectoderm) for the three germ layers in comparison to iPS cells was observed (Figure 10b).
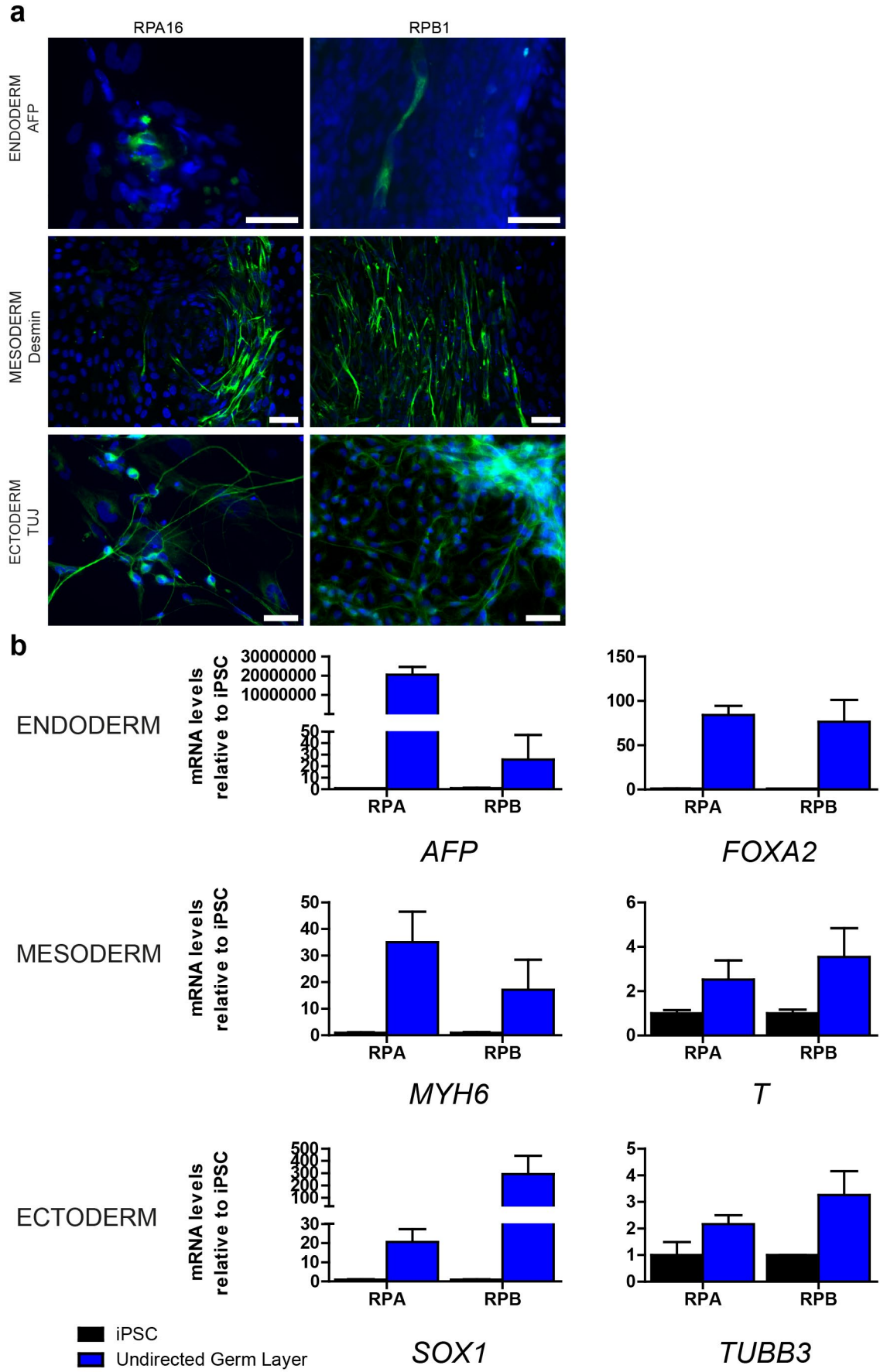
Figure 10- Germ layer differentiation of retinitis pigmentosa patient iPS cell lines

(a) Representative immunofluorescence staining of two iPSC lines (RPA16, RPB1) which were differentiated into an undirected germ layer mixture for 21 days. Cells were stained for the endoderm marker AFP (top row), mesoderm marker DESMIN (middle row) and the ectoderm marker TUJ (bottom row). (b) Gene expression analysis of germ layer markers. mRNA level of germ layer differentiation markers from RPA4 and RPB12 compared to respective iPSC (n= 3). Endoderm markers were *FOXA2* and *AFP*, mesoderm markers *MYH6* and *T* and ectoderm markers *SOX1* and *TUBB3* (n= 3). DAPI = blue. Error bars: S.E.M. Scale bars: (a) 50 µm.

6.4. Retinal organoid differentiation of RP iPSC and unaffected controls

After the iPS cell lines from the two patients were characterised, these lines were used for retinal organoid differentiation. The protocol used is described in the respective methods section 5.2.7. For both, control persons and RP patients, adherent cultured eye field areas were lifted on day 24 and cultured in suspension for up to one year. The retinal organoids derived from both patient lines showed normal appearance of optic vesicle-like stages (Figure 11a) and marker expression for the neural retina progenitor marker VSX2 (CHX10) (Figure 11b). In detail, the organoids outer layer displayed typical stripes caused by the pseudoepithelial organisation of retinal progenitors starting from the day of suspension culture (d24). With time, the layering of the neural retina becomes apparent with a distinct PRC layer (Figure 11a, Figure 15a). In accordance to that, VSX2-positive progenitors, which are initially found throughout the neural retina, are later limited to the inner layers sparing the exclusive PRC layer (Figure 11b). Finally, the mRNA profiles of retinal differentiation markers were compared. In RP patients, no change in expression level for *VSX2* and *RX* was observed (Figure 11c).

In summary, iPS cells from RP patients and controls are able to differentiate to retinal organoids displaying markers for neural retina with no apparent changes in organoid structure, mRNA or protein levels for both RP patient lines.
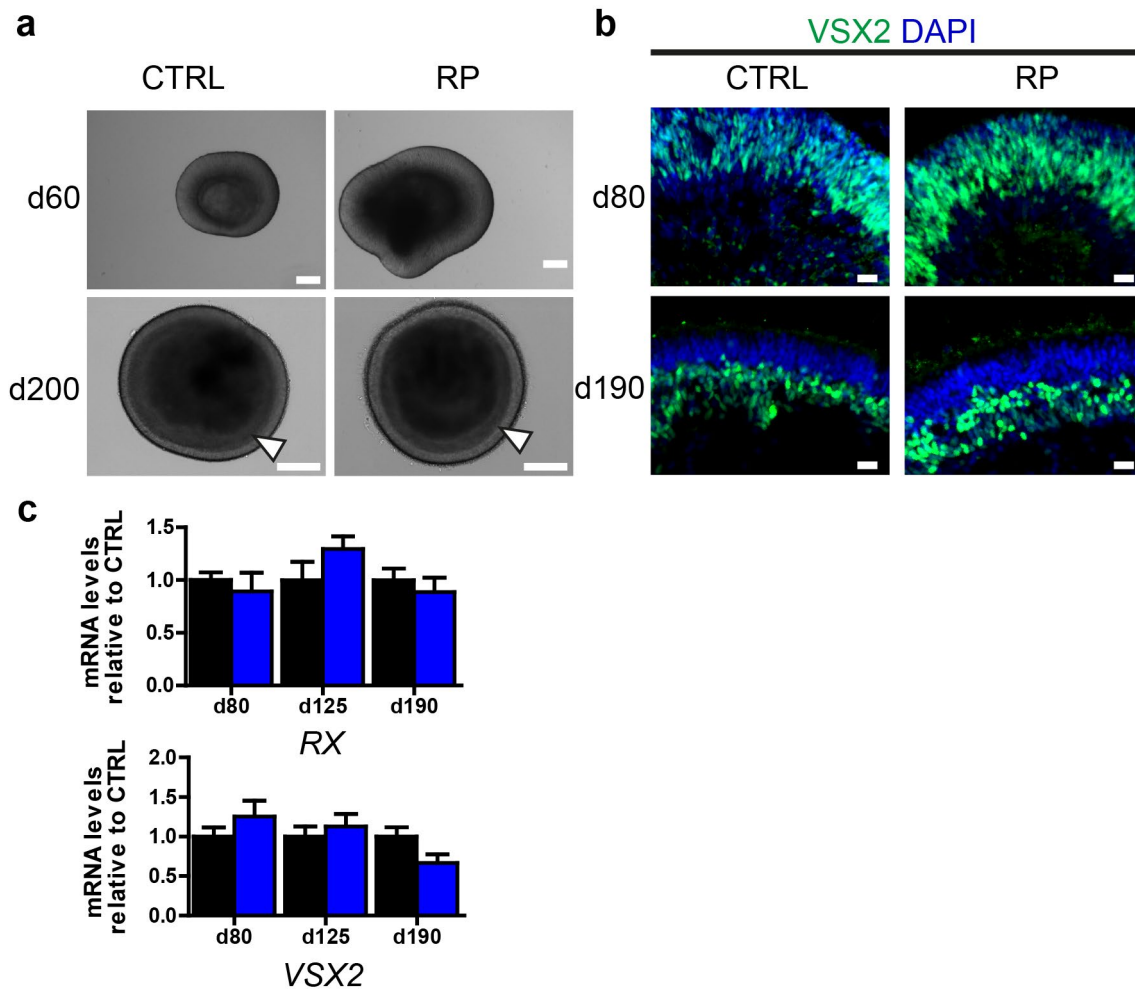
Figure 11- Retinal organoid differentiation of RP iPSC and unaffected controls

(a) Brightfield images of d60 and d200 retinal organoids of RP patients and unaffected controls. Arrowheads indicate the border of the photoreceptor layer (outer part) and the inner layers (inner part). (b) d80 and d190 retinal organoids of RP patients and unaffected controls stained for the neural retina progenitor marker VSX2 (green). (c) Gene expression analysis of the retinal progenitor markers *RX* and *VSX2* comparing day 80, d125 and d190. Values were normalised to the housekeeping gene *GADPH.* In the graph, RP values (blue) are depicted relative to expression level of unaffected controls (black) at each time point (n= 6- 23). DAPI= blue. Error bars: S.E.M. Scale bars: (a) 200 μm, (b) 20 μm.

6.5. Assessment of proliferation capacity of retinal progenitors during retinal differentiation

For examining retinal cell and especially retinal progenitor cell proliferation, cells were loaded with BrdU on day 79 of differentiation for 24 hours, fixed and stained with a BrdU antibody. The resulting images revealed that at d80, most of the retinal progenitor cells were still proliferating (Figure 12a). This was confirmed by the mitosis marker KI67. KI67-positive nuclei mostly overlapped with the BrdU-positive nuclei (Figure 12a). At d190, only few progenitor cells (VSX2+) were still left and only a small fraction of these cell was still proliferating (Figure 12b). Retinal organoids from RP patients showed a comparable amount of proliferative cells at both d80 and d190 (Figure 12a, b). mRNA expression analysis however revealed a significant increase of the cell cycle gatekeeper *CCND1* at day 80 but no changes for *CCNE1* expression (Figure 12c).
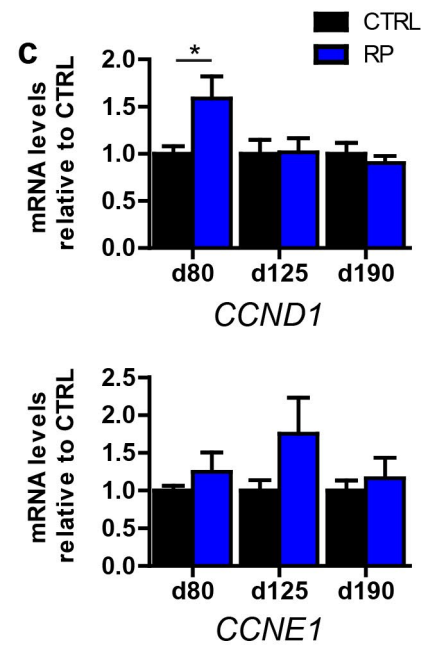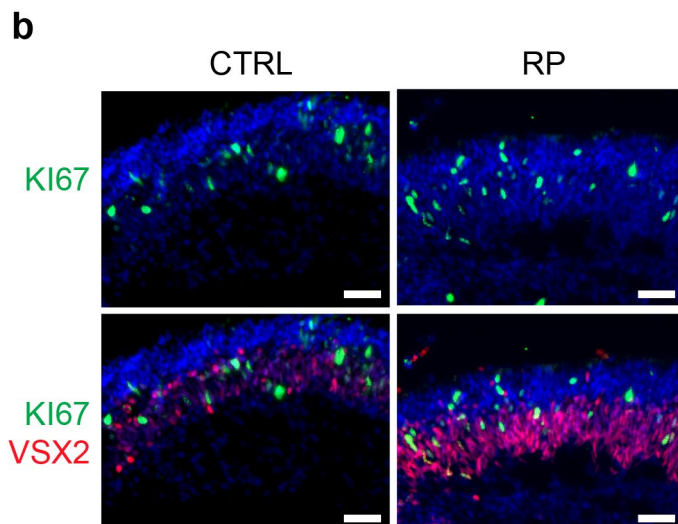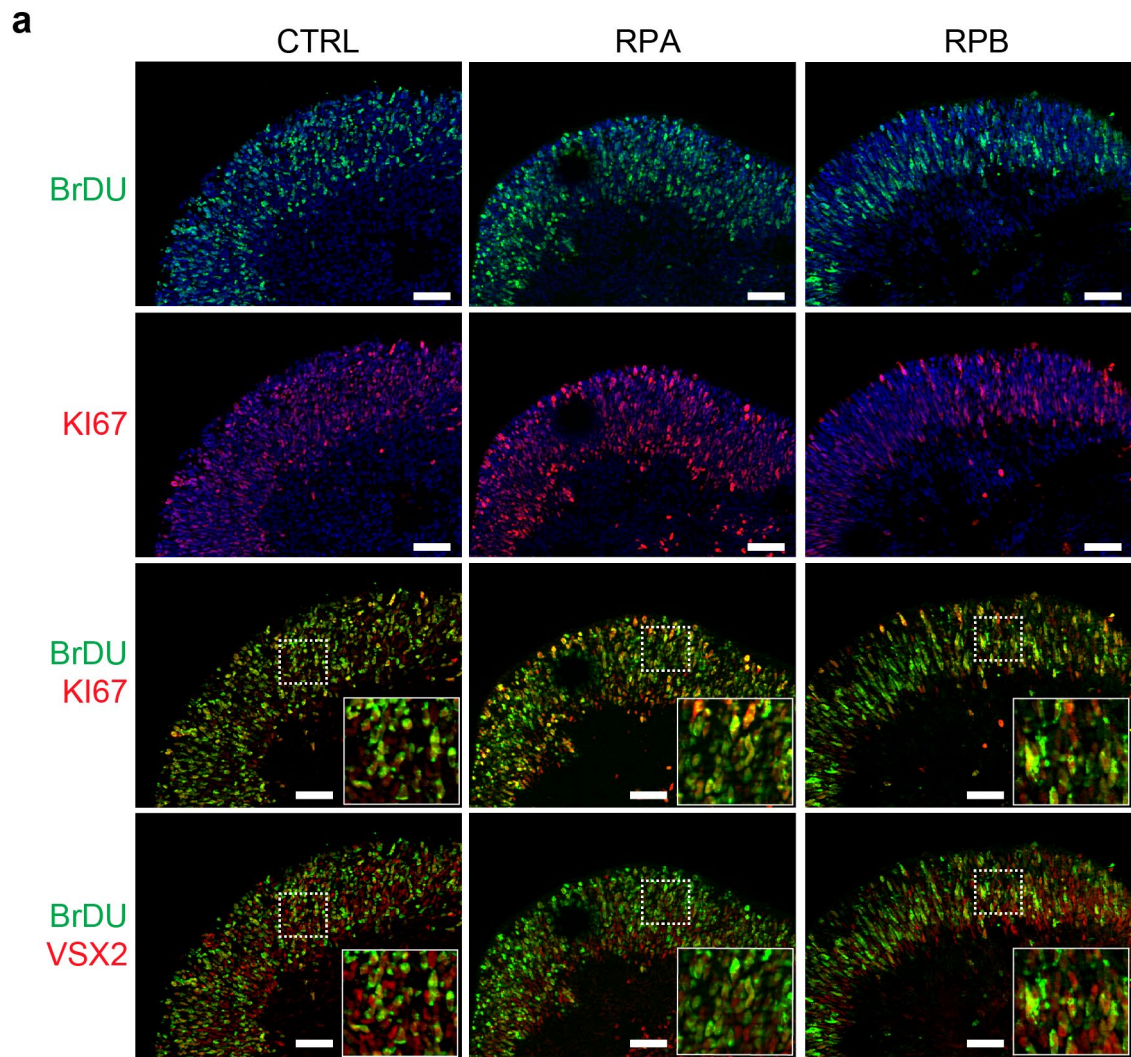
Figure 12- Assessment of the proliferation capacity of retinal progenitors during retinal differentiation

(a) d80 retinal organoids of controls, RPA and RPB were supplemented with BrDU for 24 hours and stained with a respective antibody (BrDU, green). Samples were co-stained for the mitosis marker KI67 (red). A combination staining of BrDU and KI67 (third row) and with the neural retina marker VSX2 (last row) is shown. Spotted squares indicate the magnified areas shown adjacent to the individual images. (b) CTRL and RP retinal organoids from day 190 of differentiation were stained for KI67 (green) and VSX2 (red). (c) Gene expression analysis of cell cycle-related genes *CCND1* and *CCNE1*. RP and control retinal organoids of differentiation day 80, d125 and d190 were normalised to the housekeeping gene *GADPH.* In the graph, values are depicted relative to expression level of unaffected controls at each time point (n= 6- 23 per condition). DAPI= blue. Error bars: S.E.M. * $p < 0.05$. Scale bars: (a, b) 50 µm.

6.6. Evaluation of cell death in retinitis pigmentosa retinal organoids

A striking aspect of retinitis pigmentosa pathology is the progressive loss and cell death of PRCs. To assess, whether PRC death could be observed in RO, a TUNEL staining was performed at advanced stages of differentiation (d260 and d365). In these stages, most photoreceptor cells show a mature configuration including inner and partly outer segment formation (Figure 13a, Figure 15). Co-staining of Click-it™ TUNEL 488 and photoreceptor markers Recoverin and Rhodopsin showed that only few cells/PRCs in CTRL and patients were labelled as apoptotic (Figure 13a). A quantification of TUNEL-positive punctae within the PRC layer revealed a significant decrease of TUNEL staining in RP patients for both time points (Figure 13b). Additional staining for cleaved caspase 3 showed almost no positive signals within the retina (data not shown).

In conclusion, RP RO showed no increase of cell death during late stages of PRC development. On the contrary, a decreased number of dead cell within the matured photoreceptor layer was observed compared to control RO.
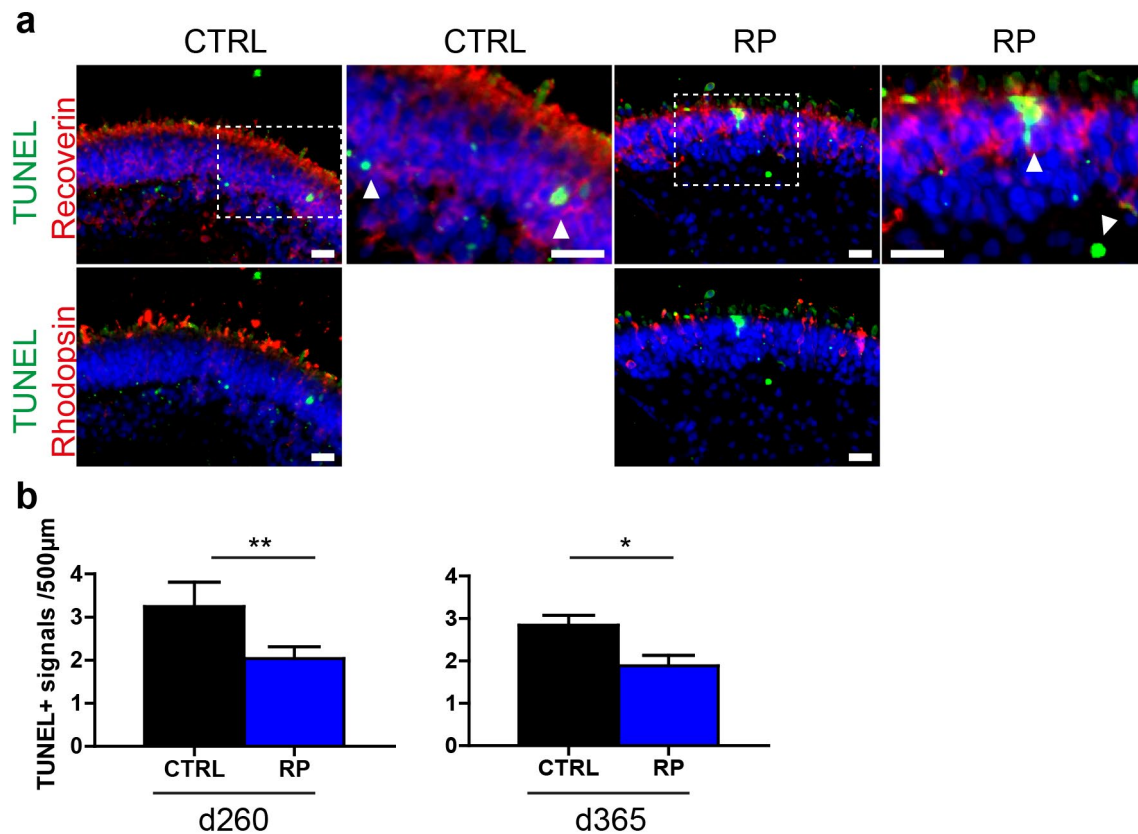
Figure 13- Evaluation of cell death in retinitis pigmentosa retinal organoids using the TUNEL assay

(a) CTRL and RP retinal organoids were stained with the Click-it™ TUNEL 488 Kit (green) to label dead cells at day 260 of differentiation. Co-staining with photoreceptors (Rhodopsin, red) is shown in the second and fourth column. Arrowheads point to TUNEL-positive cells. (b) Quantification of TUNEL-positive individual signals (stained with Click-it™ TUNEL 488 Kit) in the photoreceptor layer (identified by Rhodopsin co-staining) at d260 and d365. Bar graphs show positive punctae per 500 µm of organoid outer circumference for CTRL and RP lines (n= 15- 36 organoids per condition). DAPI = blue. Error bars: S.E.M. * p<0.05, ** p<0.01. Scale bars: (a) 20 µm.

6.7. Retinal subtype differentiation and layering in retinitis pigmentosa retinal organoids

In order to check whether the *CRB1* mutation in RP patients affects the differentiation process and neural subtype differentiation in retinal organoids, a

set of marker proteins was selected to assess retinal subtype differentiation. As already described, the differentiation of retinal dells from RPCs is a tightly orchestrated process and the time of emerge and number of each individual subtype highly conserved.

As the first retinal cell type, ganglion cells can be detected starting from day 40 (earliest time point examined) until around day 100. In both RP patients and controls, BRN3B- positive ganglion cells could be observed in a comparable timeframe and number (Figure 14a). Similar observations were made for the interneuron marker Calbindin and AP2α staining amacrine and horizontal cells (Figure 14b, c). In each case, individual cells could be identified in the inner non-photoreceptor layer for different time points starting from day 40. Of note, the innermost layer containing ganglion cells completely disappeared after day 100, a commonly known phenomenon of current retinal organoid cultures. Further, bipolar cells were stained with the markers PKCα (Figure 14d) and G0α (Figure 14e). They could be detected frequently starting from day 190 adjacent to the photoreceptor layer (see also Figure 17). Again, no obvious differences in number and morphology between the RP patients and controls could be observed (Figure 14d, e). These results are in contrast to the results obtained with mRNA from ROs harvested at day 80, d125 and d190. Here, a significantly higher expression for the ganglion cell marker *ATOH7*, amacrine cell marker *NEUROD2* and neural marker *TUBB3* could be observed in RP ROs at day 80 (Figure 14f). At day d190, a significant decrease of the genes *PKCA* (bipolar cells) and *PROX1* (horizontal cells) was observed for RP RO.

In summary, RO from patients and controls contain ganglion cells and respective marker expression. Although the patients show a difference in mRNA profiles for markers of these cell types, no striking differences in number, localisation or morphology could be observed.
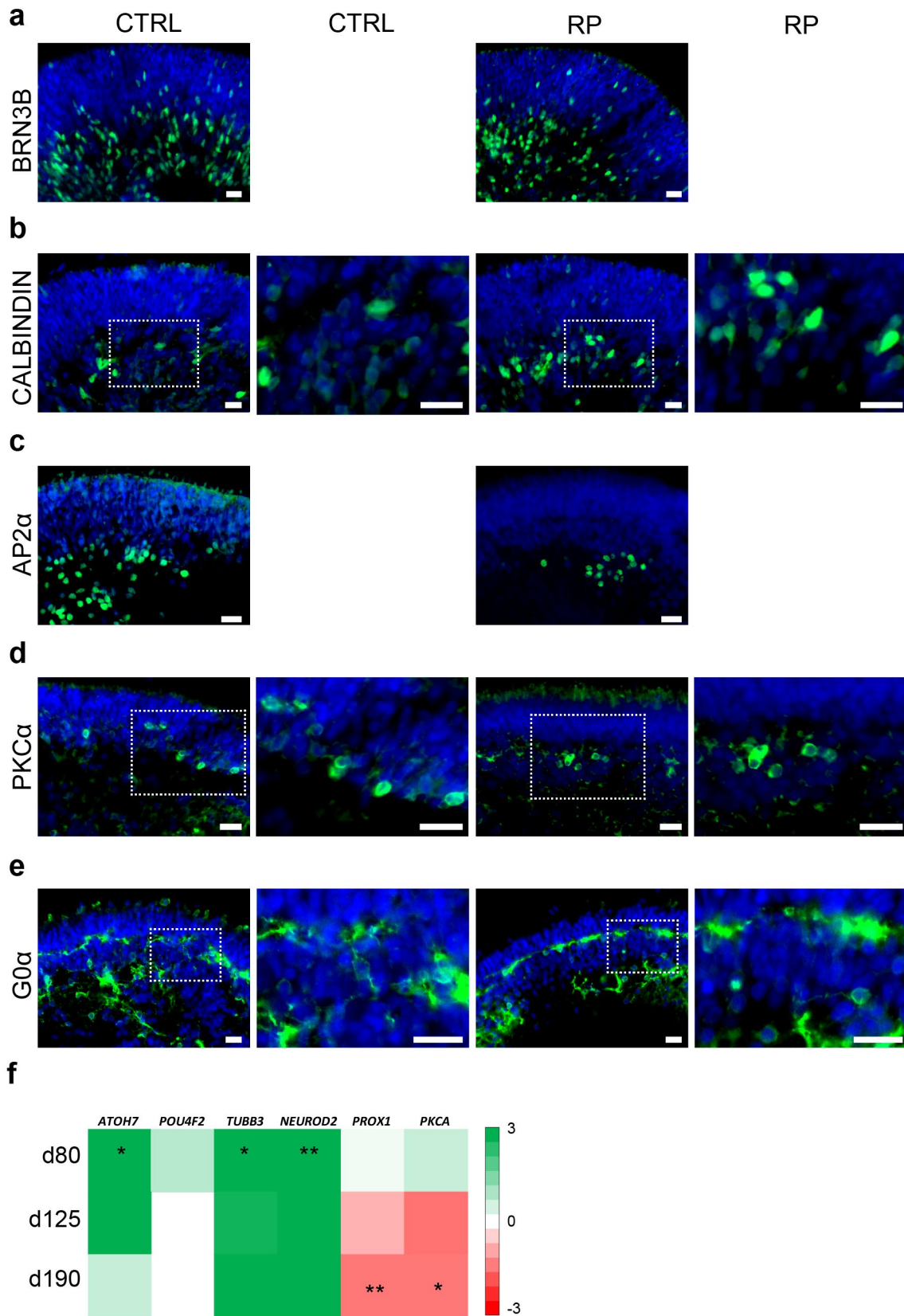
Figure 14- Retinal subtype differentiation and layering in retinitis pigmentosa retinal organoids

(a) CTRL and RP retinal organoids from day 80 of differentiation stained for the retinal ganglion cell marker BRN3B (green). (b) CTRL and RP retinal organoids from day 80 of differentiation stained for the amacrine/horizontal cell marker Calbindin (green). (c) CTRL and RP retinal organoids from day 260 of differentiation stained for the amacrine/horizontal cell marker AP2α (green). (d) CTRL and RP retinal organoids from day 260 of differentiation stained for the bipolar cell marker PKCα (green). (e) CTRL and RP retinal organoids from day 365 of differentiation stained for the bipolar cell marker G0α (green). (f) Gene expression analysis of retinal neural cell types. Markers for ganglion cells (*ATOH7, POU4F2, TUBB3*), amacrine/horizontal cells (*NEUROD2, PROX1*) and bipolar cells (*PKCA*). RP and control retinal organoids of differentiation day 80, d125 and d190 were normalised to the housekeeping gene *GADPH*. In the graph, expression changes to the individual controls are depicted as a colour heat map. Shades of red indicate decrease, shades of green increase of expression in RP in comparison to the control (n= 6- 23) as indicated by a colour bar. DAPI = blue. Error bars: S.E.M. * $p < 0.05$, ** $p < 0.01$. Scale bars: (a-e) 20 µm.

6.8. Rod and cone photoreceptor maturation in healthy and retinitis pigmentosa retinal organoids

As the light-sensitive cells of the retina, the photoreceptors are indispensable for the functionality of the retina, a partial loss of photoreceptors as seen in *e.g.* retinitis pigmentosa is leading to a decreased eyesight; a full loss of photoreceptors is leading to blindness.

In ROs, first PRCs (positive for Recoverin) appear at around day 40 (data not shown). They steadily increase in number and at around day 125, they form an exclusive outer photoreceptor layer, which is stable throughout the further development (Figure 15a). However, the occurrence of PRCs outside of this layer is frequently observed (see *e.g.* Figure 15c, e).

Respective markers can stress the subspecialisation to rod and cone photoreceptors. First cone cells (marked by ARR3, Figure 15b) can be observed at day 80, whereas rod cells identified by Rhodopsin appear later (starting from day 125) (Figure 15d). In contrast, single cones stained for Opsin cannot be found before day 190; at larger numbers at day d365 (Figure 15c). For Opsins, short-

wave (S, blue) and middle/long wave (L, red and M, green) can be distinguished via immunofluorescence (data not shown). Double staining for L/M- and S-Opsins and Rhodopsin show that almost all rod and cones exclusively express one or the other markers (Figure 15e). The pattern of rod and cone distribution among different organoids within or between different lines was variable (data not shown). Especially, the appearance of Rhodopsin- labelled rods strongly varied between individual organoids (data not shown).

Next, RO from RP were analysed and compared to control differentiation. Emerge and maturation of rods and cones did not seem to be affected by the *CRB1* mutation (Figure 15a- e). For both RP lines, rods and cones appeared at similar time points and at comparable rates. Comparing the expression profiles of RP and controls, a mild increase of rod and cone markers (*RHO*, *ARR3*, middle and short wave opsins (*OPN1MW, OPN1SW*)) was observed (Figure 15f). However, only the levels of *OPN1MW* at d80 were significantly changed.

In summary, differentiation and maturation of rod and cone photoreceptors was observed in control ROs. The number and expression pattern of rod and cone cells and markers was comparable in RP patient lines.
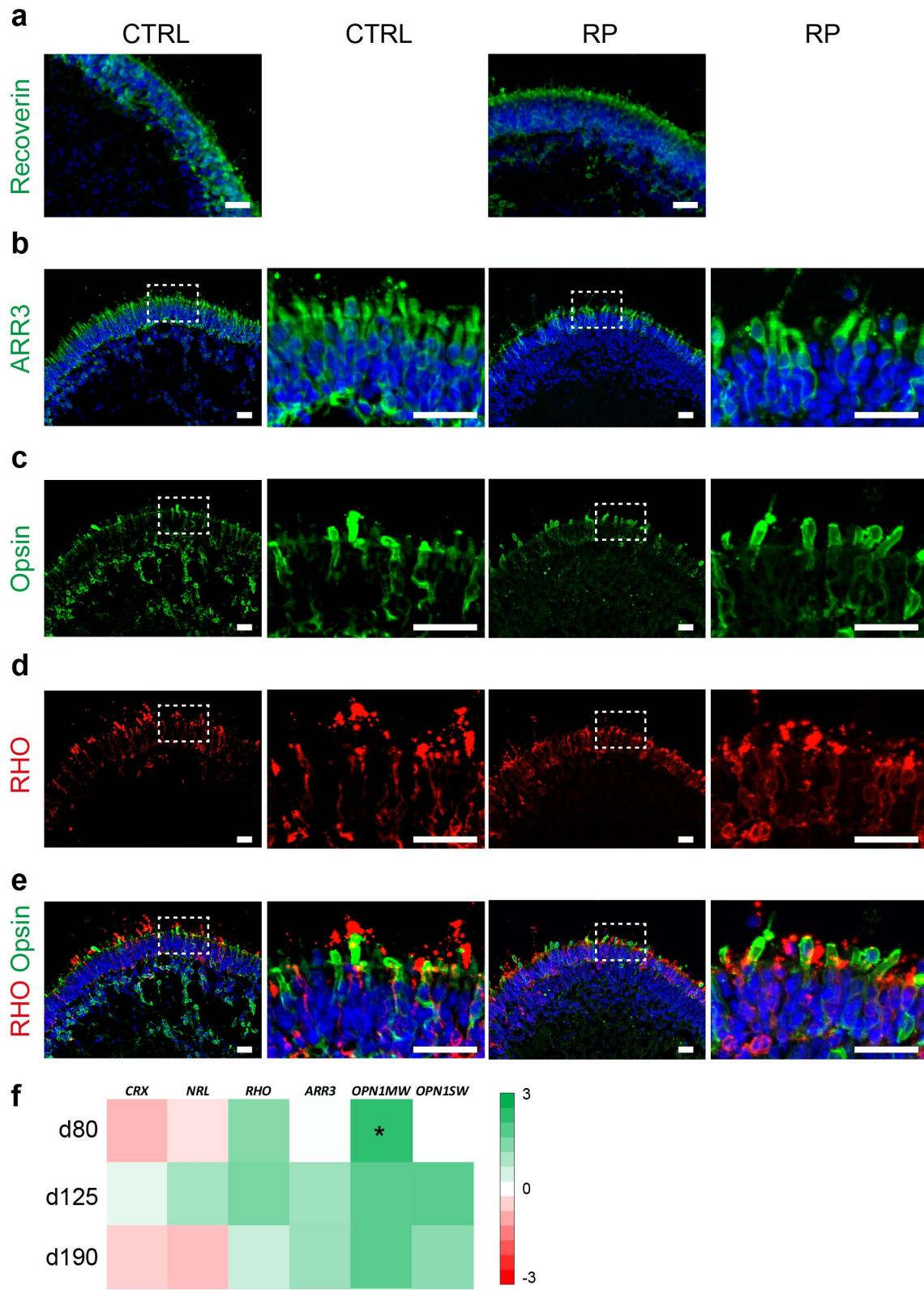
Figure 15- Rod and cone photoreceptor maturation in retinitis pigmentosa retinal organoids

(a) CTRL and RP retinal organoids from day 260 of differentiation stained for photoreceptor cell marker Recoverin (green). (b) CTRL and RP retinal organoids from day 365 of differentiation stained for the cone marker ARR3 (green). (c) CTRL and RP retinal organoids from day 365 of differentiation co-stained for cone photoreceptor cell markers L/M-Opsin and S-Opsin (Opsin, both in green). (d) CTRL and RP retinal organoids from day 365 of differentiation stained for the rod photoreceptor marker Rhodopsin (red). (e) Composite image of (c) and (d) showing Rhodopsin (red) and L/M/S-Opsin (Opsin, green). Images in the second and fourth column are magnification of the respective areas (marked with dotted line squares) in the first and third column. (f) Gene expression analysis of photoreceptor genes *CRX*, *NRL*, *RHO*, *ARR3*, *OPN1MW* and *OPN1SW*. RP and control retinal organoids of differentiation day 80, 125 and 190 were normalised to the housekeeping gene *GADPH*. In the graph, expression changes to the individual controls are depicted as colour heat map. Shades of red indicate decrease, shades of green increase of expression in RP in comparison to the control (n= 6- 23) as indicated by a colour bar. DAPI = blue. Error bars: S.E.M. * $p < 0.05$. Scale bars: (a- e) 30 µm.

6.9. Photoreceptor segment formation in retinitis pigmentosa retinal organoids

Starting from day 125, PRC of ROs started to form segment-like structures. Using electron microscopic imaging, the ultrastructure of the photoreceptor segments could be evaluated (Figure 16a). Most of the segments found in ROs showed an inner segment-like morphology growing out of the organoid body. At the base of the outgrowth, an electron-dense outer limiting membrane (OLM)-like structure could be identified. Above the OLM, the inner segments showed variable size but almost all were filled with a high number of mitochondria, sometimes strongly clustered to the apical end (Figure 16a, left top image). In some cases, cilia outgrowing of the inner segment could be observed (Figure 16a, right image). The occurrence of outer segments was a rare event in RO of day 190. In some cases, simple formations of membrane stacks were found; most probably early forms of OS disks (Figure 16a, left bottom image).

Between day 80 and d365, the segments increased in number (Figure 16b, c) and length (Figure 16b, d); the longest reaching a length of 40 μm and more (Figure 16e). For RP ROs, numbers and length of segments were comparable to CTRLs (Figure 16b- d). To have a detailed look, the segment lengths were categorised in 5 μm steps starting from the OLM as basis line (Figure 16e, f). Over time, the proportion of segments, which were 10 μm and more steadily increased. In RP lines, the same was observed at day 365. The amount of segments above 25 μm in the analysed images was higher than for the CTRLs (Figure 16f).

Next, the presence of the bona fide outer segment marker ROM1 in CTRL and RP lines was analysed (Figure 16g- i). ROM1-positive puncta outside of the organoid were present starting from d190 (Figure 16g). In order to quantify the immunofluorescence signal, the ImageJ/R based macro "Slope Approach" was used (details see material and methods section 5.2.24). For both analysed time points (d190 and d365), the mean signal intensity in the segment ranges (with the OLM set as 0 point) of 0- 40 μm was comparable (Figure 16h). Comparing the signal intensity in 10 μm ranges between d190 and d365 revealed an increase

of ROM1 signal for both CTRL and RP (Figure 16i). A significant change between the CTRL and RP at the individual time points was not observed.

Finally, in order to assess the validity of ROM1 as outer segment marker, ROs were stained with ROM1 in combination with the bona fide inner segment marker Na$^+$/K$^+$ ATPase α3 (Figure 16j). At day d365, some of the PRC segments (labelled by the cone marker ARR3) showed a membrane staining for Na$^+$/K$^+$ ATPase α3 with positively stained apical ROM1 puncta (Figure 16j). This was found in a similar fashion for RP lines (Figure 16j).

In summary, the number and length of segments is comparable in RP retinal organoids compared to controls, as well as the signal strength and distribution of the outer segment marker ROM1. In addition, ROM1 was identified as a potential outer segment and Na$^+$/K$^+$ ATPase α3 as an inner segment marker.
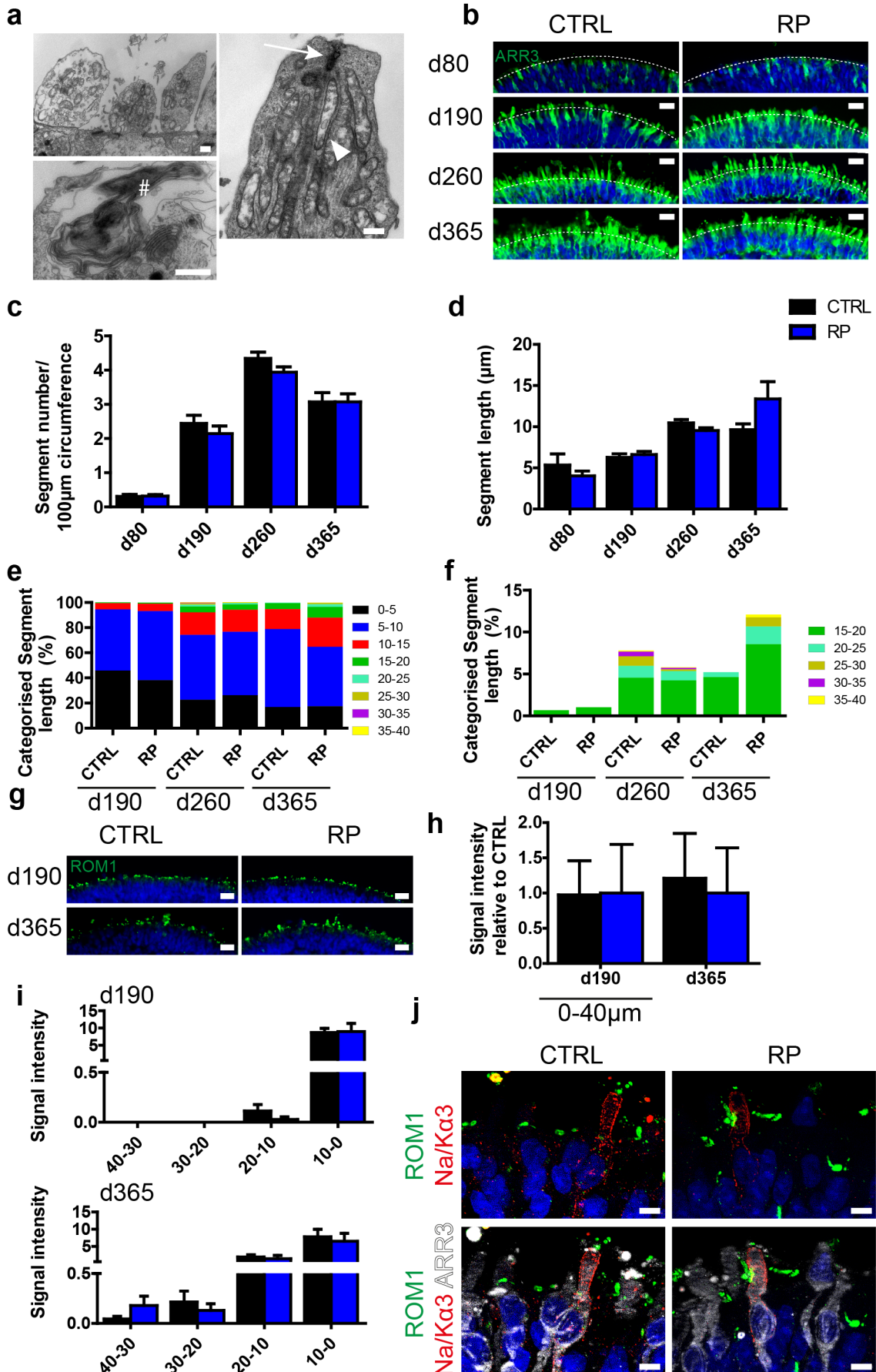
Figure 16- Photoreceptor segment formation in retinitis pigmentosa retinal organoids

(a) Electron microscopic visualisation of formed inner (left top, right) and outer segments (bottom left) in d190 retinal organoids. Arrowhead marks inner segment mitochondria, Arrow marks connecting cilia, (#) marks assumed outer segment discs. (b) CTRL and RP retinal organoids from day 80, 190, 260 and 365 of differentiation stained for ARR3 (green) representing the length and number of (cone) segments. Dotted line indicates organoid rim. (c) Quantification of segment number per 100 µm organoid circumference comparing CTRL and RP retinal organoids at day 80, 190, 260 and 365. (d) Measurement of the average segment length (in µm, from OLM to the segment tip) comparing CTRL and RP retinal organoids at day 80, 190, 260 and 365. (e) Distribution analysis of d190, d260 and d365 CTRL and RP segment lengths based on the data shown in (c) and (d). Different shares indicate the proportion of segments of a specific length range in 5 µm intervals (*e.g.* 0 - 5 µm) as indicated in the legend on the right. (f) Categorised segment lengths of d190, d260 and d365 CTRL and RP in 5 µm intervals between 15 and 40 µm length based on the data of (d) and (e). (g) CTRL and RP retinal organoids from day 190 and 365 of differentiation stained for the bona fide outer segment marker ROM1 (green). (h) Quantification of the summed fluorescence signal of ROM1 from control and RP RO outside the organoid using the "Slope Approach" macro. Values are compared for range 0- 40 µm of OLM distance at d190 and d365 (2 CTRL lines n= 14- 26 images, 4 RP lines n= 17- 23 images). (i) Distribution of mean fluorescence signal for ROM1 at day 190 (top image) and d365 (bottom image) in specified distance ranges (0- 10 µm, 10- 20 µm, 20- 30 µm, 30- 40 µm from the OLM) based on the data acquired for (h). (j) CTRL and RP retinal organoids from day d365 of differentiation stained for the bona fide outer segment marker ROM1 (green) and the potential inner segment marker Na$^+$/K$^+$ ATPase α3 (red) and ARR3 (white). DAPI = blue. Error bars: S.E.M. Scale bars: (a) 500 nm, (b, g) 20 µm, (j) 5 µm.

6.10. Synaptic wiring in retinitis pigmentosa retinal organoids

Next, I examined whether organoids from RP and CTRL were able to form synaptic connections. In human retina, synapses are located in two gatherings in the outer and inner plexiform layers.

In RO, ribbon synapses were identified using ultrastructural analysis (Figure 17b). The electron microscopic image shows ribbons that are loaded with gatherings of vesicles. Further, stainings for the PRC synapse marker Bassoon (data not shown) and the ribbon protein Ribeye (CTBP2) (Figure 17a) were performed to further validate the identity of the synapse. In a co-staining with the cone marker

ARR3 and the bipolar marker PKCα, a co-localisation of cone end-feet, ribbon synapses and bipolar branches could be shown (Figure 17a, arrow). In RP patients, similar patterns were observed showing no obvious difference in ribeye positive puncta or co-localisation with cone end-feet (Figure 17a).

In conclusion, RO from controls and RP patients form ribbon synapses are probably interconnecting PRC and bipolar cells forming the first synapse in phototransduction.
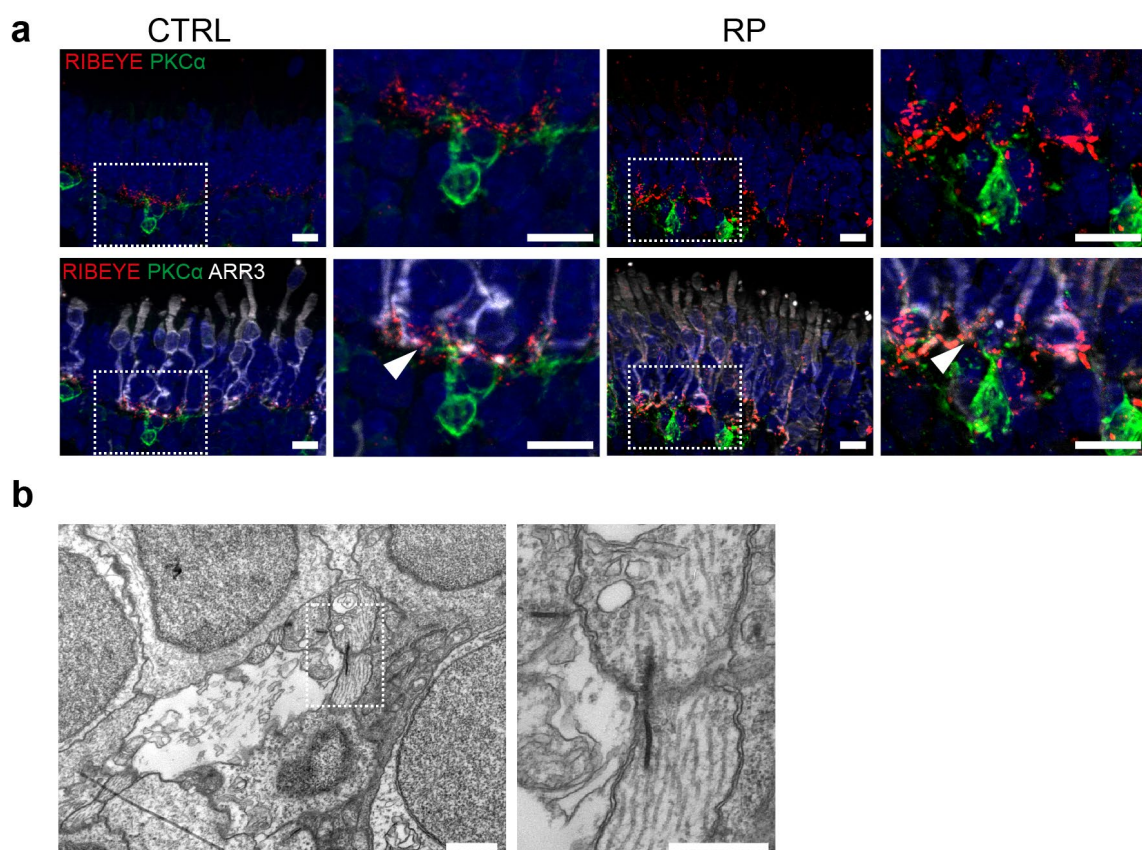

Figure 17- Synaptic wiring in retinitis pigmentosa retinal organoids

(a) CTRL and RP retinal organoids from day d260 stained for the ribbon synapse marker Ribeye (CTBP2, red), the bipolar cell marker PKCα (green) and the cone marker Arrestin3 (ARR3, white, bottom row). Images in the second and fourth column are magnification of the respective areas (marked with dotted line squares) in the first and third column. Arrowhead point to putative ribbon synapses between stained cones and bipolar cells. (b) Electron microscopic images of CTRL d190 RO showing electron dense ribbon synapse with clustered vesicles. Right image is a

magnification of the dotted lined marked area in left image. DAPI = blue. Scale bars: (a) 10 µm, (b) 1 µm.

6.11. Müller glia formation in retinitis pigmentosa retinal organoids

In adult human retina, CRB1 was seen to be expressed by PRCs and Müller glial cells (120) and was even proposed to influence the development of Müller glia cell features (191). Therefore, I checked whether RO of RP patients showed a changed Müller glia cell distribution pattern. Using the marker CRALBP (Figure 18a), no obvious differences in the expression pattern could be found. In both cases, beginning from day 190, the staining could be found in the inner layers, sparing out the PRC layers except for long processes ending in the presumable OLM belt (Figure 18a).

Using the analysis tool "Slope Approach", at d260 and d365 for two analysed regions (OLM and PRC layer) of the organoids, no striking difference between CTRL and RP was observed. At d260, in RP ROs a significant decrease of CRALBP signals within in the innermost layers was detected. At d365 however, these changes could not be observed anymore. Using another bona fide Müller glia maker, the Glutamine synthetase, only at d365 a strikingly positive signal in cell bodies could be seen. This was however comparable in RP and in control lines. Additionally, I checked for the activated form of Müller glia by staining with GFAP antibodies (data not shown). In some organoids, strongly stained active Müller glia cells were found, however in no correlation to CTRL or RP patient lines. mRNA levels of the Müller glia related genes at day 80, 125 and 190 showed an increase for *ANXA4* in RP RO at d125, a significant increase for the Glutamine synthetase gene *GLUL* at day 80 and decrease at day 190. For *HES5*, the mRNA levels were increased at d80 and decreased at d190 similarly to *GLUL*, however slightly above significance.

In summary, I could establish two markers for Müller glia cells, CRALBP and Glutamine synthetase. Both did not show striking changes in RP retinal organoids, except for an increase of CRALBP in the INL at 260. Finally, the

analysis of Müller glia-related genes showed changed expression levels of *HES5* and a significant change of Glutamine synthetase (*GLUL*).
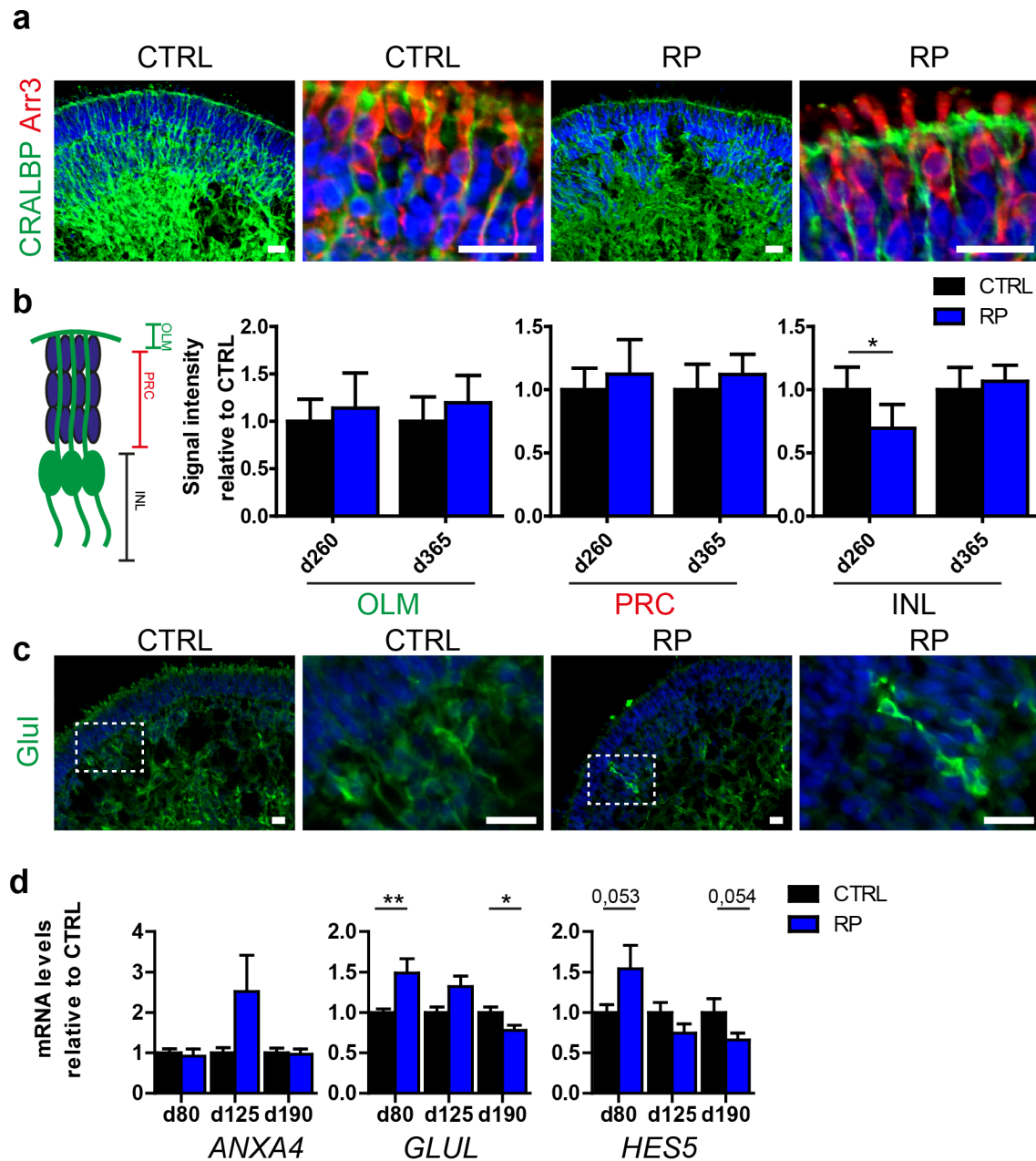

Figure 18- Müller glia formation in retinitis pigmentosa retinal organoids

(a) CTRL retinal organoids from day 365 of differentiation stained for the Müller glia marker CRALBP (green) and ARR3 (red). Second and fourth image are z-projections of magnified areas of the first and third image (b) Quantification of the summed fluorescence signals of CRALBP from control and RP RO along the OLM with the "Slope Approach" macro. Signal was summed

in specific regions as indicated in the scheme (OLM: 0 - 10 μm below the OLM, PRC: 10 – 30 μm below the OLM, organoid: 30 – 70 μm below the OLM). 2 CTRL lines, n= 14 - 36 images; 2- 4 RP lines, n=9- 46 images. (c) CTRL retinal organoids from day 365 of differentiation stained for the Müller glia marker Glutamine synthetase (GLUL, green). (d) Gene expression analysis of the Müller glia related genes *ANXA4*, *GLUL* and *HES5*.   RP and control retinal organoids of differentiation day 80, 125 and 190 were normalised to the housekeeping gene *GADPH*. In the graph, values are depicted relative to the individual controls (n = 6 - 23). DAPI = blue. Error bars: S.E.M. * $p < 0.05$, ** $p < 0.01$. Scale bars: (a, d) 20 μm.

6.12. Examination of the outer limiting membrane in retinitis pigmentosa retinal organoids

In the vertebrate retina, CRB1 is part of the crumbs complex, which is situated in the apical region adjacent to the adherens junctions of the outer limiting membrane. To check, whether the mutation in the *CRB1* gene influences the formation of the adherens junction and the OLM, RO were stained with OLM markers. A frequently used marker for the OLM is ZO-1. As expected, in RO ZO-1 stained the outer rim of the retinal organoid (Figure 19a), which could be identified as the OLM using electron microscopy (Figure 19c). Here, the OLM is visible as electron dense belt flanking outgrowing segments. A quantification of fluorescence stainings of ZO-1 using the "Slope Approach" macro showed that the signal was comparable for d80, d125 and d365, but significantly decreased in RP patients at d190 and d260.

In summary, the RO of control and RP patients present an intact OLM, which can be stained by ZO-1 and visualised by electron microscopy. In RP, a strong decrease of signal intensity was observed for two of the analysed time points, but remained unchanged for the others.
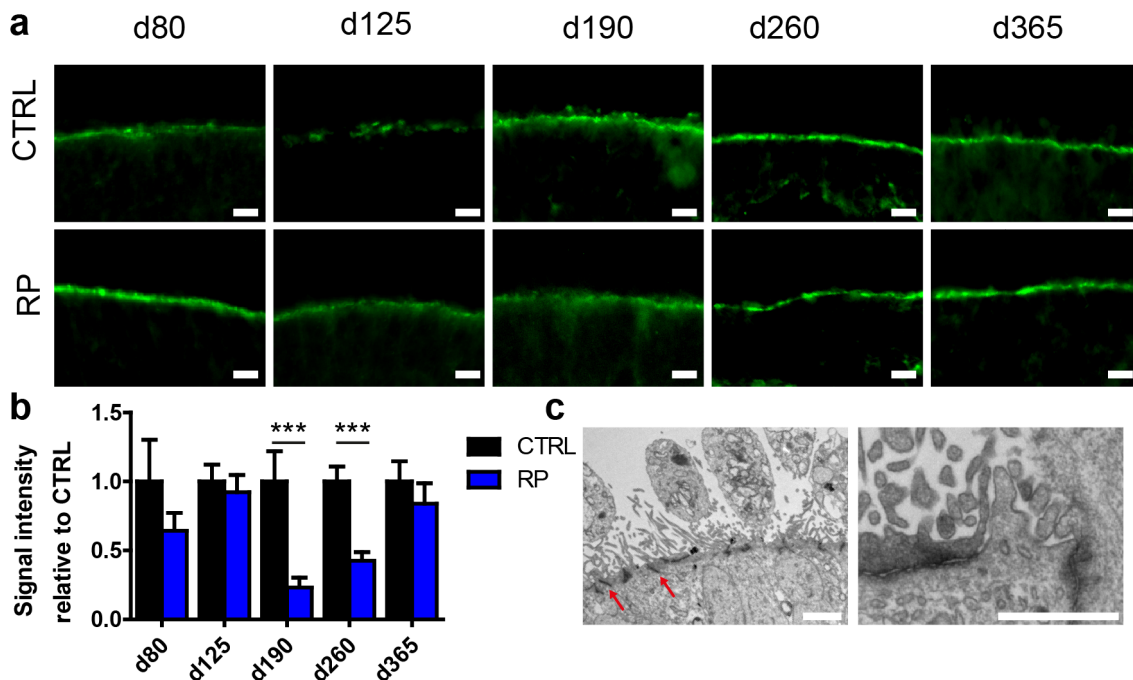
Figure 19- Examination of the outer limiting membrane in retinitis pigmentosa retinal organoids

(a) CTRL and RP retinal organoids from day 80, 125, 190, 260 and 365 of differentiation stained for ZO-1 (green). (b) Quantification of the summed fluorescence signal of ZO-1 from control and RP RO along the OLM with the "Slope Approach" macro. Signal was summed between the OLM and 10 µm distance above and below (2 CTRL lines, n= 14- 36 images; 2- 4 RP lines, n= 9- 46 images). (c) Electron microscopic image of a day 190 retinal organoid showing photoreceptor segments and electron dense OLM (red arrows). Right image shows a similar area at a higher magnitude. DAPI = blue. Error bars: S.E.M. *** p < 0.001. Scale bars: (a) 10 µm, (c) 2 µm.

6.13. CRB1 localisation and expression during retinal organoid development

As initial experiment, 2 different antibodies for CRB1 were tested in order to visualise the developmental changes of CRB1 localisation and expression (Figure 20a). The first antibody was directed against an immunogen in the central region of CRB1 (thereafter called CRB1c) and the second to an N-terminal region within CRB1 (CRB1n). Both antibodies stained the outer rim of the retinal organoid representing the OLM area. At day 40, CRB1c staining was still punctual and non-continuous (Figure 20a), whereas at later time points, CRB1c staining was found as a continuous belt on all sides of the organoid (Figure 20a). CRB1n

staining was already seen as a continuous streak at day 80 decreasing slightly over time (Figure 20a, bottom row). At day 365, the signal at the organoid outer rim was not detectable anymore. Co-localisation of both antibodies showed a partly overlapping, however CRB1c was seen slightly more apical than CRB1n (Figure 20b).

Next, the CRB1c signal was compared with to the signal of the OLM marker ZO-1 (Figure 20c). For d80 and d365, CRB1c was strictly apical from the ZO-1 signal. Comparing the signal of the segment surface marker PNA lectin with CRB1c at d80 showed that CRB1 is located in close apposition to the not yet fully formed segments (Figure 20d). At d365, the outgrowing segments are flanked at the base by the CRB1c signal, yet none of the signal was located inside the segments or the photoreceptor cell soma.

As next experiment, I checked whether *CRB1* mRNA (the confirmed splice variants) were expressed throughout the development. In that course, I made use of primers directed against different splice mRNAs published previously (120). Analysing the time points d80, d190 and d365 of differentiation revealed that all variants which have a confirmed expression in the retina (*CRB1 V1*, *V2* and *VSec*, details see Figure 4) are expressed at a detectable level throughout the development (Figure 20e). CRB1 *V2* mRNA showed a significantly decreased expression comparing d80 to d190 and d365 in RO (Figure 20e). In contrast to that, the variant *CRB1 VSec* was increasing steadily during the measured time points. When comparing the *GAPDH*-relative mRNA levels of *CRB1 V2* and *VSec* to primer mixes which also detected *V1*, the levels of the latter were almost 10-fold higher (Figure 20e). The combined mRNA levels of all variants (*V1/V2/VSec*) however did not show the same dynamics as *V2* and *VSec* but remained at constant levels throughout the examined time points.

Finally, to assess whether the expression of CRB1 is at least partly taking place in photoreceptors, I used an IRBP promoter driven-fluorophore (GFP), labelling photoreceptor cells (Figure 20f, left image). Since IRBP-GFP expression was also observed in RPE cells (data not shown), pigmented RPE areas were manually removed. Afterwards, GFP-positive cells were sorted via FACS and the RNA was

analysed via Fluidigm (Figure 20f, right image). At day 125, in 4 out of 7 IRBP+ samples *CRB1* was detected; at day 190 in 5 out of 8. Of note, the expression levels were in a comparable magnitude to the *CRB1* expression of whole organoid mRNA samples (data not shown).

In summary, throughout retinal organoid development, both CRB1c and CRB1n antibodies could detect CRB1 protein. The signal was seen to be apically to the OLM and in close apposition to developing segments. Finally, I found that the confirmed human splice variants are expressed in retinal organoids and photoreceptor cells in particular, presenting dynamic mRNA levels changes *of the CRB1* variants *V2* and *V4*.

a

d80   d125   d190   d260   d365

CRB1c

CRB1n

b

CRB1n CRB1c

c   d80   d365

CRB1c ZO-1

d   d80   d365

CRB1c Lectin

e

CRB1 Variants

d80
d190
d365

mRNA levels relative to *GADPH*

V2   VSec   V1/2/Sec   V1/2   V1/Sec

f

mRNA levels relative to *GADPH*

CRB1

d125
d190

IRBP+
FACS SORTED
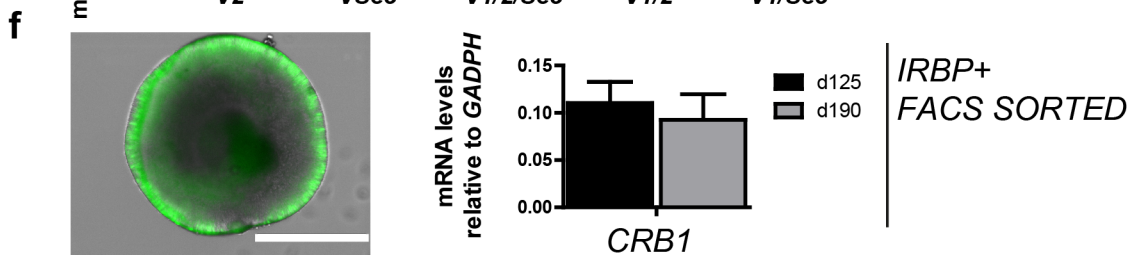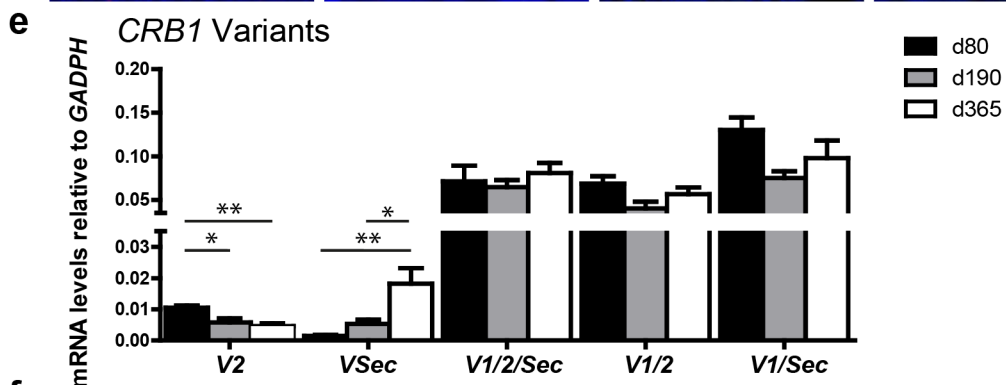
Figure 20- CRB1 localisation and expression during retinal organoid development

(a) CTRL retinal organoids from day 80, 125, 190, 260 and 365 of differentiation stained by a CRB1 antibody directed against the protein centre (CRB1c, green) and against the N-terminus (CRB1n). (b) CTRL retinal organoid from day 260 co-stained with a CRB1 antibody directed against the pr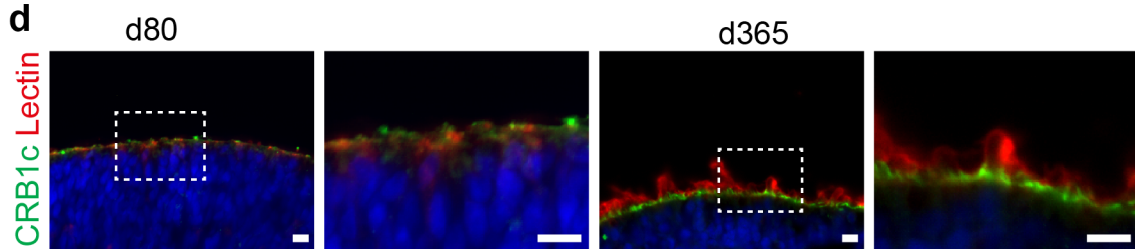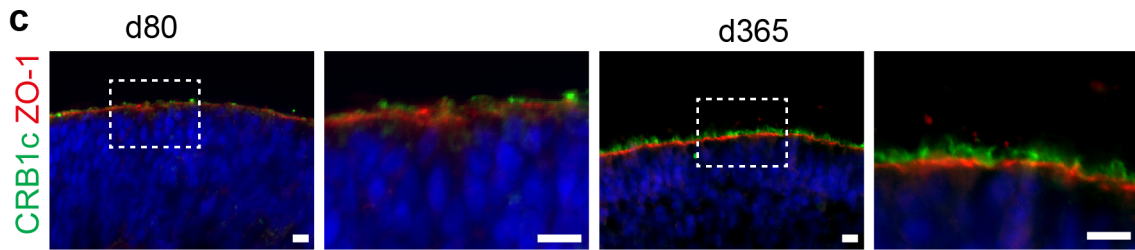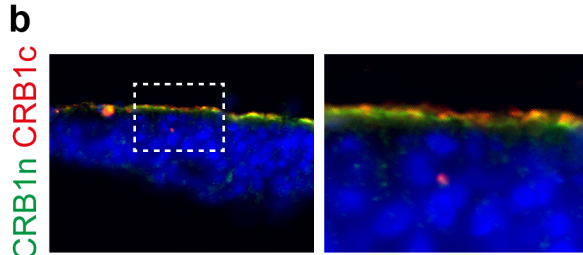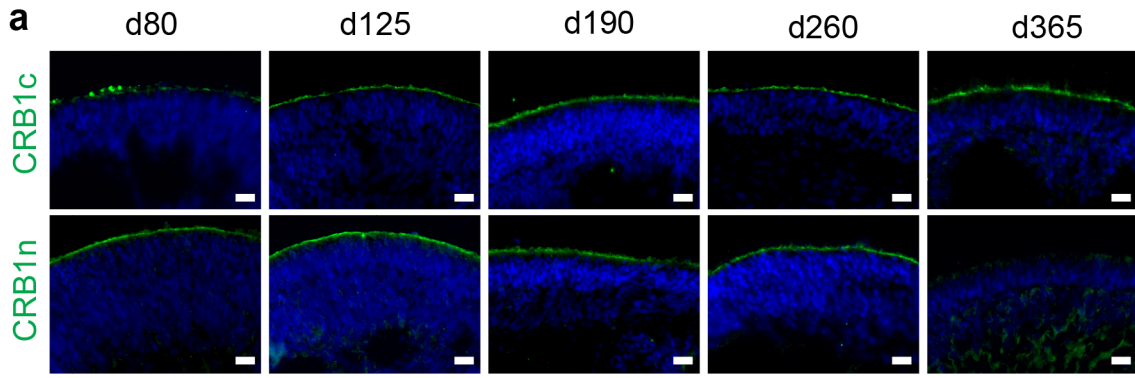otein centre (CRB1c, green) and against the N-terminus (CRB1n). (c) CTRL retinal organoid from day 80 and 365 co-stained with CRB1c and ZO-1. Images in the second and fourth column are magnification of the respective areas (marked with dotted line squares) in the first and third column. (d) CTRL retinal organoids from day 80 and 365 co-stained with CRB1c and ZO-1. Images in the second and fourth column are magnification of the respective areas (marked with dotted line squares) in the first and third column. (e) Gene expression analysis of *CRB1* splice variants (*V1, V2, VSec*) as indicated in the graph using specific primer pairs (right graph). RP and control retinal organoids of differentiation day 80, 190 and 365 were normalised to the housekeeping gene *GADPH* (n = 6- 12). (f) Brightfield/Fluorescence composite image of a d125 retinal organoid transfected with an IRBP-GFP promoter construct (green) labelling photoreceptor cells. Graph shows *CRB1* (Qiagen Primer) expression in the FACS-sorted IRBP-positive cell fraction at day 125 and 190 (n= 7- 8 individual samples). DAPI = blue. Error bars: S.E.M. * $p < 0.05$, ** $p < 0.01$. Scale bars: (a, b) 20 µm, (c- e) 10 µm, (f) 400 µm.

6.14. CRB1 in retinitis pigmentosa retinal organoids

As already mentioned, the mutation of both RP patients is located in the central region of the CRB1 protein (amino acid 947). In order to check whether the mutation has an influence on the protein amount and localisation, I compared antibody stainings of controls and both RP patients at 5 different time points (d80, d125, d190, d260, d365) (Figure 21a-d). Signal quantification was performed with the ImageJ/R Macro "Slope Approach". Stainings for CRB1c showed that in particular at the early time points, the signal is decreased in RP RO. At d125, the decrease was slightly below significance, whereas at d190 and d260 the decrease was highly significant (Figure 21b).

The N-terminal CRB1 antibody signal at the apical OLM region was not present in RP patients at all (Figure 21c). This was also reflected by signal quantification, which demonstrated CRB1n antibody signal to be significantly decreased throughout all analysed time points (Figure 21d). Notably, at d365, the CRB1n signal at the apical OLM is neither present in the RP nor in CTRLs. Still, the

quantified signal intensity in the OLM region was significantly lower in the RP patients (Figure 21d). Finally, I compared the mRNA levels of the *CRB1* splice variants, showing no aberrations in RP patients' ROs in comparison to the controls (Figure 21e).

In conclusion, the CRB1 protein expression in RP patients carrying a *CRB1* mutation was decreased in the earlier time points (d125-d260) using the CRB1c antibody and not present at all using the CRB1n antibody. In contrast to that, the mRNA expression pattern of all detected *CRB1* splice variants was unaltered.
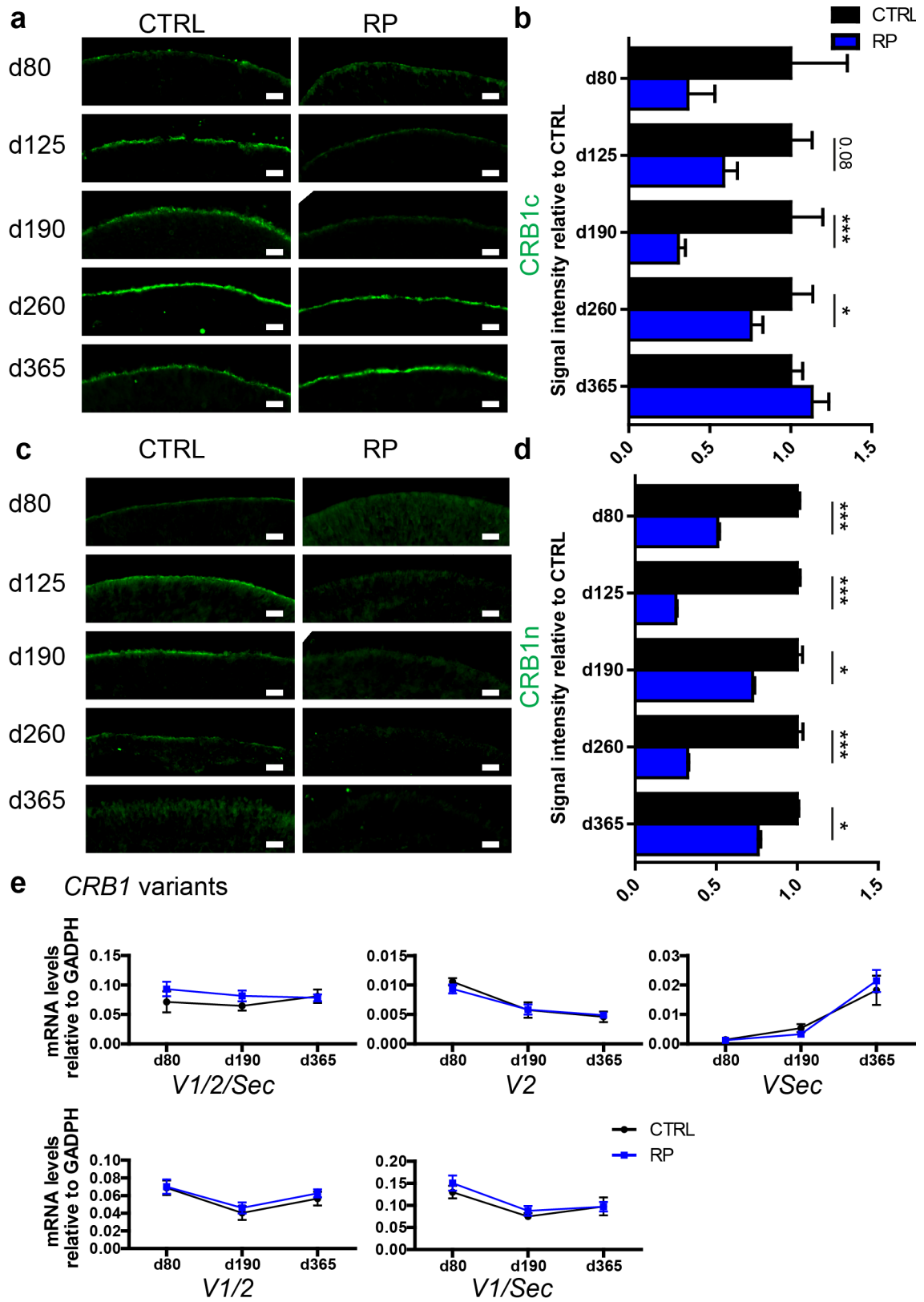
Figure 21- CRB1 in retinitis pigmentosa retinal organoids

(a) CTRL and RP retinal organoids from day 80, 125, 190, 260 and 365 of differentiation stained with a CRB1 antibody directed against the protein centre (CRB1c, green). (b) Quantification of the summed fluorescence signal of CRB1c from control and RP RO along the OLM with the "Slope Approach" macro. Signal was summed between the OLM and 13 µm distance above and below (2 CTRL lines, n= 14- 36 images; 2- 4 RP lines, n= 9- 46 images). (c) CTRL and RP retinal organoids from day 80, 125, 190, 260 and 365 of differentiation stained with an N-terminal CRB1 antibody (CRB1n, green). (d) Quantification of the summed fluorescence signal of CRB1n from control and RP RO alongside the OLM with the "Slope Approach" macro. Signal was summed between the OLM and 13 µm distance above and below (2 CTRL lines, n= 11- 28 images; 2- 4 RP lines, n= 17- 434 images). (e) Gene expression analysis of *CRB1* splice variants as indicated in the individual graphs using specific primer pairs. RP and control retinal organoids of differentiation day 80, 190 and 365 were normalised to the housekeeping gene *GADPH* (n= 6 - 12). DAPI = blue. Error bars: S.E.M. * $p < 0.05$, *** $p < 0.001$. Scale bars: (a) 20 µm.

6.15. Expression of crumbs complex members in retinitis pigmentosa retinal organoids

Next, I questioned whether the mutated CRB1 would influence the expression and localisation of other crumbs complex members. For that, RO were stained for the CRB1 interaction partner PALS1 (Figure 22a-c) and CDC42 (Figure 22a-f). At day260, PALS1 signal was found in similar regions than the CRB1c signal (Figure 22a). However, the expression did not seem to be limited to the apical region but also stained part of the photoreceptor segments (Figure 22a). To quantify the protein amount and localisation, the "Slope Approach" was used. A comparison of the total signal intensity (40 µm above and below the OLM termed as "Outside" and "Inside", respectively), no significant difference between CTRL and RP was observed. However, for both regions, the RP ROs showed a slightly increased signal. A more detailed classification of the examined regions in 10 µm steps showed a similar increase for most of the evaluated regions. However, none of them was affected significantly.

Another indirect interaction partner of CRB1 is CDC42. At day 365, the protein was found throughout the inside of the organoid, however not in clear contact to the apical region of the OLM (Figure 22d). Signal quantification showed a

significant increase of CDC42 inside of the RP ROs (0 – 40 µm) (Figure 22e-f). Interestingly, in the outside region, the pattern was reversed showing a signal decrease. A more detailed region classification in 10 µm steps showed that especially in the innermost layers, the signal increase was striking. Comparison of CTRL and RP ROs mRNA levels of *CDC42* confirmed that at all examined time points, an increase of expression was taking place in RP ROs (Figure 22g). At d80 and d125, this change was significant. The mRNA level of other Crumbs complex members and interaction partners (*CRB2*, *INADL*, *MPP5/PALS1* and *PPKCI*) was not changed. Of note, mRNA of the crumbs protein *CRB3* could not be detected (Figure 22g).

a

CRB1c PALS1 — CTRL | CTRL | RP | RP

b

Signal intensity relative to CTRL — Outside, Inside

c

Signal intensity

(-40)-(30) | (-30)-(-20) | (-20)-(-10) | (-10)-(0) | (0)-(10) | (10)-(20) | (20)-(30) | (30)-(40)

■ CTRL
■ RP

d

ARR3 CDC42 — CTRL | CTRL | RP | RP

e

Signal intensity relative to CTRL — Outside, Inside **

f

Signal intensity

(-40)-(30) | (-30)-(-20) | (-20)-(-10) | (-10)-(0) | (0)-(10) | (10)-(20) | (20)-(30) | (30)-(40)

■ CTRL
■ RP

g

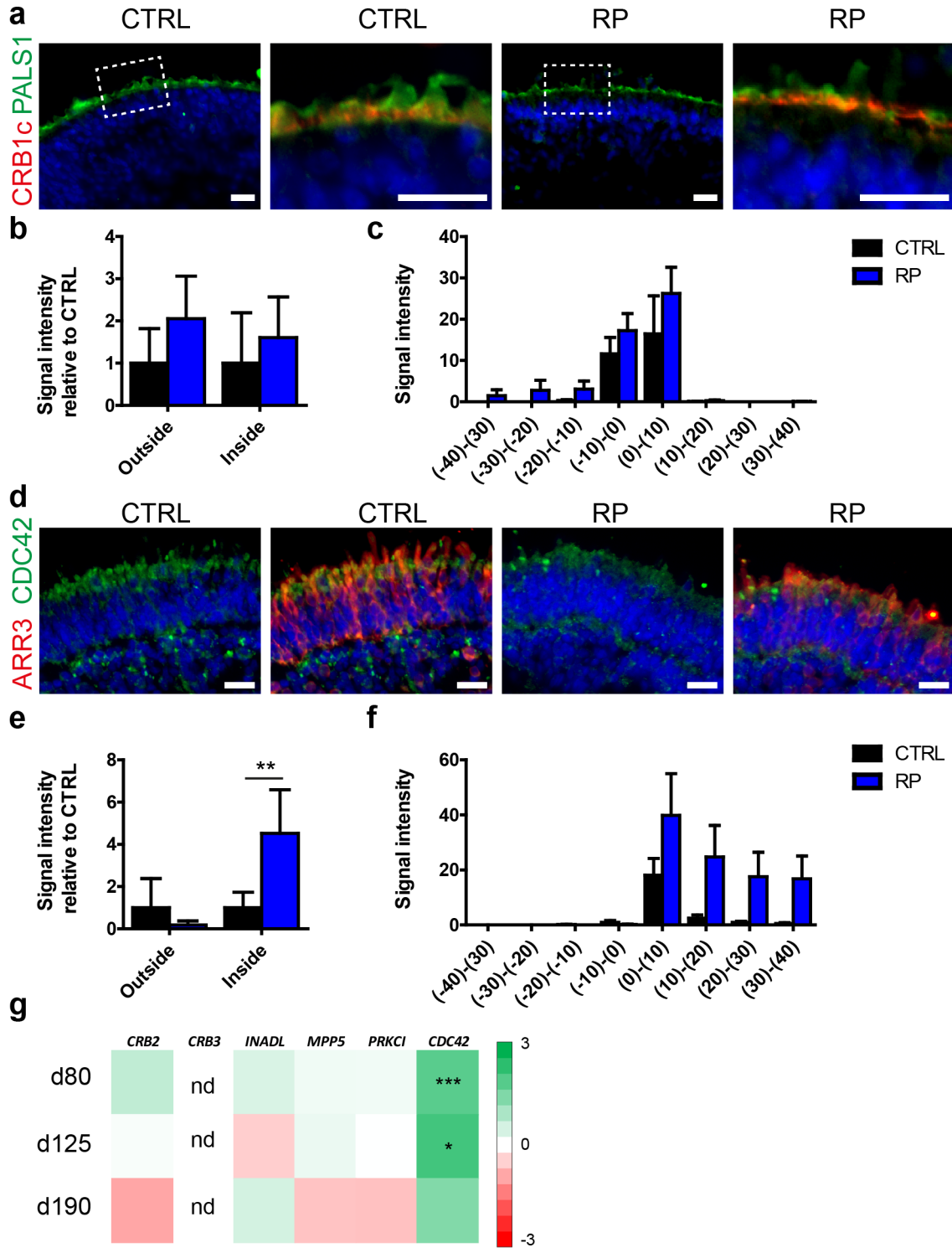|	*CRB2*	*CRB3*	*INADL*	*MPP5*	*PRKCI*	*CDC42*
d80		nd				***
d125		nd				*
d190		nd				

3
0
-3

Figure 22- Crumbs complex members in controls and retinitis pigmentosa retinal organoids

(a) CTRL and RP retinal organoids from day 365 of differentiation stained for PALS1 (green) and CRB1c (red). Spotted squares indicate the magnified areas shown adjacent to the individual images. (b) Quantification of the summed fluorescence signal of PALS1 from control and RP RO (d260) inside and outside of the organoid with the "Slope Approach" macro. Signal was summed between the OLM and 40 µm distance above ("Outside") and 40 µm below ("Inside") (1 CTRL lines, n= 11 images; 2 RP lines, n= 20 images). (c) Distribution of summed fluorescence signal for PALS1 in specified segments ((-30)-(-40) µm, (-20)-(-30) µm, (-10)-(-20) µm, (-10)-0 µm, 0-10 µm, 10-20 µm, 20-30 µm and 30-40 µm distance from the OLM; negative value are outside, positive value inside the organoid) based to the data acquired for (b). (d) CTRL and RP retinal organoids from day 365 of differentiation stained for CDC42 (green) and ARR3 (red). (e) Quantification of the summed fluorescence signal of CDC42 from control and RP RO (d365) inside and outside of the organoid with the "Slope Approach" macro. Signal was summed between the OLM and 40 µm distance above ("Outside") and 40 µm below ("Inside") (2 CTRL lines, n= 13 images; 2 RP lines, n= 14 images). (f) Distribution of summed fluorescence signal for CDC42 in specified segments ((-30)-(-40) µm, (-20)-(-30) µm, (-10)-(-20) µm, (-10)-0 µm, 0-10 µm, 10-20 µm, 20-30 µm and 30-40 µm distance from the OLM; negative value are outside, positive value inside the organoid) based to the data acquired for (e). (g) Gene expression analysis of crumbs complex members *CRB2*, *CRB3*, *INADL*, *MPP5*, *PRKCI* and *CDC42*. RP and control retinal organoids of differentiation day 80, 125 and 190 were normalised to the housekeeping gene *GADPH*. In the graph, expression changes to the individual controls are depicted as colour heat map. Shades of red indicate decrease, shades of green increase of expression in RP in comparison to the control as indicated by a colour bar (n= 6- 23). DAPI = blue. Error bars: S.E.M. ** p < 0.01. nd= not detectable. Scale bars: (a, d) 20 µm.

6.16. Expression analysis of signalling pathways potentially affected by CRB1 mutations

Previous publications showed that CRB1 has an influence on several developmental and cell cycle related pathways in the mouse retina (143). Therefore, I checked several of these pathways in RP retinal organoids by using Taqman™- assay based qPCR (Figure 23a-d).

At day 80, expression of all notch related genes was seen upregulated in RP RO (Figure 23a). The expression of Nicastrin (*NCSTN*), *PEN2* and *Presenilin-1* (*PSEN1*) was significantly increased d80. Interestingly, the expression of *HEY1*, a gene that is activated by the notch pathway was initially increased at day 80 and significantly decreased at d125 and d190. Alongside with this, also *APH1* levels decreased significantly at d190.

Next, I looked at genes, which are related to the wnt pathway (Figure 23b). At day 80 of differentiation, all tested genes were upregulated. 8 of the wnt genes (*CTNNB*, *CTNND1*, *LRP6*, *LEF1*, *DVL1*, *GSK3B*, *MYC*, *MYCN*, *DKK3*) were even significantly increased. In contrast to that, at day 190, 6 wnt genes, were seen to be decreased with beta-catenin (*CTNNB*) even been downregulated significantly (Figure 23b).

From the mTOR pathway- related genes, only *TSC2* was found to be increased significantly at d80 (Figure 23c). Finally, I measured the expression of some genes which previously have been observed to be upregulated in Crb1 or Crb2 KO mouse models (143) (Figure 23d). Among these genes, the sonic hedgehog gene *GLI2*, the histone protein *HIST3H2BB (H2BB)*, and *PTTG1* and *PTTG2* were significantly upregulated at day 80. *ESCO1*, a gene which is involved in sister chromosome pairing during mitosis, was also significantly increased at d125.

In summary, for many of the tested genes concerning different pathways and interaction proteins where CRB1 is potentially involved (Notch, wnt, mTOR, cell cycle and chromosomal organisation) an increase of expression at day 80 was observed. In contrast to that, some of the genes showed a decrease of expression at later stages.
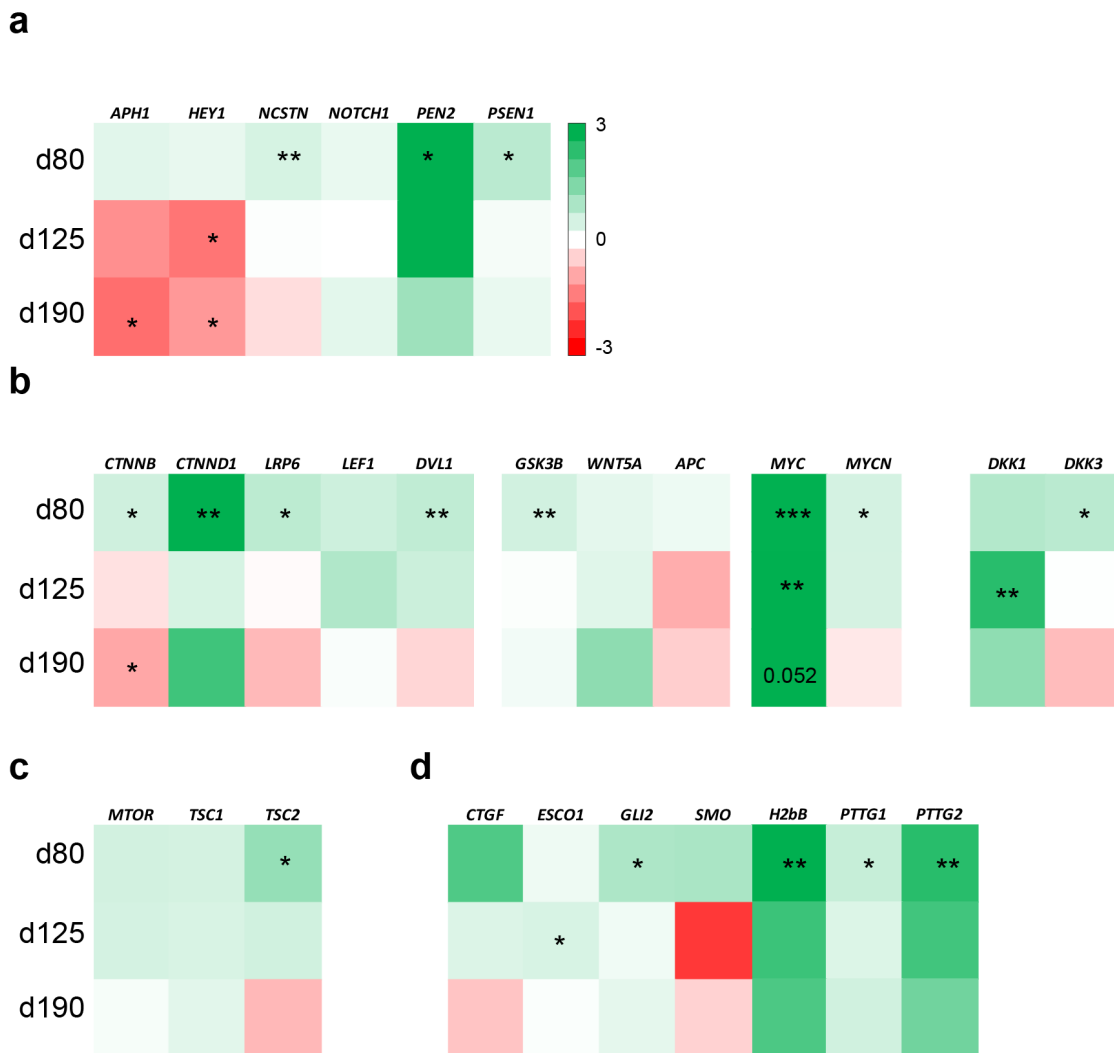
Figure 23- Expression analysis of signalling pathways potentially affected by *CRB1* mutations

Gene expression analysis of pathways potentially influenced by mutated *CRB1*. RP and control retinal organoids of differentiation day 80, 125 and 190 were normalised to the housekeeping gene *GADPH*. In the graph, expression changes to the individual controls are depicted as colour heat map. Shades of red indicate decrease, shades of green increase of expression in RP in comparison to the control (n= 6- 23) as indicated by a colour bar.(a) Notch- related genes *APH1*, *HEY1*, *NCSTN*, *NOTCH1*, *PEN2*, *PSEN1*. (b) Wnt related genes *CTNNB, CTNND1, LRP6, LEF1, DVL1, GSK3B, WNT5A, APC, MYC, MYCN, DKK1, DKK3*. (c) mTOR related genes *MTOR*, *TSC1*, *TSC2*. (d) Genes *CTGF, ESCO1, GLI2, SMO, H2BB(HIST3H2BB), PTTG1, PTTG2*. Error bars: S.E.M. * p < 0.05, ** p < 0.01, *** p < 0.001.

6.17. Assessment of calcium dynamics and photosensitivity in photoreceptor cells of retinitis pigmentosa patients

RO from patients and controls could be matured to a relatively advanced stage of differentiation with clear formation of inner segments and partly of outer segments (Figure 16). Further, the light sensing proteins Rhodopsin and cone-Opsins could be detected by mRNA and protein stainings (Figure 15). Therefore, I tested whether RO from controls and patients are sensitive to light exposure and perform downstream signalling on light stimulation.

For that, organoids were incubated with FURA-2-AM dye to measure the intracellular calcium concentrations (Figure 24a). In order to see calcium dynamics in PRC, cells in the exclusive PRC layer, which can be found on the surface of the organoid, were monitored for 5 minutes and 5 five-seconds-lasting light flashes were executed (see also material and methods section 5.2.17). Individual cells were identified and an activity map (number of calcium spikes in each cell) was created (Figure 24a). Interestingly, some of the recorded cells were spiking independently from the light stimulation, some reacted on the first light flash with calcium outflux, some cells on the last stimulus (Figure 24b). In-depth analysis of the spiking and counting of positive cells over several experiments showed that at day 200, around 2.5 % of the measured cells from CTRL RO reacted on light stimulation with calcium spiking and significantly less prior to the flashes (Figure 24c, d). For RPB, the number of cells reacting to light was much lower (~1 %), but significantly increased in comparison to the pre-stimulation period (Figure 24c, d). RPA RO showed a strong activity during and before the light stimulation (3 % of the cells), however independent of the light stimulation (Figure 24c, d). Finally, to assess the cell response, which can be attributed to the light stimulation, I calculated the difference of stimulated cells between stimulation and none stimulating period (Figure 24e). Here, both patients RPA and RPB showed a significant decrease of light-dependent calcium responses in comparison to the CTRLs. For RPA, the difference was even negative, reflecting a slight signal decrease during the stimulation period.

In summary, a substantial number of PRC from control persons are able to react with calcium outflux on light stimulation at day 200 of differentiation. In contrast

to that, patient RPA and RPB show a reduced calcium spiking in response to light stimulation.
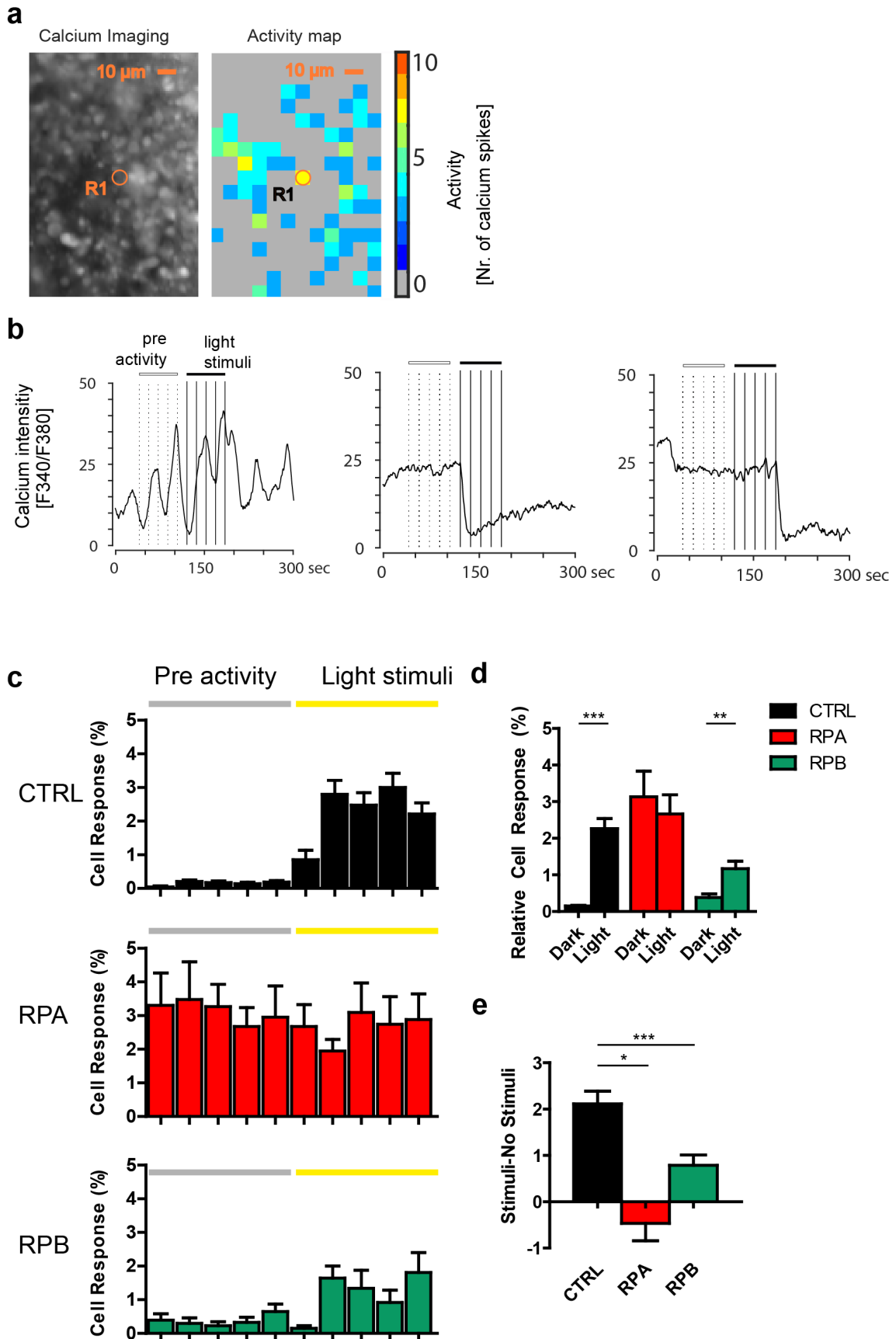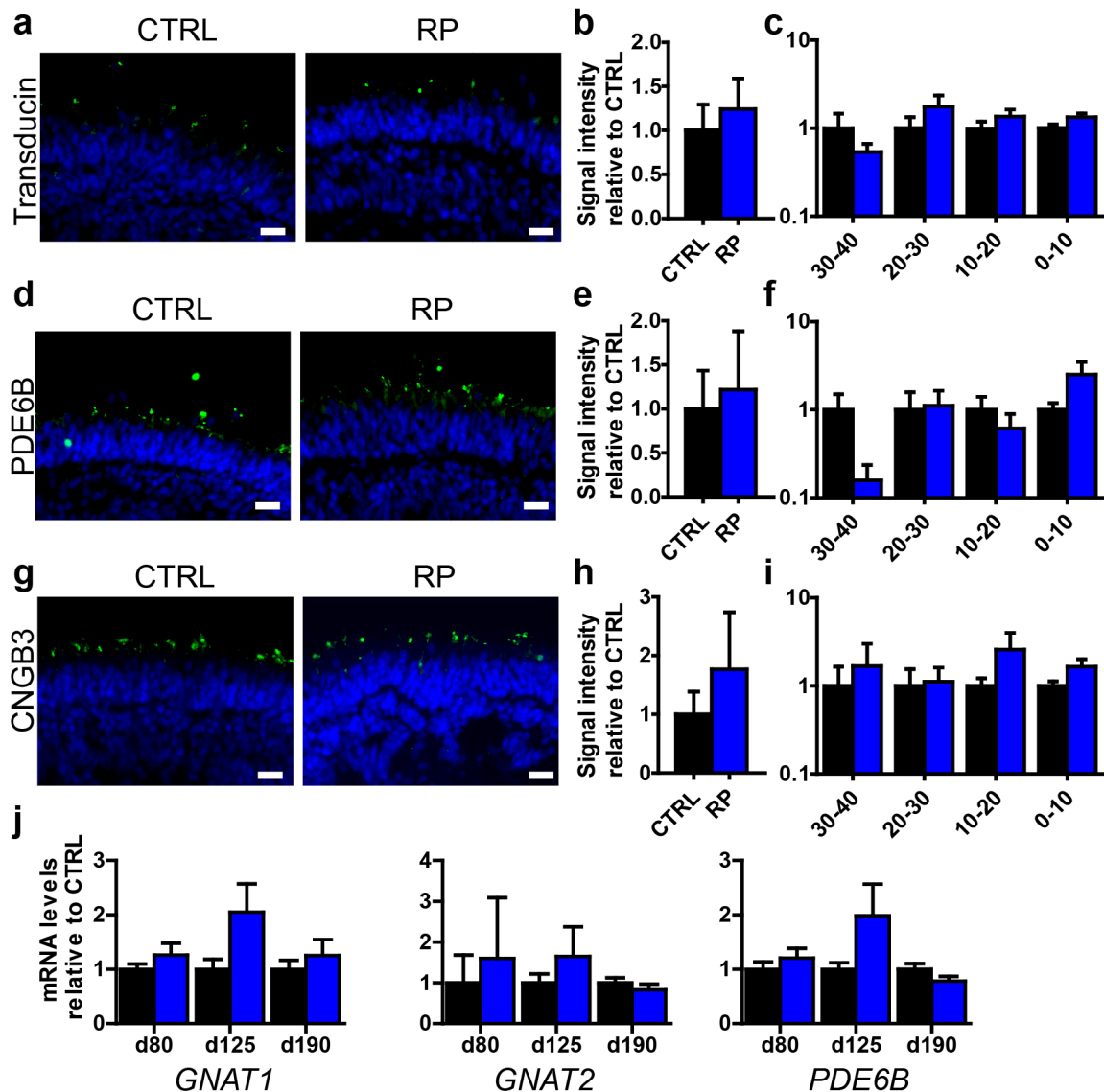
Figure 24- Assessment of calcium dynamics and photosensitivity in photoreceptor cells of retinitis pigmentosa patients

(a) Representative image of a d200 RO marked with the calcium dye Fura-2-AM (F340/380 Ratio) (left) and the respective activity heat map (right). Colour indicates the number of spikes during the measurement (300 s) in each spot. Spot size was chosen so that it contains approximately 1 cell. An example spot (R1) is marked in the centre. (b) Exemplary measurements of calcium intensity (F340/F380 ratio) of three individual cell measurements. Dotted lines indicate 5 pre-activity time points to determine baseline activity. Continuous lines indicate 5 light flashes (5 s each). Images indicate three different activity types: light-independent calcium spiking (left), calcium efflux on first light stimulus (middle), calcium efflux on last light stimulus (right). Total measured time was 300 s. Y-axis depicts F340/380 signal ratio, which is directly related to the calcium concentration. (c) Comparison of cell response between CTRL, RPA and RPB in d200 RO. Number of active ("spiking") cells (% of all cells) during the 10 marked positions shown in b). First 5 bars are pre-activity (baseline) measurements; last 5 bars are measured during light stimulation n= 15- 33 cells, 9 individual measurements with > 3 different sets of experiments. 2 control lines (k3, k8), 4 patient lines (RPA4, RPA16, RPB1, RPB12). (d) Comparison of mean "baseline" and "light stimuli" cell numbers from CTRL, RPA and RPB. Baseline values were calculated as mean of the 5 pre-activity positions illustrated in b) and c). Light stimuli values were taken from the 5 light stimulation positions. e) Difference between the number of cells active during light stimulation and pre-activity (baseline) for CTRL, RPA and RPB. Error bars: S.E.M. * $p < 0.05$, ** $p < 0.01$, *** $p < 0.001$. Scale bars: (a) 10 µm.

6.18. Analysis of proteins involved in the phototransduction cascade

The observation that ROs from RP patients show less light induced signals led to the question whether the phototransduction within the PRC segments is intact in RP photoreceptor cells. Therefore, I compared mRNA levels as well as protein levels by immunostaining and analysed the signal intensity with the "Slope Approach" tool (Figure 25). First, RO were stained for rod transducin, a G-protein which is activated by Rhodopsin conformation change (192). At day 365, transducin immunofluorescence signals was found in the PRC segments outside the organoid (Figure 25a-c). Comparing the total signal intensity outside the ROs (0- 40 µm), a slight increase of transducin in RP patient ROs (Figure 25b). Looking at the signal distribution in 10 µm steps showed that this increase was found for all ranges between 0- 30 µm, however not for 30- 40 µm (Figure 25c). Next, I stained ROs for the Phosphodiesterase 6β (PDE6B) (Figure 25d-f). At day 365, a similar signal pattern as for transducin could be observed. The total signal intensity in RP and controls was comparable, however in the range between 30-40 µm of segment length, RP ROs presented less signal intensity (Figure 25e, f). Similar results were observed for the CNG channel CNGB3. Here, in all measured ranges RP ROs were comparable to CTRLs (Figure 25g-i). Finally, I looked at the gene expression of the rod and cone transducin subunit alpha (*GNAT1* and *GNAT* 2, respectively) as well as *PDE6B* and *PDE6A* (Figure 25j and data not shown). For *PDE6A,* no expression was monitored, whereas *PDE6B*, *GNAT1* and *GNAT2* showed no significant aberration in RP retinal organoids.

In conclusion, I could not identify any apparent changes of phototransduction proteins in RP retinal organoids neither on mRNA nor on protein level.

Figure 25- Analysis of proteins involved in the phototransduction cascade

(a) CTRL and RP retinal organoids from day 365 of differentiation stained for rod transducin (Transducin) (green). (b) Quantification of the summed fluorescence signal of rod transducin from control and RP RO outside the organoid with the "Slope Approach" macro. Signal was summed between the OLM and 40 µm distance above (2 CTRL lines, n= 26 images; 4 RP lines, n= 26 images). Values are normalised to CTRL. (c) Distribution of summed fluorescence signal for rod transducin in specified distance segments (30- 40 µm, 20- 30 µm, 10- 20 µm, 0- 10 µm) from the OLM based to the data acquired for a). Values are shown on a logarithmic (log 10) scale and are normalised to CTRL. (d) CTRL and RP retinal organoids from day 365 of differentiation stained for PDE6B (green). (e) Quantification of the summed fluorescence signal of PDE6B from control and RP RO outside the organoid with the "Slope Approach" macro. Signal was summed between

the OLM and 40 µm distance above (2 CTRL lines, n= 24 images; 4 RP lines, n= 25 images). Values are normalised to CTRL. (f) Distribution of summed fluorescence signal for PDE6B in specified distance segments (30- 40 µm, 20-30 µm, 10- 20 µm, 0- 10 µm) from the OLM based to the data acquired for (d). Values are shown on a logarithmic (log 10) scale and are normalised to CTRL. (g) CTRL and RP retinal organoids from day 365 of differentiation stained for CNGB3 (green). (h) Quantification of the summed fluorescence signal of CNGB3 from control and RP RO outside the organoid with the "Slope Approach" macro. Signal was summed between the OLM and 40 µm distance above (2 CTRL lines, n= 25 images; 4 RP lines, n= 23 images). Values are normalised to CTRL. (i) Distribution of summed fluorescence signal for CNGB3 in specified distance segments (30- 40 µm, 20- 30 µm, 10- 20 µm, 0- 10 µm) from the OLM based to the data acquired for (g). Values are shown on a logarithmic (log 10) scale and are normalised to CTRL. (j) Gene expression analysis of phototransduction related genes *GNAT1*, *GNAT2* and *PDE6B*. RP and control retinal organoids of differentiation day 80, 125 and 190 were normalised to the housekeeping gene *GADPH*. In the graph, values are depicted as relative to d80 expression of control retinal organoids (n= 6- 23). DAPI= blue. Error bars: S.E.M. Scale bars: (a, d, g) 20 µm.

6.19. Improvement of *in vitro* retina modelling by introducing a novel microfluidic device called retina-on-a-chip

All previously performed experiments using retinal organoids to model a degenerative retinal disease such as retinitis pigmentosa *in vitro* led to the question whether there are feasible improvements increasing the validity and physiological value of the model. The retinal organoids, which were described in detail and studied in this thesis, showed features such as layering, synaptic connections and light induced responses, however lack certain features such as *e.g.* the crucial connection between photoreceptor segments and RPE cells. In that course, together with the Fraunhofer IGB Stuttgart, a next-generation microfluidic device based on the organ-on-a-chip technology (Figure 26) was designed and developed. A version of this "retina-on-a-chip" device is shown in Figure 26b. The chip was designed so that the organoid could be cultured in close apposition to an adherent layer of RPE inside a physiological hydrogel (Figure 26a). The chip itself can be nourished *e.g.* by medium which was applied by a pump from below the RPE layer (labelled as (S)). This configuration allowed the direct Interaction of rod and cone segments and RPE cells (Figure 26a, right image). In addition, the microfluidic chip system enables a closely physiological culture without mechanical stress, with a controlled flux of media, nutrition and compounds as well a physiological extracellular matrix. To observe the RPE-RO interaction site, living retinal organoids where marked with a fluorophore-labelled peanut agglutinin (PNA Lectin Alexa Fluor™ 568). In Figure 26c, a three-dimensional visualisation of a d260 retinal organoid with PNA lectin marked segments is depicted. The RPE cells could be transfected with an IRBP-GFP protein construct, which is able to mark RPE cells in green. After the chip was assembled, both PRC segments (Figure 26c-d, left top) and an RPE layer (Figure 26d, left bottom) could be observed individually via fluorescence microscopy. Using an Apotome microscope, an x-z view and a three dimensional image of the interaction side could be produced showing the close apposition of segments and RPE cells (Figure 26d, right images).

In summary, I created a new organoid-on-a-chip technology based device, which paves the way for improved next generation *in vitro* retina modelling, allowing the interaction of photoreceptor cells and RPE and combining it with the advantages of the microfluidic organ-on-a-chip technology.
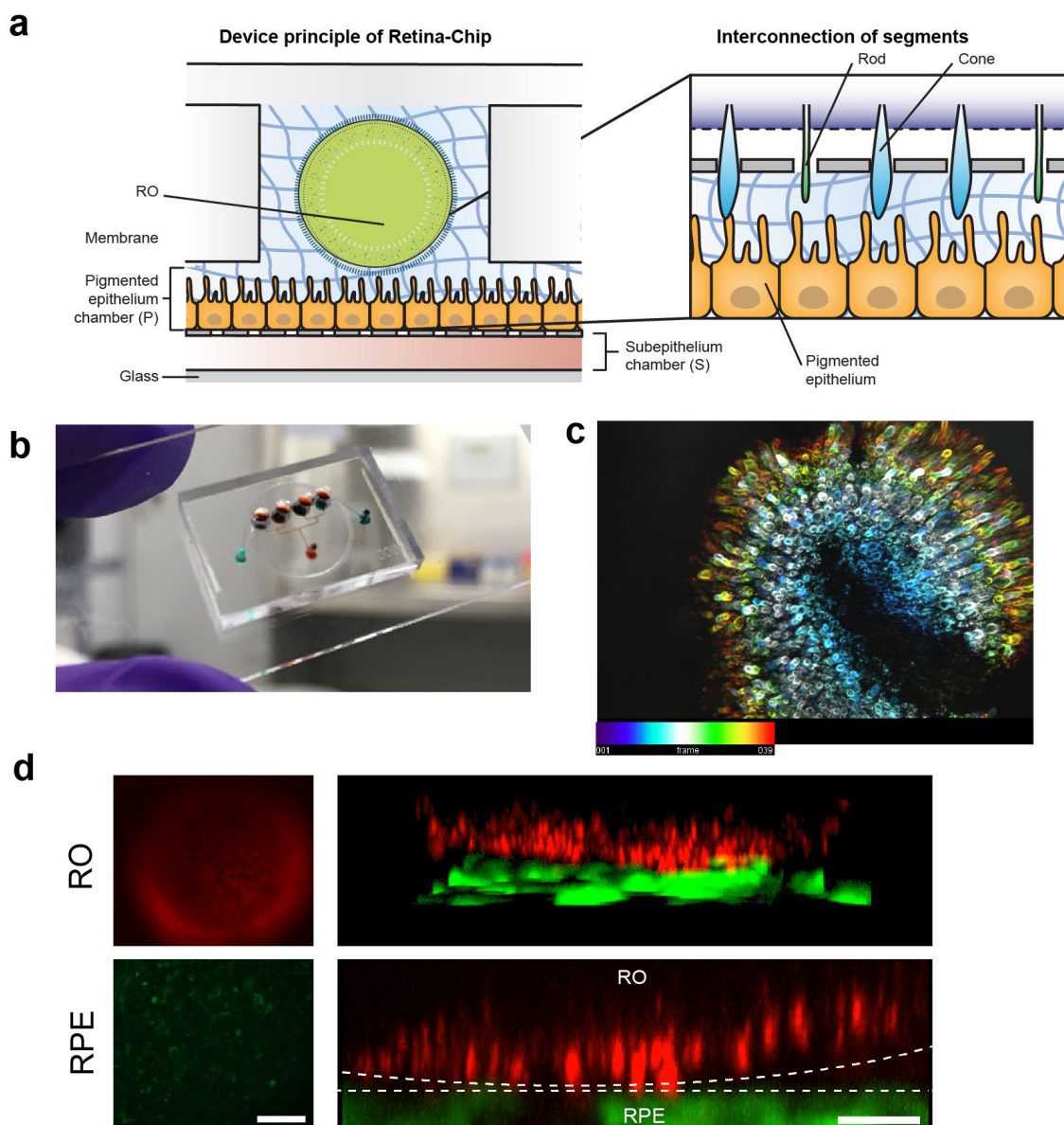
Figure 26- The retina chip as next-generation disease model

(a) Schematic image of the retina-on-a-chip device (left image). The chip has a RPE-organoid compartment, in which first the RPE (yellow) and then the organoid (green) is loaded. The RPE is cultured on top of a permeable membrane, which separates the culture chamber from the subepithelial chamber (S). Through this channel, the medium is supplied. The culture well is filled with hyaluronic acid-based hydrogel (HyStem®-C, indicated by blue grid). The set up enables the direct interconnection of RO segments from rod and cones (right image) with the RPE. (b) Picture of the actual engineered chip fabricated out of polydimethylsiloxane (PDMS). (c) Three dimensional reconstruction of a RO (day 260) dyed with PNA Lectin and taken with an Apotome microscope (Zeiss). To indicate different heights within the z-stack, a frame dependent colour coding was used as indicated by the colour bar. (d) Retina-on-a-chip with a PNA Lectin dyed RO (day 260) and RPE that was beforehand transfected with lentiviral IRBP-GFP construct. Left images shows a top view of the PNA Lectin labelled segments (red) and the IRBP-GFP labelled RPE (green). Image at the bottom right shows the x-z axis

of the z-stack taken with an Apotome microscope (Zeiss). Top right show a three-dimensional projection of the same recording. Scale bars: (d) 200 µm (left), 20µm (right).

7. Discussion

The main achievements of my work are: I) the establishment of a valid retina *in vitro* model based on iPSC derived retinal organoids and thereby setting the hallmarks of differentiation using bona fide cell markers and transcriptomic analysis. II) The establishment of methods analysing the differentiation and the functionality of these ROs including FACS- based transcriptomics, electron microscopy and calcium imaging. III) The application of the retinal organoids to model retinitis pigmentosa caused by *CRB1* mutations revealing an aberrant CRB expression pattern, alongside with potential changes in signalling and photoreceptor functionality. Finally, IV) the invention of a next-generation *in vitro* retina model introducing a microfluidic retina-on-a-chip device.

The following discussion will focus on four main aspects of this thesis:

1) Retinal organoid as a model for human retina development
2) The usage of an image analysis tool set for immunofluorescence signal quantification in retinal organoids
3) Modelling of retinitis pigmentosa caused by a *CRB1* mutation using retinal organoids
4) The application and perspective of the novel *in vitro* model retina-on-a-chip

7.1. Human iPSC-derived retinal organoids as a model system for the human retina

The development of *in vitro* retina models came a long way from primary retinal cell types to the establishment of stem cell derived single retinal cell protocols to the astonishing development of complex stratified retinal organoids showing physiological layering and function. The major aim of this thesis was to exploit the possibilities of these retinal organoids to answer developmental and pathophysiological questions by modelling retinitis pigmentosa caused by a *CRB1* mutation. In this section, I will discuss the potential of retinal organoids as an *in vitro* retina model as well as features, advantages and current drawbacks.

7.1.1. The use of iPSC-derived retinal organoids as *in vitro* model

The possibility to culture human embryonic stem cell (hESC) *in vitro* (176) and the discovery of human induced pluripotent stem cell (hiPSC) derived tissues in 2006 by Takahashi and Yamanaka (159) opened up new possibilities for creating new model systems as *e.g.* for the human retina. Before that, *in vitro* human system modelling was merely possible using cultured primary cells or immortalised cell lines. However, these models could not fully reflect all cell types and especially not their complex interactions. These requirements could be fitted by organotypic human explants, however those cannot be cultured for a long period, are limited in availability (especially for patients suffering from a specific retinal disease) and cannot be used for studying retinal embryology. Human ESCs and hiPSCs on the other hand are able to create virtually all tissues and cell types. Recently, the discovery of self-assembling organ-like-tissues derived from hESCs and hiPSCs brought *in vitro* models another step forward (183). So-called organoids are not only single or multiple cell types cultured in a dish, but reflect complex, three-dimensional layered structures building up physiological interconnections.

This opened new venues for the modelling of the human retina, which was until now predominantly done using animal models such as rodents, rabbits, dogs or pigs. Although these organisms share a common basic makeup with humans (also of the retina), they cannot fully reflect all aspects of the human retina. The mouse retina for example lacks trichromacy, contains a different photoreceptor distribution pattern and has no fovea centralis. Moreover, none of the mentioned animals shares the exact same molecular biology concerning the mRNA or protein equipment. Of note, studies involving apes and monkeys, which are quite similar to human, are expensive, time-consuming due to the long live span of the animal and above all ethically questionable.

In contrast, human iPSCs can be derived from virtually every individual and therefore patient-specific disease modelling is possible. In this thesis, I chose two patients suffering from retinitis pigmentosa caused by a single mutation within the *CRB1* gene. In mouse models, Crb1 KO could not fully reflect the phenotype observed in affected human beings (121). For the mentioned reasons, I decided to use hiPSC- derived retinal organoid to study the human retinal embryogenesis and the pathogenesis of retinitis pigmentosa caused by *CRB1* mutations.

7.2. Cell types and cell type markers of retinal organoids

7.2.1. Retinal pigmented epithelium

A detailed characterisation of RPE cells in retinal organoids was not shown in this thesis. Therefore, it will only described here briefly. RPE is one of the earliest cell types in the retina, which commits to its fate. During the establishment of the optic vesicle, retinal progenitors divide into neural retinal progenitors and RPE cells (72). Thereafter, the cells mature and become pigmented. Markers such as MITF, RPE65 and BEST1 can be found starting from different stages of development (74). In retinal organoids, which strongly resemble the optic vesicle stages, these cells can be found either as clusters attached to one side of the organoid or sometimes distributed throughout the organoid (data not shown). When extracted, these cells can be stained positively for the respective markers or cultured and propagated in an adherent culture (data not shown).

7.2.2. Ganglion cells

Ganglion cells are amongst the first retinal neurons, which can be found in a developing retina. Therefore, they are referred to as "early born". In human retina, they appear starting from fetal week 8 (193) and later form the optic nerve which projects to the lateral geniculate nucleus (LGN) inside the midbrain. In retinal organoids, ganglion cells were discriminated by the marker BRN3B, which can be found starting from day 40 (earliest time point analysed). Other publications come to similar results (184). Starting from this time, the cells will form a layer, which resembles the ganglion cell layer in the human retina. At later stages, the retinal ganglion cells start to disappear. At d125, they are cannot be identified anymore. The same effect has been also observed by others (184). A possible explanation might be a lack of adequate synaptic connection between the GC and brain neurons of the LGN. It has been observed previously that neurons, which form connections to the wrong targets cells, are likely to undergo apoptosis presumably due to the inappropriate release of neurotrophins by the target cells (194). Another explanation could be the central organoid malnutrition (due to missing vascularisation) or the missing of certain external survival factors usual provided by the surrounding cell types (such as NGF, GDNF or BDNF supplied *e.g.* by astroglia) (195).

7.2.3. Bipolar cells

In vivo, bipolar cells make the connection between photoreceptor cells and ganglion (or amacrine) cells. During vertebrate development, they are among the last cells which can be identified in the retina (77,196). In this thesis, two widely accepted markers for bipolar cells were used: PKCα and G0α. In human retina, both were identified as ON-bipolar markers (197). In retinal organoids, first positive cells were identified at late time points, namely at d190 of differentiation. These cells clustered at the outer synaptic layer (identified by bassoon and CTBP2, see Figure 17) and presumably formed synapses with adjacent photoreceptors (discussed in section 7.2.8).

7.2.4. Amacrine and horizontal cells

The family of amacrine and horizontal cells each consists of several subtypes (amacrine: around ~ 30 in mammalians, horizontal: 3 for humans) (198,199). Therefore, distinguishing between the individual subtypes is sometimes only possible due to morphological cues. In retinal organoids, amacrine and horizontal cells can only be identified due to certain markers proteins. In this thesis, Calbindin and AP2α were used. However, for both markers it was reported that they stain certain subtypes of both AC and HC (200,201) and in case of Calbindin even cones (201). Consequently, it was not possible to distinguish between the individual populations with absolute certainty. One hint might be soma positioning within the organoid. Staining for AP2a mostly stained the innermost cells (*e.g.* at day 260, Figure 14c), where amacrine would be expected. In some cases however, AP2α-positive nuclei could be also found adjacent to the photoreceptor layer, indicating a horizontal cell identity (data not shown). Similar observations were also made for Calbindin (Figure 14b). The first signals for both antibodies could be observed starting from day 80, which fits to the long period in which amacrine and horizontal cells are established (76).

7.2.5. Müller glia

As the most abundant glial cell type in the retina, Müller glia are of great importance for the function and stability of the retina. For instance, their end-feet generate the inner and outer limiting membrane and form apical microvilli in the subretinal space (53). In retinal organoids, first Müller glia can be observed at around d190. From this time ongoing, the marker CRALBP strongly labels the inner layers of the organoid, where small processes penetrate the outer nuclear (photoreceptor) layer and generate connections to the outer rim, where the OLM is located (Figure 18). This is comparable to what can be observed in the mammalian retina (202). Another known marker for mature Müller glial cells is Glutamine synthetase (203). Interestingly, this marker can be found at the same developmental time-point; however, at later time-points (d365), the staining becomes restricted to a distinct cell population (Figure 18). This could mean that at late stages of development, mature Müller glia produce much larger amounts of the Glutamine synthetase, and the protein therefore could be used as a potent marker for mature Müller glial cells. Of note the protein GFAP, which is strongly expressed in astroglia or activated Müller glia (204), can only occasionally be observed in retinal organoids (data not shown). Either this could proof the presence of astroglia in RO or that, triggered by external stimuli like degeneration or malnutrition, activation of Müller glia is taking place. If the latter would be the case, GFAP could be considered as marker for tissue injury such as retinal degeneration.

7.2.6. Photoreceptor cells

As the light-detecting cell, the photoreceptor is the most crucial component of the retina. A degeneration even of a fraction of the photoreceptor cell population can lead to severe conditions such as retinitis pigmentosa, age-related macular degeneration, amongst others (103,205).

Retinal organoids harbour all four known photoreceptor types found in human: rods, small-, long-, and middle-wave cones. The first signs of photoreceptor cells can be found at around day 40. At this time, first cells can be stained for the bona fide photoreceptor marker Recoverin. This is much like previous publications had already shown (183,184). The population of Recoverin- positive PRCs would enlarge over time and around d100- 125, the photoreceptor will occupy the complete outer layer of the

retinal organoid (Figure 15a). This layer can be seen as the equivalent of the outer nuclear layer *in vitro*. Of note, unlike in the healthy human retina, the occurrence of photoreceptor cell bodies outside the photoreceptor layer is common even in ROs from unaffected persons. The markers used for distinguishing photoreceptors, rods and cones in peculiar were chosen from previous publications and are based on the observed *in vivo* expression in animals and man. The marker Arrestin 3 for example was observed to be a suitable marker for cones, as its expression was seen to be present already early in cone development (31,206). Marker proteins such as Rhodopsin, L/M-opsin and S-Opsin are obvious and can be seen as "definition" of a rod or cone cell classes, respectively. Photoreceptors *in vivo* show two major important functional domains, which should be reproduced in a valid *in vitro* model: The end-feet containing the ribbon synapses and the inner and outer segments containing the chromophore and a specialised shape ("rod" or "cone"). The first shall be discussed in the "synaptic connections" section (7.2.8.).

The observation of segments is one of the most astonishing and intriguing features of the three dimensional retinal organoids. Before that, only simple process-like structures could be observed in *in vitro* adherent cultures, which could be hardly recognised as segment structures, neither by markers nor by ultrastructure ((177,179)). In ROs, the makeup of segments is reminiscent of the *in vivo* segments: Beginning from day 125, inner segments can be distinguished, outgrowing from the retinal organoid rim. Initially, only striving few micrometres in length, inner and possibly outer segments have been found with more than 40 µm (Figure 16). Inner segments in ROs display numerous mitochondria, which later even cluster at the most apical inner segment regions (Figure 16, data not shown). Both features are shared with the human retina as well as the formation of connecting cilia at the inner segment tip. The formation of outer segments, which *in vivo* are formed by double lipid membranes forming stacks (called disks), was only rarely observed. Even at very late time points (d190, d260), only a handful of these structures were found by electron microscopy. This could be the consequence, at least in part, be partly due to the relatively rigid process of fixation and staining, but also by the mechanical stress, which is put onto the fragile structures in suspension dish cultures. In addition, as pointed out later, I assume that the lack of RPE is fatal for the final maturation of these structures.

A vital part of this thesis was to identify potential inner and outer segment markers in order to distinguish between these structures in immunofluorescence images. Amongst them are markers which have shown to be specific in *e.g.* rat retina (207) and human (208). From the tested outer segment markers Pepherin2, ROM1, Rhodopsin, Opsins, PDE6B amongst others, most were already found early in the development (*e.g.* Peripherin2, Rhodopsin at day 125, data not shown) and in close apposition to the OLM. In combination with the information gained from ultrastructural analysis, I assume that these markers are expressed already in early forming segments, which are most likely not containing disks or outer segments. ROM1 as well as PDE6B were amongst the most promising markers. Their expression was rare even at late time points (d190) and showed a more apical distribution pattern. In co-staining with Na$^+$/K$^+$ ATPase α3, I could show that ROM1 is very often but not exclusively expressed apically from "inner segments" which can be labelled by the Na$^+$/K$^+$ ATPase α3 (Figure 16j). I therefore assume that the markers tested might staining outer segment- like structures, however not exclusively. A valid exclusive outer segment marker is therefore yet to be found.

One way to overcome this issue would be the finding of a reliable inner segment marker. An interesting candidate is the Na$^+$/K$^+$ ATPase α3, which was found to be specific for inner segments in rat tissue (207). In RO, it showed a specific staining of some segments at late time points (d260, Figure 16j). From that it could be hypothesised, that this marker is indeed specific of inner segments. However, only at a mature state.

In summary, both inner and outer segments can be stained for markers, which have been established for this purpose *in vivo*. Still, these markers might not be compartment- specific during development or the retinal organoid develop differ in this respect from the embryonic development.

7.2.7. Retinal organoid layering

Amongst the most astonishing features of the retinal organoids is their ability to form an accurate layering of the retinal cell types with distinct cell types in each layer. In the organoids described in this thesis, most of the vertebrate retinal layers can be identified

and are organised in the correct order. The inner most layer is an exclusive ganglion cell layer (until the GC disappears), whereas the inner nuclear layer contains amacrine, bipolar, horizontal nuclei as well as Müller glia. In the outermost organoid layer, photoreceptor nuclei and cell bodies are found exclusively, forming segments, which grow outside the organoid. This outside organoid layer could be compared with the segment layer, which *in vivo* contains exclusively the inner and outer segments of photoreceptors. Between the inner and outer nuclear layer, a distinct gap can be found starting from day 125. This gap is free of nuclei and instead filled with synapses which can be stained positively by the ribbon synapse markers Ribeye (Figure 17) and Bassoon (data not shown). In contrast to that, the synapse layer, which would be expected between the ganglion cell layer and the inner nuclear layer, was not found and to my knowledge not described in the literature yet. This might be caused by the early degeneration of ganglion cells (before day 125) before the bipolar cells can even form (starting from day 190 on). Finally, the retinal organoids display inner and outer limiting membranes, from which only the outer limiting membrane sustains at later time points (inner limiting membrane was not shown in this thesis) making up the outer rim of the organoid. The OLM can be identified with a respective marker (ZO-1) and by ultrastructural imaging (Figure 19). In RO, they separate the cell bodies of the photoreceptors from the PRC segments, a feature reminiscing of a human retina.

7.2.8. Synaptic connections and wiring

The retina contains two exclusive synaptic layers representing one of its main features, the pre-processing of the visual information before it enters the brain and the consciousness. Therefore, the presence of synaptic structures are a crucial aspect for reflecting the retinal functionality in a model. Retinal organoids have already been described to contain so-called ribbon synapses (185). These ribbon synapses have a specialised makeup containing anchor points for numerous Ca^{2+} and glutamate containing vacuoles in order to the supply the great demand of synaptic transmitter which is necessary for the constant dark current (33). Therefore, these structures can be easily identified by respective markers (CTBP2= Ribeye or Bassoon) or in ultrastructural analyses. I could identify the presence of these synapses between the photoreceptor layer and bipolar by immunofluorescence and electron microscopy

(Figure 17). In addition, I could see that the puncta of ribeye are located between the end-foot of photoreceptors and the processes of bipolar cells. Therefore, I can assume that indeed these synapses are formed between PRC and bipolar cells and are potentially functional. As described in the previous section, synapses between ganglion cells, bipolar cells and/or amacrine cells have not yet been found or identified. Moreover, the so-called triad between PRC, BC and amacrine cells was not yet found.

7.2.9. Light responsiveness

The most vital function of the retina is to detect light quanta and process this information into the brain. Therefore, a potent *in vitro* model should be able to recapitulate this important functionality. In the vertebrate retina, the proteins Rhodopsin and Opsin are responsible for the light absorption. Thereafter, a cascade of proteins multiplying and passing on the information until a CNG channel inside the membrane of the photoreceptor segments is closed causing a hyperpolarisation of the photoreceptor membrane (28). Ultimately, this leads among other effects to a decrease of calcium ions and a decrease of glutamate exocytosis (25). To reproduce this process *in vitro,* all the necessary proteins need to be expressed and found in the right location. As already described, photoreceptors of retinal organoids for inner segments and primitive outer segments contain some membrane stacks. As previously shown by others, I could confirm as well that the most vital proteins for phototransduction are expressed and can be found in the formed segments (Figure 25 and (184)). One way of measuring the response of the photoreceptor cells is patch clamp electrophysiology, already performed in Zhong *et al*. (184) and Busskamp *et al*. (209). Both could show individual cells reacting with current changes on light stimuli. However, those cells were only few in number and by electrophysiology only single cells and events could be monitored.

In my thesis, I used calcium imaging, a live cell method based on the fluorescence labelling of calcium inside cells. In my experiments, which were performed in cooperation with Wadood Haq, I could show that photoreceptor cells were spontaneously displaying calcium in- and efflux. However, applying white light stimulation of 5 s to d190 organoids, I could show that around 3 % of the recorded cells per experiment (around 6 cells/recording) showed calcium dynamics during the phase

of light stimulation. When adding up all performed experiment, this is a far larger number of cells than what has been reported before (184,209). From this, I can conclude that at d190, a small fraction of cells are light sensitive and calcium imaging is a useful tool to detect numerous light induced signals, making it a useful readout method for the functionality of the retina organoid.

7.2.10.   Current drawbacks

Although retinal organoids can reproduce many complex and astonishing aspects of a mammalian retina, they still lack many important features and the protocols are in need of optimisation and adjustment. Following the Zhong protocol, retinal organoids are derived from an ectodermal differentiation to neuroepithelial cells (184). Hence, they lack all cell types, which are originating from other germ layers and non-retinal tissues such as (embryonic) mesoderm (epithelial cells, microglia, extra-retinal mesoderm). Further, they share with other organoids the problem of a missing vascularisation. Therefore, they are limited in (organoid) size and are prone to central malnutrition and degeneration.

Another important feature missing is the fovea centralis. At this structure, a special make up is implemented (only cones, specialised ganglion cells, etc.). In diseases such as the age-related macular degeneration, it is especially vulnerable to degenerative effects. In the future, a specialised modelling of this structure would be of enormous interest.

Finally, the retinal organoids are facing the problem of an uncompleted maturation. This becomes most obvious for the photoreceptors, which are present for more than one year in RO but never reach a fully matured segment structure. The inner and outer segment-like structures described in this thesis and by others (184,185) are still immature and especially the stack formation of outer segments is incomplete and unorganised. This could have three major reasons: first, in a non-static suspension culture, the segments are always exposed to mechanical stress and therefore the fragile outer segment structures might be lost. Second, the segments are usually implemented in a specialised extracellular matrix (interphotoreceptor matrix), which supplies mechanical stability and important growth and developmental factors (210).

Third and most importantly, the photoreceptors lack the direct connection to the RPE, which are crucial for the survival and maintenance of the segments (211). Therefore, it was already surprising that segments are generated without a direct connection to the RPE at all. It can only be assumed that for the survival and the final maturation of the segments, the RPE is still indispensable. In other publications, the problem of RPE-segment interaction was solved by using more advanced retinal organoids, which have been developed to optic cups (212). Here, the RPE-neural retina are already faced to each other and the interaction can occur. However, these structures were only shown to be cultured for around 100 days, which was insufficient for a matured segment development. In this thesis, I tried to solve this problem by implementing retinal organoids and RPE in a microfluidic chip and get them in close interaction. The features of this chip will be discussed in the last sections.

7.3. Stereotypical image analysis

One of the major problems one has to face when working with *in vitro* models is first to find meaningful readouts for developmental and pathological changes and second to find efficient and reproducible ways to quantify them. Especially data gained from microscopic fluorescence images is hard to analyse in a fast and unbiased way. In the endeavour to solve these problems, I created a set of semiautomatic ImageJ/R- tools called "Slope Approach". This toolset is able to analyse large sets of image data and to create numerous ways of quantifying intensity and position of fluorescence signals. In the next sections, I want to describe which prerequisites the data needs to fulfil, which kind of analysis can be done with this tool, which limitations it holds and finally where this tool could be useful.

7.3.1. Overview of the Slope Approach tool and image prerequisites

The "Slope Approach" tool is based on the assumption that the imaged structures (or slices of them) have a stereotypical makeup. This should mean that relative to a definable zero line, every orthogonal to each point on the zero line has the same principle layout. In the case of the retinal organoid, the zero line can be defined as the OLM and all the retinal layers are organised in an orthogonal orientation to it. For

example, the PRC segments can only be found above the OLM (approx. -40- 0 µm from the OLM), the photoreceptor layer beneath it (0- 40 µm). The inner layer which follows the PRC layer should then always be in the same distance to the OLM (approx. 40 µm and more). If the thickness and orientation of these distances are stable over single organoid images or several organoids of a condition, they can be summed up to a stereotypical profile, which is representative for every organoid or every sample category (examples can be found in the methods section 5.2.24). Since sectioned organoids are circular, the tool takes the curvature in account and produces a corrected straightened image (Figure 7a,d). Since organoids are not perfect in many respects (especially the round shape), the selection of the zero line has to be performed manually. This makes the tool "semi-automatic" and enables the maximum processing of 60 -120 images per hour.

7.3.2. The Slope Approach tool box

Once the tool processes the pictures, those can be used for numerous analyses. A simple way of analysis would be to produce a reconstructed image from the values, which have been recorded initially (Figure 7d). This straightened image can be used for *e.g.* counting of segments and measuring the length with another ImageJ macro called "CountingHighest". This tool enables the user to mark structures (*e.g.* segments) at a certain position (*e.g.* the tip of a segment). From this data, the tool can calculate the number of segments in a certain organoid circumference and measure the length from the tip of the segment to the OLM. This analysis form was performed in Figure 16 to measure the length and number of segments at different time points of RO development.

A more complex version of analysis is the profile line (see Figure 7b). This line is a representation of the signal intensity of a fluorescence staining in relation to the OLM (as zero point). A marker protein that is expressed in the segment layer will show a peak in the negative range, in the PRC layer a peak in the positive range, respectively.

If the intensity information of the individual pixel is not demanded, a background threshold can be set and the images can be analysed in binary "signal- no signal"-way.

This is *e.g.* useful when the compared images are not stained with the same antibody dilution or if the image is partly overexposed.

7.3.3. Limitation of the Slope Approach tools

Major limitations can be found in the variability of the data. Especially in older organoids, in which central areas are partly degenerated, some of organoids lack the inner layers, compromising the summed pixel values for these ranges. Therefore, the images have to be preselected carefully as well as the range for the analysis.

Another major issue is debris or background on the slides or the images. Debris can compromise the data set strongly. Hence, preselection of the area that is being analysed is vital. In addition, the programme recognises automatically strongly stained or overexposed areas and removes them from the data set (replaced by a background value). To remove background, two options are thinkable: First, the values for the background can be set manually and chosen from the acquired images. Second, a second antibody control for each sample can be used as background values. In this thesis, the first way was used.

7.3.4. Use of the Slope Approach tools as read out method

Some of the possible applications for the tool are presented in this thesis: first, it can be used to compare the number and length of certain structures starting from a zero-point (here: segments). Second, it can be used to quantify and compare signals from total ranges or small portions of ranges in order to recognise if certain markers are differentially expressed only in some areas. Third, it can be used to identify shifts of signal distributions. For example, an increase of segment length during the organoid development can cause outer segments markers too shift away from the organoid. Fourth, the tool can be used to identify the purpose and layer position of a certain marker. If *e.g.* a marker is strongly expressed in the OLM, its function is potentially linked to this location. On the base of this for each marker, a stereotypical profile plot can be created. Figure 27 shows this for some of the markers used in this thesis. In the future, the tool could be used for unknown proteins. Here, the profile line could

make a prediction of the expression and hence maybe function in an unbiased and automatic way.

In summary, the Slope Approach tool set is a promising tool for fast analyses of data gained from retinal organoids. It might be able to serve data for readouts in disease or compound testing studies, where certain marker protein are altered or their location is changed. Of note, the tool might not only be used for retinal organoid data but could be applied to any other stereotypical data sets. One possible could be *e.g.* sections of a mouse or human retina, which has, depending on the position, a similar stereotypical makeup.
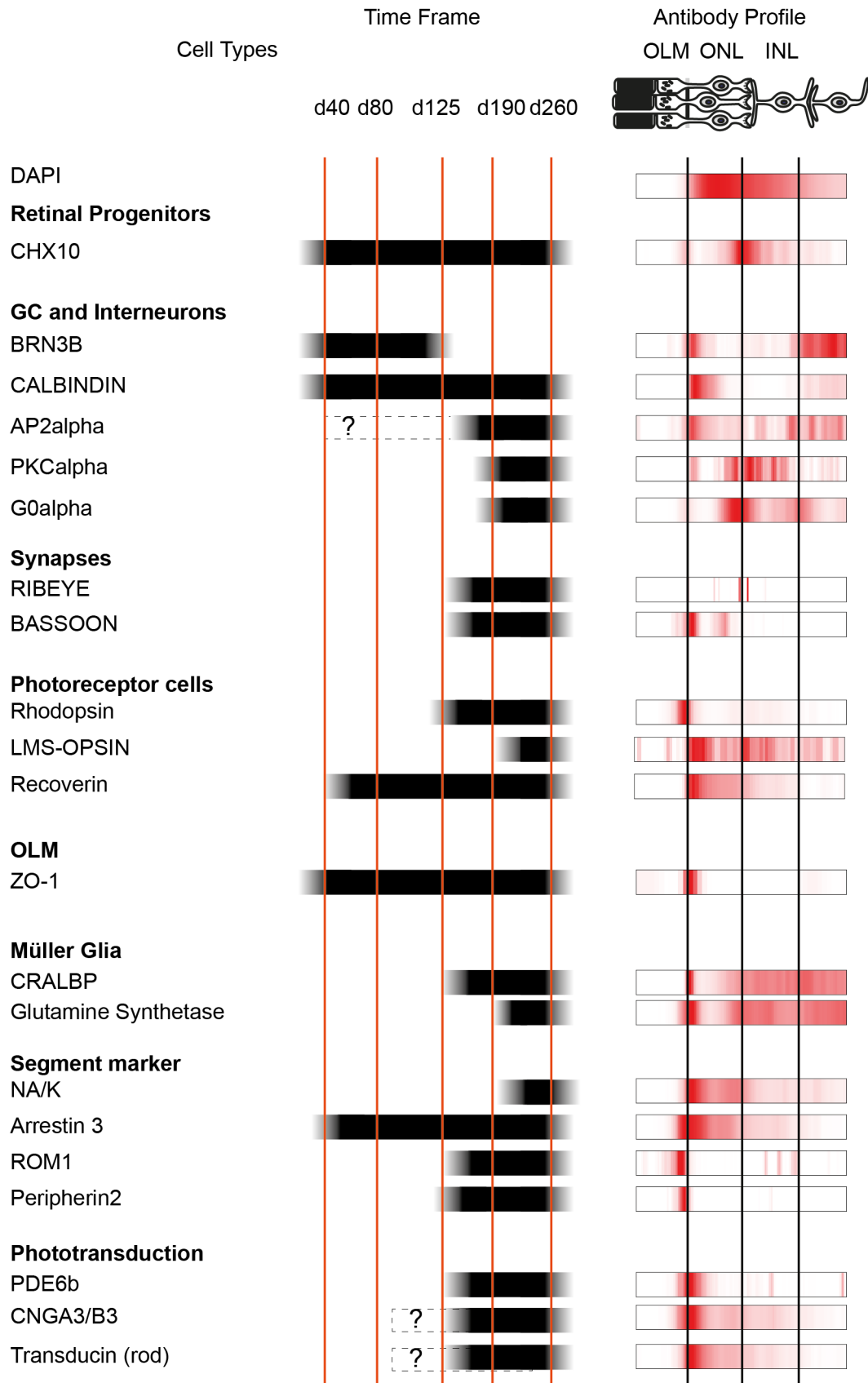
Figure 27- Expression patterns of retinal organoid cells and structure specific markers

This figure shows markers for retinal cell types and structures as listed. For each marker, the expression time frame during the organoid differentiation was assessed and is depicted as bar (middle column). Time points where expression is assumed but has not been evaluated are marked with dotted bars and question marks. Right column shows the vertical stereotypic profile for each antibody staining within the retinal organoids analysed at d80 (BRN3B, Calbindin) and d365 (all others). An approximated depiction of the retinal layers was added for comparison (top).

7.4. CRB1 RP disease modelling

The main goal of this thesis was to use retinal organoids as a disease model for retinitis pigmentosa caused by a genetic mutation. For that purpose, I chose *CRB1*, a gene most likely related to the establishment and maintenance of cell polarity (123,131). In photoreceptors, it is assumed to stabilise the formation of segments and to organise the proper positioning of cell types (136). In mice, *Crb1* KO leads to the formation of rosettes which are unorganised areas within the retina (121). In human patients, *CRB1* mutations lead to a thickening of retina, probably caused by an increase of proliferation (or decrease of embryonic apoptosis) as well as progressive photoreceptor cell death (117). CRB1 has been linked to retinitis pigmentosa and Leber's congenital amaurosis, which are both similar in the main features of retinal cell death, but differ in the age of onset. The two patients whose cells have been examined in this study were diagnosed with early-onset retinitis pigmentosa with first symptoms appearing during early childhood, but not present at or right after birth as it is observed in LCA patients. Both patients are brothers and have been diagnosed with a point mutation leading to a 1 amino acid exchange (cysteine -> tyrosine) at position 948 of the CRB1 gene (C948Y). While working at this thesis, this diagnose was confirmed by sequencing (see Figure 8). If the patients also share the common CRB1 RP feature of a thickened retina is not known. Interestingly, both patients displayed a different severity of the disease with the older brother (RPA) being blind at age 23 and the younger brother still able to see (age 18). This is not surprising since the C948Y mutation is known to cause a wide range of different onsets and syndromic features (110). In this thesis, I mostly focused on changes that occurred in both RPA and RPB organoids and therefore no patient-specific data is shown (except for calcium imaging). For the future, a more detailed

examination between the two patients might reveal some specific cues, which could influence the severity, onset and pathophysiology of the disease.

7.4.1. Main findings of this study comparing CRB1 retinitis pigmentosa retinal organoids and controls

The main findings of this study comparing CRB1 retinitis pigmentosa retinal organoids and controls are summarised in Table 16. In the following sections, they are discussed in detail.

Table 16: Summary of results

Feature	Major patient findings
RO morphology	Normal RO morphology
Retinal progenitor cells	No changes for the progenitor marker VSX2
Apoptosis	Decreased number of apoptotic cells in the PRC layer
Proliferation	No changes observed
Neural cell types	All neural cell types present
Synapses	Normal synapse formation
PRC	Normal rod and cone formation
Müller glia	Decreased protein signal in inner layer at d260, decreased mRNA expression for *GLUL* and *HES5* at d190
CRB1	Decreased protein signal, unchanged mRNA
Crumbs complex	Increase of CDC42 protein signal and mRNA expression
Developmental pathways	Increased mRNA levels for Notch, mTor and wnt genes at d80
Light sensitivity	Decreased light sensitivity at d190
Phototransduction	Unchanged protein signal for PDE6B, Rod transducing and CNGB3

7.4.2. Differences in retinal organoid development and cell type specification

Overall, retinal organoids from CRB1 RP showed a normal morphological appearance and no obvious signs of an altered cell type composition (Figure 11- Figure 18). Quantification of the cell distribution was not feasible, since the retinal neurons and especially photoreceptor cells showed a variable distribution pattern and occasionally formation of rosettes even in controls. Therefore, the mislocalisation of cell types and the half-rosettes observed in knockout animal models for Crb1 (121) or Crb1/Crb2 conditional KO in retinal progenitors (cKO) (143) could not be evaluated in organoids. Another aspect in the human CRB1 RP pathology was the observation of an unusual thickened retina (117) in patients. In addition, in Crb1/Crb2 cKO, an increase of proliferation was observed (143). Based on this data, I hypothesised that *CRB1* mutated retinas either harbour an increased pool of retinal progenitors, have an increased proliferative potential or undergo less apoptosis during the development. I could not find hinds for the first and second hypothesis, since no increase of proliferation (KI67, BrDU application for 24 hours, Figure 12) was found. However, matching to the third hypothesis, I saw a decreased rate of apoptosis in the photoreceptor layer at later time points (d190-d260, Figure 13). Nevertheless, the quantification of the organoid growth during a defined developmental period (d60- d80) showed no apparent differences (data not shown) and therefore an increase of proliferating progenitors is still in question.

One further pathological feature which was observed in Crb1/Crb2-cKO mice was an increase of late born cells (Bipolar cells, Müller glia, glycinergic amacrine cells and GABAergic amacrine cells), and their progenitors (143). Expression analysis of marker genes in RP retinal organoids showed a significant increase for several early born cell types (*ATOH7* for ganglion cells; or *NEUROD2* for amacrine cells) and a decrease for the late born bipolar cells (*PKCA*). *PROX1*, a marker for horizontal cells (late and early-born). These results could however not be confirmed by immunofluorescence staining of the respective antibody markers, where most cell types appeared to be too variable in number and localisation to be quantified. For rod photoreceptors for example, a high variability within a group of samples was observed (from 0 % to more than half of all photoreceptors, data not shown), which made a meaningful quantification hardly possible. In the future, a possible solution to this might be a more defined external

environment *e.g.* by the implementation into an organ-on-a-chip system with a constant medium supply.

Next, I was especially interested whether the *CRB1* mutation of the two patients examined could influence the number and morphology of Müller glia cells. The Müller glia cells are, beside the PRC, one of the assumed cell types that express CRB1 in the human retina (120). Besides, Crb1 KO mice displayed a decreased size of Müller glia cell villi in the inferior temporal quadrant, accompanied by increased GFAP expression in the same area (191). In ROs, I found that the quantified signal for the Müller glia CRALBP was significantly decreased in the innermost layers at d260 (Figure 18). This data however has to be seen with great caution since central degeneration occurred in many organoids independent of controls and patient groups and a more detailed study of the Müller glia fate has to be undertaken. However, in line with the decreased antibody signal, a decrease of mRNA levels of Müller glia markers (*GLUL* and *HES5*) was observed, which would fit to the quantified protein signals. The occurrence of GFAP-positive activated glia was a rare event in retinal organoids (data not shown) and could not be attributed to patient or control ROs.

Lastly, I checked whether the degeneration of photoreceptor cells was reproducible in RP ROs. For that cause, I first examined the development of rod and cone photoreceptors and especially the proper formation of the segments. For both aspects, I could not find obvious degeneration events or changes in the localisation and compositions of the photoreceptor population (Figure 15 and Figure 16). On the other hand, some examined markers of photoreceptors and segments (ARR3, PDE6B) seemed to be increased in RP ROs (Figure 16 and Figure 25). Moreover, the number of apoptotic cells at late differentiation states (d260, d365) was even decreased (Figure 13). The reasons for the absence of photoreceptor degeneration could lie in the lack of incomplete photoreceptor development and/or the missing photoreceptor-RPE interaction. As described earlier, the photoreceptor-RPE interaction is usually crucial for the survival and maintenance of the photoreceptors and the observation that they can survive and mature for a long time in RO without RPE was quite surprising. Concerning the onset of degeneration, this interaction might be crucial, since potentially only fully established photoreceptors are prone to the subtle degenerative processes caused by the lack of normal CRB1. Another explanation could be the lack

of prolonged light stimulation of the PRC. In Crb1 KO mice, long-term illumination with light leads to a substantial worsening of the observed degeneration (121). Similar effects are also known for human RP patients, where light deprivation is one of the suggested treatments to slow down the PRC degeneration (103).

In summary, the overall differentiation of RP retinal organoids was comparable to the controls and could so far not reproduce the observed phenotype in mice or patients. Future actions to induce stronger phenotypic changes will be discussed below (Section 7.4.7).

7.4.3. Changes in CRB1 expression and location

One of the central aims of this thesis was to learn more about the role of CRB1 during development, its expression and its role in the pathology of retinitis pigmentosa. Initially, I examined the expression of CRB1 with two different antibodies (CRB1c, CRB1n) at several time points ranging from early (d40) to late (d365) development. The immunogen used for CRB1c was located in the centre of CRB1 (no further details are provided by the company), whereas the immunogen for CRB1n is found at the N-terminal. In theory, both should be able to detect all splice variants of *CRB1* (*V1*,*V2* and *VSec*), which are confirmed for the human retina (120). Note that in previous studies, the CRB1n antibody was already verified in human retinal tissue (120). Examination of control organoids from day 40 to 260 showed a comparable pattern for both antibodies (Figure 20). The signal was found apically adjacent to the outer limiting membrane. This fits well for what was known before from human and mouse adults and developing retina (120). Interestingly, at day 365, the CRB1n antibody did not show this specific apical region staining as in earlier time points (Figure 20a).

In order to check whether the human *CRB1* variants were also differently expressed on mRNA levels at different stages of the development, qPCR from all confirmed splice variants was performed (*V1*, *V2* and *VSec*) (Figure 20). The expression pattern revealed that *V1* is decreasing significantly over time, whereas the *VSec* increases within the same period. Of note, the mRNA levels resulting from the primer pairs detecting combinations of *V1* and *VSec* with *V1* show a ten times higher expression

(0.1 x *GAPDH* to 0.01 x *GAPDH*). This makes it likely that variant *V1* is by far more expressed then the other variants *V2* and *VSec*.

Another important issue is the cell type, which produces CRB1. In the literature, it has been assumed that in humans, both glia and photoreceptors are able to express CRB1 (120,131). In human RO, this could not be clarified using the CRB1 antibodies, since the expression was seen at the OLM and not associated to any cell type. FACS sorted photoreceptor cell RNA (sorted by IRBP-GFP promoter construct) showed that most of the measured PRC population expressed normal levels of *CRB1* (Figure 20f). This strongly suggested that CRB1 is at least partly expressed by PRC.

Finally, I compared protein levels of CRB1c and CRB1n antibodies of RP patients with healthy controls and found a decrease for CRB1c antibody signal at some of the measured time points (Figure 21). At day 125, the decrease was significant. For CRB1n, for day 40- d260, no apical region signal could be detected at all and indeed fluorescence signal analysis was significantly decreased for all time points. This was also true for day 365 where the signal was more diffuse, however still significantly stronger than in RP patients (Figure 21c-d). The lowered CRB1 protein levels might be explained by the C948Y mutation causing an aberrant translation or localisation pattern. The C948Y mutation is found in one of the protein-protein EGF-like binding regions. Hence, it might be important for the clustering of the protein and of the cells to the OLM. In line with this hypothesis, the signal of the OLM protein ZO-1 was also decreased at two of the examined time points (d190, d260) (Figure 19). In Crb1 KO mice, a disruption of the OLM was also observed (121).Therefore, the disturbed CRB1 pattern at the apical region might influence the localisation and/or stability of the OLM.

7.4.4. Crumbs complex members might be affected by the *CRB1* mutation

The crumbs complex is an important regulator of cell polarity in epithelia especially during the development of neuroepithelial tissues (131). Mutations and changes in the protein composition of the crumbs complex protein (Crb1-3, Pals1, Patj, Mupp1) as well as the associated PAR complex (Par6, aPKC, Cdc42, Par3) are associated with adhesion and polarity loss and in many cases retinal degeneration (reviewed in (131)). mRNA profiling of the crumbs complex members in RP RO showed a high upregulation

of *CDC42* at day 80 and day 125 (Figure 22). Cdc42 is GTPase of the Ras family involved in growth cone regulation (213), cell polarisation and cell cycle progression (214). In drosophila, Cdc42 is involved in PRC morphogenesis and polarity (215). In a retina-specific knockout study in mice, Cdc42 had a strong effect on the correct layering and organisation of the retina (216). Another study showed that the Cdc42 protein was accumulating in light-induced degenerative photoreceptor cells before they became apoptotic (217). This suggests either a role in early cell death induction or a protective role against cell death. The overexpression of *CDC42*, which was observed in RP RO, might therefore have a potential anti-apoptotic effect, which fit to the decrease in TUNEL-positive cells (Figure 13).

The expression of CRB2 did not show any signs of aberration on mRNA (Figure 22) and protein level (data not shown). The staining of CRB2 showed similarities to CRB1 but was more punctuated and might be located within the segments rather than at the adherens junctions (data not shown). As its structure and function is strongly related to CRB1, it is still one of the main candidates as a phenotype-modulating factor. As described in the introduction, RP caused by *CRB1* mutations has a weak genotype-phenotype correlation, where one mutation can lead to very different onset and severities of the disease. I could however not find any difference so far between the CRB2 expression and the observed difference in the two examined patients (data not shown).

7.4.5. *CRB1* mutation might influence major developmental pathways

In previous publications, crumbs proteins and crumbs complex members were observed to influence many critical differential and signalling pathways. Especially in knockdown mice, several differentially regulated genes have been observed (143,191,218). In order to examine whether this could be also observed in ROs from CRB1 RP patients, I checked for mRNA levels of important components of these pathways as well as effector genes (Figure 23). First, I checked for notch pathway, which is crucial for neural development and especially retinogenesis (95,145,147). I observed a significant increase of notch pathway components (*PEN2*, *PSEN1*, *and NCSTN*) in early d80 differentiated RP ROs. At later time points, a decrease of *APH1* and *HEY1* was apparent. With exception of *HEY1,* all these genes are associated with

an increase of gamma-secretase activity, which is crucial for notch pathway activity (144). *HEY1* however is one of the target genes, which is influenced by notch. In drosophila, the crb1 analogue crb was observed as a notch inhibiting factor by inhibiting the internalisation of the Notch receptor (151). A potential inhibition of the gamma secretase activity was observed in drosophila and humans (for CRB1-3) in cell lines and cell free assays (148). In another study, the extracellular domain of crb was able to bind and inhibit the notch receptor (150). Interestingly, like CRB1, the notch receptor contains multiple EGF-like repeats and Ohata and colleagues suggested this as one of the potential binding sites (150). Keeping in mind that the mutation present in the CRB1 RP patients studied in this thesis is located within this region, this interaction site might not be functional in our patients. This would therefore fit to the observed early overexpression of notch components, however could not explain the reduction of notch component expression in the later time points. One possibility is that an early notch overactivation lead to a changed cell composition in the RO, which could potentially alter all involved pathways. However, contradicting to that, no drastic changes in the cell population could be observed. Future studies could check for notch pathway activity and expression of pathway components specifically in photoreceptors and/or Müller glia.

Next, I checked for potential changes in the canonical wnt pathway. Previous studies suggested that crb could be important for the correct localisation of ß- and P120 catenins due to their influence on the adherens junction formation (142). In a study from 2013, ablation of Crb1 and Crb2 in mouse retinal progenitors led to a mislocalisation of ß-catenin at the adherens junction of the OLM to other layers (143). Almost all measured wnt genes showed a significant increase of mRNA levels at d80 (B-catenin (*CTNNB*), p120 catenin (*CTNND1*), *LRP6, VL1, GS3B, MYC, MYCN, DKK3*). Antibody staining for ß-catenin showed no convincing staining in ROs and was therefore not included in the examination (data not shown). From this data, I hypothesise that the CRB1 might influence the wnt signalling and the expression of wnt components. Wnt signalling can influence stem cell maintenance and influences cell cycle regulation and cell survival (219), (220). The excessed activation of wnt could therefore be a potential explanation for the thickened retina observed in CRB1 RP patients (117) as a result of an increased stem cell population. However, in this work, no increased proliferation was observed. Another potential role of wnt could be a

protective role against apoptosis of photoreceptors. In several studies, wnt has shown to regulate neurotrophin release and might therefore be a potential response against ongoing cellular stress (221,222). The wnt regulator DKK3, which was significantly upregulated at day 80 (mRNA level), was found to be upregulated in rd1 mice during ongoing rod photoreceptor cell death and also serves as pro-survival signal (222,223). In concordance to that, I observed a significant decrease of apoptosis (Figure 13).

The next potentially regulated pathway was the mTOR pathway. In the retina, tit could play a role in cone function and prevention of oxidative stress in photoreceptor cells (224), (225). In the rd1 retinitis pigmentosa mouse model, activation of mTOR signalling was able to increase to long-term survival of cones (226). Crb1 could act in this pathway through its complex members Patj, which is able to bind Tsc2 via a PDZ domain (156). Tsc2 as a part of the Tsc1/Tsc2 complex is an important inhibitor of mTor. In RP RO, *TSC2* was significantly upregulated, which could potentially lead to an imbalance of photoreceptor metabolism.

Finally, I checked for genes that were in some way connected to the cell cycle. The proteins Pttg1 and Pttg2 take part in chromatid separation inhibition (191,218). Moreover, Pttg was associated with p53, modulating its function (218,227,228). *PTTG1* was seen to be downregulated in white light exposed Crb1 KO mice (218). In this thesis, both genes (*PTTG1* and *PTTG2*) were seen to be upregulated at d80. Again, a protection of cell death might take place here, resulting in increased survival of PRCs or progenitors.

7.4.6. *CRB1* mutation might lead to a decreased light sensitivity of PRC

Ca^{2+}-ions are key regulating elements in the light adaption and control almost every element of the phototransduction (229). For instance, the intracellular Ca^{2+}-concentration in outer segments regulates the activity of cGMP synthesis by the guanylate cyclase (via the GC activating protein (GCAP) and GC inhibiting protein (GCIP)). Unlike other Ca^{2+}- binding proteins, GCAP is inactivated by Ca^{2+} (229). During light adaption, cGMP sensitive CNG channels are closed, lowering the intracellular Ca^{2+}- concentration. This in turn leads to more active GCAP molecules and subsequent activation of GC (229). With rising cGMP production by the GC, CNG

channels re-open and the calcium concentration (and dark current) normalises again. Further, Ca^{2+} influence the binding affinity of rhodopsin to transducin as well as direct control over the CNG channels (229). Consequently, the dynamics of Ca^{2+} concentration is a meaningful indicator for light stimulation and adaption in photoreceptor cells.

By tracing Ca^{2+}- ions using live cell imaging with the calcium dye Fura-2-AM, a dynamic change of intracellular calcium concentrations before and during light stimulation could be observed (Figure 24). Comparing day 190 RO from CRB1 RP patients, a robust decrease of the number of cells that were activated during light stimulation, was recorded. The decrease was observed in two independent sets of experiments and in both patient lines (RPA and RPB). Further, I analysed the data by comparing the number of cells, which were activated in the periods shortly during light stimulation and in periods beforehand (dark). This clearly showed that patient cells unlike control cells showed almost no calcium peaks during the light induction phase in comparison to an inactive phase. Since the occurrence of calcium dynamics is a crucial aspect of the phototransduction and the restoring afterwards, it can be hypothesised that the CRB1 RP patients RO display a defect in the transduction cascade.

In order to test this hypothesis, I checked for levels and localisation for several phototransduction proteins (Figure 25). However, no signs of an aberrant expression patterns for Rod transducin, PDE6B and CNG channel subunit β3 was found. Additionally, examination of the GCAP1 protein levels was not possible since the signal of the used antibody was not conclusive (data not shown). Since most prerequisites for a working phototransduction cascade are given, it can only be speculated that the missing light response is caused by some factors or mislocalisation, which have not been examined or observed yet. In future experiments, calcium imaging of even later time points (here d200), where transduction proteins are most abundantly expressed. Further, other protein of the phototransduction cascade such as GCIP, GCAP-2 or Calmodulin could be used for a detailed analysis.

7.4.7. Possible lessons learned for next-generation disease models

The findings of this thesis led to the question, which improvements have to be undertaken to be able to see profound degeneration in retinitis pigmentosa models and in which way the model can be made more physiological. One potential mean could be the use of prolonged light exposure. Although necessary for the functionality of the retina, ongoing light exposure can induce stress and cell death even in the healthy retina (230). In drosophila, the CRB1 analogue crumbs prevents light-induced photoreceptor degeneration (231). In a Crb1 KO model, white light exposure increased the pathological changes and accelerates cell death (121).

Another way might be a drug- induced cell death model. Photoreceptor cells, which are compromised by a decreased stability of photoreceptor segments, might be less able to compensate drug-induced stress. One recent example for a drug induced degenerative phenotype was performed with tamoxifen in mouse ROs (232). Tamoxifen had a toxic effect on ROs and displayed selective PRC cell death.

Finally, the retinal organoid model could be improved by adding more components, which are potentially involved in the onset of the disease. As pointed out, ROs lack the interaction between RPE and mature PRC. Therefore, they cannot reproduce this crucial interaction. Although seemingly not needed for initial establishment of segments (183,184), RPE death in human patients leads to a secondary cell death of PRC and retinal degeneration (233). In RP caused by *CRB1* mutations, RPE is usually lost indicating a primary or secondary role in the degenerative process (234,235). A possible way to achieve this is the retina-on-a-chip device presented in this thesis (Figure 26).

7.5. The microfluidic retina-on-a-chip device

The retina-on-a-chip device was developed to overcome the problems of current retinal organoids cultures described in previous sections. The main idea is to get the photoreceptor segments in close proximity to RPE cells, which is so far not or only uncontrolled taking place in RO cultures. For example, in the Zhong protocol, RPE is usually adhered at a random side as a large cluster (184). Therefore, most of the PRC segments are not in contact or near to RPE cells. Although RO photoreceptor cells

show the presence of inner and partly of outer segment formation, especially the observed outer segments were still rare, small and unorganised (see *e.g.* Figure 16). In the retina-on-a-chip device, this problem is faced by bringing RO in close apposition to an adherent cultured layer of hiPSC-derived RPE cells generated from the same or from other donors. To prevent any unwanted overgrowth between the two cell types and to create a certain "spacing element", the ROs are embedded in a hydrogel based on hyaluronic acid. This hydrogel should also resemble the natural so-called interphotoreceptor matrix, which is crucial for photoreceptor and RPE development and interaction (discussed in (210,236)).

In a proof-of-principle study, the assembly of the RO-RPE co-culture chip was possible and that the organoids and RPE cells survived for at least three days without any observation of uncontrolled outgrowing of RO cells or degeneration. Moreover, RPE and segment from organoids could be marked by fluorophores and subsequently be monitored. This revealed a close apposition of both structures (Figure 26d). In the future, a detailed evaluation of this interaction site will be performed. A special focus lies on the effect of the RPE cells on the segment growth and maturation.

The retina-on-a-chip is based on the organ-on-a-chip technology. The idea behind the OoC is to use primary or stem cell (or more often iPSC) derived cells to reflect one or several functional aspects of a tissue in a microfluidic environment. This enables the introduction of mechanical cues, extracellular matrix or cell-cell or tissue interactions. One famous examples it the breathing lung, where alveolar and endothelial cells or combined on a membrane introducing the breathing movement of a lung (186). Amongst major advantages of the microfluidic culture systems is the controlled and dynamic medium flux (usually provided by a pump) in small physiological volumes (nl) and volume-to-cell ratios. Moreover, the chip system provides mechanical stability, controlled placing and distancing of different cell types. Due to the defined components, OoC technologies are highly standardisable and can be upscaled to large automated culture systems (*e.g.* due to the automatic pump medium supply).

By creating the retina-on-a-chip device, all these features can be implemented to the retinal organoid culture. In addition, to my knowledge it is the first time that (retinal) organoid have been combined with another adherent cell type. In the future, we plan to use the chip not only for disease modelling but also for drug screening approaches,

where highly standardisable and upscalable culture models are demanded to test the effects of drugs and compounds on the human retina.

7.5.1. Current drawbacks of the retina-on-a-chip and future improvements

The retina-on-a-chip could potentially be a next-generation disease modelling and drug screening device. Still, there are some hurdles to overcome.

First, the retina chip requires a good and reproducible quality of retinal organoids and RPE cell. Especially the long-term cultured organoids vary in quality and degree of central degeneration and organisation. Therefore, a set of quality markers and criteria has to be set up, which can ensure a sustaining quality and standard over many experiments. This could be achieved by introducing a microscope–based pattern recognition step recognising and selecting ROs of a demanded quality. Potential criteria could be *e.g.* the number and size of visible segment formation, the integrity of the central tissue and the visibility of layering in brightfield images. Another important issue is the time, which is necessary to produce organoids of advanced stages (*e.g.,* to study segment formation occurring starting at day 125). One way to surpass this is cryopreservation of organoids which makes them readily available (183). Next, the RPE-organoid chip still lacks several crucial features involved in many retinal and retinogenic processes. As already pointed out, the most important missing features are vascularisation, immune cells such as microglia, an optic nerve connecting the retina to brain neurons and the presence of a specialised fovea centralis.

In order to achieve a vascularisation, I am currently planning to implement primary (and later iPSC- derived) endothelial cells into the organoids as well as a choroid layer separated from the RPE by a semipermeable membrane. Second, I plan to flush microglial cells into the chip and let them invade into the tissue. An optic nerve could be implemented by stitching an artificial tube structure inside the organoid and let ganglion cell axons grow outside of the RO into an outside chamber. This chamber could be filled by brain neurons or brain organoids serving as connection point to the optic nerve axons. Preliminary experiments showed the feasibility of this approach (data not shown). Finally, I plan to establish a fovea centralis inside the tissue using a gradient of known (and to be identified) paracrine factors influencing the fovea fate.

For chicken area centralis, some of these factors have been identified (237) and might be applicable to the human retinal organoid.

In summary, the retina-on-a-chip system designed during this thesis is a novel and potent disease modelling and drug testing tool showing several improvements over classically cultured retinal organoids. Still, some drawbacks need to be overcome and improvements have to be made in order to achieve a physiological and amongst all applicable *in vitro* retina model.

.

8. References

1. Kolb H. Gross Anatomy of the Eye. In: 2005 May 1 [Updated 2007 May 1] In: Kolb H, Fernandez E, Nelson R, editors Webvision: The Organization of the Retina and Visual System [Internet] Salt Lake City (UT): University of Utah Health Sciences Center; 1995-. Available from: https://www.ncbi.nlm.nih.gov/books/NBK11533/;

2. Achberger K, Haderspeck JC, Kleger A, Liebau S. Stem cell-based retina models. Adv Drug Deliv Rev. 2018 May 16;

3. Kolb H. Simple Anatomy of the Retina. Kolb H. Simple Anatomy of the Retina. 2005 May 1 [Updated 2012 Jan 31]. In: Kolb H, Fernandez E, Nelson R, editors. Webvision: The Organization of the Retina and Visual System [Internet]. Salt Lake City (UT): University of Utah Health Sciences Center; 1995-. Available from: https://www.ncbi.nlm.nih.gov/books/NBK11533/;

4. Fuhrmann S. Eye morphogenesis and patterning of the optic vesicle. Curr Top Dev Biol. 2010;93:61–84.

5. Cajal SR. La retine des vertebres. Cellule. 1893;9:119–255.

6. Curcio CA, Sloan KR, Kalina RE, Hendrickson AE. Human photoreceptor topography. J Comp Neurol. 1990 Feb 22;292(4):497–523.

7. Ahmad KM, Klug K, Herr S, Sterling P, Schein S. Cell density ratios in a foveal patch in macaque retina. Vis Neurosci. 2003;20(2):189–209.

8. Bowmaker JK, Dartnall HJ. Visual pigments of rods and cones in a human retina. J Physiol. 1980 Jan;298:501–11.

9. Anderson DH, Fisher SK. The photoreceptors of diurnal squirrels: Outer segment structure, disc shedding, and protein renewal. J Ultrastruct Res. 1976 Apr 1;55(1):119–41.

10. Villegas GM. Ultrastructure of the human retina. J Anat. 1964 Oct;98(Pt 4):501–13.

11. Bowmaker JK, Dartnall HJ, Mollon JD. Microspectrophotometric demonstration of four classes of photoreceptor in an old world primate, Macaca fascicularis. J

Physiol. 1980 Jan;298:131–43.

12. Hecht S, Shlaer S, Pirenne MH. Energy, quanta and vision. J Gen Physiol. 1942 Jul 20;25(6):819–40.

13. Pepperberg DR. Rhodopsin and visual adaptation: Analysis of photoreceptor thresholds in the isolated skate retina. Vision Res. 1984 Jan 1;24(4):357–66.

14. Nathans J, Thomas D, Hogness DS. Molecular genetics of human color vision: the genes encoding blue, green, and red pigments. Science. 1986 Apr 11;232(4747):193–202.

15. Fain GL, Dowling JE. Intracellular recordings from single rods and cones in the mudpuppy retina. Science. 1973 Jun 15;180(4091):1178–81.

16. Purves D, Augustine GJ, Fitzpatrick D, et al., editors. Neuroscience. 2nd edition. Sunderland (MA): Sinauer Associates; 2001. Functional Specialization of the Rod and Cone Systems. Available from: https://www.ncbi.nlm.nih.gov/books/NBK10850/. In.

17. De Robertis E. Some observations on the ultrastructure and morphogenesis of photoreceptors. J Gen Physiol. 1960 Jul;43(6)Suppl(6):1–13.

18. Papermaster DS, Schneider BG, Besharse JC. Vesicular transport of newly synthesized opsin from the Golgi apparatus toward the rod outer segment. Ultrastructural immunocytochemical and autoradiographic evidence in Xenopus retinas. Invest Ophthalmol Vis Sci. 1985 Oct;26(10):1386–404.

19. Steinberg RH, Wood I, Hogan MJ. Pigment epithelial ensheathment and phagocytosis of extrafoveal cones in human retina. Philos Trans R Soc Lond B Biol Sci. 1977 Mar 28;277(958):459–74.

20. Steinberg RH, Fisher SK, Anderson DH. Disc morphogenesis in vertebrate photoreceptors. J Comp Neurol. 1980 Apr 1;190(3):501–18.

21. Kevany BM, Palczewski K. Phagocytosis of retinal rod and cone photoreceptors. Physiology (Bethesda). 2010 Feb;25(1):8–15.

22. Wald G. Molecular basis of visual excitation. Science. 1968 Oct

11;162(3850):230–9.

23. Hubbard R. Absorption Spectrum of Rhodopsin: 500 nm Absorption Band. Nature. 1969 Feb 1;221(5179):432–5.

24. Longstaff C, Calhoon RD, Rando RR. Deprotonation of the Schiff base of rhodopsin is obligate in the activation of the G protein. Proc Natl Acad Sci. 1986;83(12).

25. Fu Y. Phototransduction in Rods and Cones. 2010 Apr 1. In: Kolb H, Fernandez E, Nelson R, editors. Webvision: The Organization of the Retina and Visual System [Internet]. Salt Lake City (UT): University of Utah Health Sciences Center; 1995-. Available from: https://www.ncbi.nlm.nih.gov/books/NBK52768/;

26. Leskov IB, Klenchin VA, Handy JW, Whitlock GG, Govardovskii VI, Deric Bownds M, et al. The Gain of Rod Phototransduction: Reconciliation of Biochemical and Electrophysiological Measurements. Neuron. 2000;27:525–37.

27. Norton AW, D'Amours MR, Grazio HJ, Hebert TL, Cote RH, D 'amours MR, et al. Mechanism of transducin activation of frog rod photoreceptor phosphodiesterase. Allosteric interactiona between the inhibitory gamma subunit and the noncatalytic cGMP-binding sites. J Biol Chem. 2000 Dec 8;275(49):38611–9.

28. Karpen JW, Zimmerman AL, Stryer L, Baylor DA. Gating kinetics of the cyclic-GMP-activated channel of retinal rods: flash photolysis and voltage-jump studies. Proc Natl Acad Sci U S A. 1988 Feb;85(4):1287–91.

29. Hagins WA, Penn RD, Yoshikami S. Dark Current and Photocurrent in Retinal Rods. Biophys J. 1970 May;10(5):380–412.

30. Makino CL, Dodd RL, Chen J, Burns ME, Roca A, Simon MI, et al. Recoverin Regulates Light-dependent Phosphodiesterase Activity in Retinal Rods. J Gen Physiol. 2004 Jun;123(6):729–41.

31. Nikonov SS, Brown BM, Davis JA, Zuniga FI, Bragin A, Pugh EN, et al. Mouse Cones Require an Arrestin for Normal Inactivation of Phototransduction. Neuron. 2008 Aug 14;59(3):462–74.

32. Kolb H. Organization of the outer plexiform layer of the primate retina: electron microscopy of Golgi-impregnated cells. Philos Trans R Soc Lond B Biol Sci. 1970 May 7;258(823):261–83.

33. Sterling P, Matthews G. Structure and function of ribbon synapses. Trends Neurosci. 2005 Jan 1;28(1):20–9.

34. Stell WK. The structure and morphologic relations of rods and cones in the retina of the spiny dogfish, Squalus. Comp Biochem Physiol Part A Physiol. 1972 May 1;42(1):141–51.

35. Boycott BB, Wassle H. Morphological Classification of Bipolar Cells of the Primate Retina. Eur J Neurosci. 1991 Nov 1;3(11):1069–88.

36. Kolb H, Linberg KA, Fisher SK. Neurons of the human retina: A Golgi study. J Comp Neurol. 1992 Apr 8;318(2):147–87.

37. Kolb H. Outer Plexiform Layer. 2005 May 1 [Updated 2007 May 1]. In: Kolb H, Fernandez E, Nelson R, editors. Webvision: The Organization of the Retina and Visual System [Internet]. Salt Lake City (UT): University of Utah Health Sciences Center; 1995-. Available from: https://www.ncbi.nlm.nih.gov/books/NBK11518/;

38. Kolb H, Dekorver L. Midget ganglion cells of the parafovea of the human retina: A Study by electron microscopy and serial section reconstructions. J Comp Neurol. 1991 Jan 22;303(4):617–36.

39. Schwartz EA. Responses of bipolar cells in the retina of the turtle. J Physiol. 1974 Jan;236(1):211–24.

40. Strettoi E, Novelli E, Mazzoni F, Barone I, Damiani D. Complexity of retinal cone bipolar cells. Prog Retin Eye Res. 2010 Jul;29(4):272–83.

41. Dolan RP, Schiller PH. Evidence for only depolarizing rod bipolar cells in the primate retina. Vis Neurosci. 1989;2(5):421–4.

42. Wong-Riley MTT. Synaptic organization of the inner plexiform layer in the retina of the tiger salamander. J Neurocytol. 1974 Mar;3(1):1–33.

43. Grünert U, Haverkamp S, Fletcher EL, Wässle H. Synaptic distribution of

ionotropic glutamate receptors in the inner plexiform layer of the primate retina. J Comp Neurol. 2002 May 27;447(2):138–51.

44. Kolb H, Famiglietti E V. Rod and cone pathways in the inner plexiform layer of cat retina. Science. 1974 Oct 4;186(4158):47–9.

45. Gouras P. The function of the midget cell system in primate color vision. Vision Res. 1971 Jan 1;11:397–410.

46. Shapley R, Hugh Perry V. Cat and monkey retinal ganglion cells and their visual functional roles. Trends Neurosci. 1986 Jan 1;9:229–35.

47. Kolb H, Fernandez E, Schouten J, Ahnelt P, Linberg KA, Fisher SK. Are there three types of horizontal cell in the human retina? J Comp Neurol. 1994 May 15;343(3):370–86.

48. Diamond JS. Inhibitory Interneurons in the Retina: Types, Circuitry, and Function. Annu Rev Vis Sci. 2017 Sep 15;3(1):1–24.

49. Hirasawa H, Kaneko A. pH Changes in the Invaginating Synaptic Cleft Mediate Feedback from Horizontal Cells to Cone Photoreceptors by Modulating Ca $^{2+}$ Channels. J Gen Physiol. 2003 Dec;122(6):657–71.

50. Jackman SL, Babai N, Chambers JJ, Thoreson WB, Kramer RH. A Positive Feedback Synapse from Retinal Horizontal Cells to Cone Photoreceptors. Rieke F, editor. PLoS Biol. 2011 May 3;9(5):e1001057.

51. MacNeil MA, Masland RH. Extreme Diversity among Amacrine Cells: Implications for Function. Neuron. 1998 May 1;20(5):971–82.

52. Masland RH. The tasks of amacrine cells. Vis Neurosci. 2012 Jan;29(1):3–9.

53. Vecino E, Rodriguez FD, Ruzafa N, Pereiro X, Sharma SC. Glia–neuron interactions in the mammalian retina. Prog Retin Eye Res. 2016 Mar 1;51:1–40.

54. Uga S, Smelser. Comparative study of the fine structure of retinal Müller cells in various vertebrates. Invest Ophthalmol. 1973 Jun;12(6):434–48.

55. Das SR, Bhardwaj N, Kjeldbye H, Gouras P. Muller cells of chicken retina synthesize 11-cis-retinol. Biochem J. 1992 Aug 1;285 (Pt 3)(Pt 3):907–13.

56. Stone J, Dreher Z. Relationship between astrocytes, ganglion cells and vasculature of the retina. J Comp Neurol. 1987;255(1):35–49.

57. Schnitzer J. Astrocytes in the guinea pig, horse, and monkey retina: Their occurrence coincides with the presence of blood vessels. Glia. 1988;1(1):74–89.

58. Kim JH, Kim JH, Park JA, Lee S-W, Kim WJ, Yu YS, et al. Blood-neural barrier: intercellular communication at glio-vascular interface. J Biochem Mol Biol. 2006 Jul 31;39(4):339–45.

59. Ginhoux F, Greter M, Leboeuf M, Nandi S, See P, Gokhan S, et al. Fate mapping analysis reveals that adult microglia derive from primitive macrophages. Science (80-). 2010/10/23. 2010;330(6005):841–5.

60. Ginhoux F, Prinz M. Origin of Microglia: Current Concepts and Past Controversies. Cold Spring Harb Perspect Biol. 2015;7(8):a020537.

61. Hume DA, Perry VH, Gordon S. Immunohistochemical localization of a macrophage-specific antigen in developing mouse retina: phagocytosis of dying neurons and differentiation of microglial cells to form a regular array in the plexiform layers. J Cell Biol. 1983 Jul 1;97(1):253–7.

62. Strauss O. The Retinal Pigment Epithelium in Visual Function. Physiol Rev. 2005;85(3):845–81.

63. Erickson KK, Sundstrom JM, Antonetti DA. Vascular permeability in ocular disease and the role of tight junctions. Angiogenesis. 2007 Mar 19;10(2):103–17.

64. LaVail MM. Outer segment disc shedding and phagocytosis in the outer retina. Trans Ophthalmol Soc U K. 1983;103 (Pt 4):397–404.

65. Baehr W, Wu SM, Bird AC, Palczewski K. The retinoid cycle and retina disease. Vision Res. 2003 Dec;43(28):2957–8.

66. Steinberg RH, Linsenmeier RA, Griff ER. Three light-evoked responses of the retinal pigment epithelium. Vision Res. 1983;23(11):1315–23.

67. Steinberg RH. Interactions between the retinal pigment epithelium and the neural

retina. Doc Ophthalmol. 1985 Oct 15;60(4):327–46.

68. Seagle B-LL, Rezai KA, Kobori Y, Gasyna EM, Rezaei KA, Norris JR. Melanin photoprotection in the human retinal pigment epithelium and its correlation with light-induced cell apoptosis. Proc Natl Acad Sci U S A. 2005 Jun 21;102(25):8978–83.

69. Chow RL, Altmann CR, Lang RA, Hemmati-Brivanlou A. Pax6 induces ectopic eyes in a vertebrate. Development. 1999 Oct;126(19):4213–22.

70. Mathers PH, Grinberg A, Mahon KA, Jamrich M. The Rx homeobox gene is essential for vertebrate eye development. Nature. 1997;387:603.

71. Hyer J, Kuhlman J, Afif E, Mikawa T. Optic cup morphogenesis requires pre-lens ectoderm but not lens differentiation. Dev Biol. 2003 Jul 15;259(2):351–63.

72. Nguyen M, Arnheiter H. Signaling and transcriptional regulation in early mammalian eye development: a link between FGF and MITF. Development. 2000 Aug;127(16):3581–91.

73. Horsford DJ, Nguyen M-TT, Sellar GC, Kothary R, Arnheiter H, McInnes RR. Chx10 repression of Mitf is required for the maintenance of mammalian neuroretinal identity. Development. 2005;132(1):177–87.

74. Ramón Martínez-Morales J, Rodrigo I, Bovolenta P. Eye development: a view from the retina pigmented epithelium. BioEssays. 2004 Jul;26(7):766–77.

75. Chauhan BK, Disanza A, Choi S-Y, Faber SC, Lou M, Beggs HE, et al. Cdc42- and IRSp53-dependent contractile filopodia tether presumptive lens and retina to coordinate epithelial invagination. Development. 2009 Nov 1;136(21):3657–67.

76. Young RW. Cell differentiation in the retina of the mouse. Anat Rec. 1985 Jun;212(2):199–205.

77. Bassett EA, Wallace VA. Cell fate determination in the vertebrate retina. Trends Neurosci. 2012;35(9):565–73.

78. Marquardt T, Ashery-Padan R, Andrejewski N, Scardigli R, Guillemot F, Gruss

P. Pax6 Is Required for the Multipotent State of Retinal Progenitor Cells. Cell. 2001;105(1):43–55.

79. Muranishi Y, Terada K, Inoue T, Katoh K, Tsujii T, Sanuki R, et al. An Essential Role for RAX Homeoprotein and NOTCH-HES Signaling in Otx2 Expression in Embryonic Retinal Photoreceptor Cell Fate Determination. J Neurosci. 2011 Nov 16;31(46):16792–807.

80. Nishida A, Furukawa A, Koike C, Tano Y, Aizawa S, Matsuo I, et al. Otx2 homeobox gene controls retinal photoreceptor cell fate and pineal gland development. Nat Neurosci. 2003/11/20. 2003;6(12):1255–63.

81. Oron-Karni V, Farhy C, Elgart M, Marquardt T, Remizova L, Yaron O, et al. Dual requirement for Pax6 in retinal progenitor cells. Development. 2008 Dec 15;135(24):4037–47.

82. Brown NL, Patel S, Brzezinski J, Glaser T. Math5 is required for retinal ganglion cell and optic nerve formation. Development. 2001 Jul;128(13):2497–508.

83. Wang SW, Kim BS, Ding K, Wang H, Sun D, Johnson RL, et al. Requirement for math5 in the development of retinal ganglion cells. Genes Dev. 2001 Jan 1;15(1):24–9.

84. Poggi L, Vitorino M, Masai I, Harris WA. Influences on neural lineage and mode of division in the zebrafish retina in vivo. J Cell Biol. 2005 Dec 19;171(6):991–9.

85. Feng L, Xie Z, Ding Q, Xie X, Libby RT, Gan L. MATH5 controls the acquisition of multiple retinal cell fates. Mol Brain. 2010 Nov 18;3(1):36.

86. Vitorino M, Jusuf PR, Maurus D, Kimura Y, Higashijima S, Harris WA. Vsx2 in the zebrafish retina: restricted lineages through derepression. Neural Dev. 2009 Apr 3;4(1):14.

87. Brzezinski JA, Kim EJ, Johnson JE, Reh TA. Ascl1 expression defines a subpopulation of lineage-restricted progenitors in the mammalian retina. Development. 2011 Aug 15;138(16):3519–31.

88. Ma W, Wang S-Z. The final fates of neurogenin2-expressing cells include all major neuron types in the mouse retina. Mol Cell Neurosci. 2006 Mar;31(3):463–

9.

89.	Reese BE. Development of the retina and optic pathway. Vision Res. 2011 Apr 13;51(7):613–32.

90.	Swaroop A, Kim D, Forrest D. Transcriptional regulation of photoreceptor development and homeostasis in the mammalian retina. Nat Rev Neurosci. 2010;11(8):563–76.

91.	Morrow EM, Belliveau MJ, Cepko CL. Two Phases of Rod Photoreceptor Differentiation during Rat Retinal Development. J Neurosci. 1998;18(10).

92.	Hendrickson A, Bumsted-O'Brien K, Natoli R, Ramamurthy V, Possin D, Provis J. Rod photoreceptor differentiation in fetal and infant human retina. Exp Eye Res. 2008 Nov;87(5):415–26.

93.	Cornish EE, Hendrickson AE, Provis JM. Distribution of short-wavelength-sensitive cones in human fetal and postnatal retina: early development of spatial order and density profiles. Vision Res. 2004 Aug 1;44(17):2019–26.

94.	Jadhav AP, Mason HA, Cepko CL. Notch 1 inhibits photoreceptor production in the developing mammalian retina. Development. 2006/02/03. 2006;133(5):913–23.

95.	Yaron O, Farhy C, Marquardt T, Applebury M, Ashery-Padan R. Notch1 functions to suppress cone-photoreceptor fate specification in the developing mouse retina. Development. 2006 Apr 1;133(7):1367–78.

96.	Koike C, Nishida A, Ueno S, Saito H, Sanuki R, Sato S, et al. Functional roles of Otx2 transcription factor in postnatal mouse retinal development. Mol Cell Biol. 2007 Dec 1;27(23):8318–29.

97.	Chen S, Wang QL, Nie Z, Sun H, Lennon G, Copeland NG, et al. Crx, a novel Otx-like paired-homeodomain protein, binds to and transactivates photoreceptor cell-specific genes. Neuron. 1997 Nov;19(5):1017–30.

98.	Furukawa T, Morrow EM, Cepko CL. Crx, a novel otx-like homeobox gene, shows photoreceptor-specific expression and regulates photoreceptor differentiation. Cell. 1997 Nov 14;91(4):531–41.

151

99. Mears AJ, Kondo M, Swain PK, Takada Y, Bush RA, Saunders TL, et al. Nrl is required for rod photoreceptor development. Nat Genet. 2001/11/06. 2001;29(4):447–52.

100. Oh ECT, Khan N, Novelli E, Khanna H, Strettoi E, Swaroop A. Transformation of cone precursors to functional rod photoreceptors by bZIP transcription factor NRL. Proc Natl Acad Sci. 2007 Jan 30;104(5):1679–84.

101. Ng L, Hurley JB, Dierks B, Srinivas M, Salto C, Vennstrom B, et al. A thyroid hormone receptor that is required for the development of green cone photoreceptors. Nat Genet. 2001/01/04. 2001;27(1):94–8.

102. Wang Y, Smallwood PM, Cowan M, Blesh D, Lawler A, Nathans J. Mutually exclusive expression of human red and green visual pigment-reporter transgenes occurs at high frequency in murine cone photoreceptors. Proc Natl Acad Sci U S A. 1999 Apr 27;96(9):5251–6.

103. Hamel C. Retinitis pigmentosa. Orphanet J Rare Dis. 2006;1(1):1–12.

104. Allikmets R. Leber congenital amaurosis: a genetic paradigm. Ophthalmic Genet. 2004 Jan 8;25(2):67–79.

105. Boughman JA, Conneally PM, Nance WE. Population genetic studies of retinitis pigmentosa. Am J Hum Genet. 1980 Mar;32(2):223–35.

106. Jay M. On the heredity of retinitis pigmentosa. Br J Ophthalmol. 1982 Jul;66(7):405–16.

107. Klevering BJ, Yzer S, Rohrschneider K, Zonneveld M, Allikmets R, Born LI van den, et al. Microarray-based mutation analysis of the ABCA4 (ABCR) gene in autosomal recessive cone–rod dystrophy and retinitis pigmentosa. Eur J Hum Genet. 2004 Dec 20;12(12):1024–32.

108. Berson EL, Rosner B, Sandberg MA, Weigel-DiFranco C, Moser A, Brockhurst RJ, et al. Further Evaluation of Docosahexaenoic Acid in Patients With RetinitisPigmentosa Receiving Vitamin A Treatment. Arch Ophthalmol. 2004 Sep 1;122(9):1306.

109. den Hollander AI, Roepman R, Koenekoop RK, Cremers FPM. Leber congenital

amaurosis: Genes, proteins and disease mechanisms. Prog Retin Eye Res. 2008 Jul 1;27(4):391–419.

110. Bujakowska K, Audo I, Mohand-Säid S, Lancelot ME, Antonio A, Germain A, et al. CRB1 mutations in inherited retinal dystrophies. Hum Mutat. 2012;33(2):306–15.

111. Hanein S, Perrault I, Gerber S, Tanguy G, Barbet F, Ducroq D, et al. Leber Congenital Amaurosis: Comprehensive Survey of the Genetic Heterogeneity, Refinement of the Clinical Definition, and Genotype-Phenotype Correlations as a Strategy for Molecular Diagnosis. Hum Mutat. 2004;23(4):306–17.

112. Fahim AT, Daiger SP, Weleber RG. Nonsyndromic Retinitis Pigmentosa Overview. GeneReviews®. University of Washington, Seattle; 1993.

113. Bernal S, Calaf M, Garcia-Hoyos M, Garcia-Sandoval B, Rosell J, Adan A, et al. Study of the involvement of the RGR, CRPB1, and CRB1 genes in the pathogenesis of autosomal recessive retinitis pigmentosa. J Med Genet. 2003 Jul;40(7):e89.

114. Den Hollander AI, Ten Brink JB, De Kok YJM, Van Soest S, Van Den Born LI, Van Driel MA, et al. Mutations in a human homologue of Drosophila crumbs cause retinitis pigmentosa (RP12). Nat Genet. 1999;23(2):217–21.

115. Henderson RH, Mackay DS, Li Z, Moradi P, Sergouniotis P, Russell-Eggitt I, et al. Phenotypic variability in patients with retinal dystrophies due to mutations in CRB1. Br J Ophthalmol. 2011 Jun 1;95(6):811–7.

116. den Hollander AI, Heckenlively JR, van den Born LI, de Kok YJ, van der Velde-Visser SD, Kellner U, et al. Leber congenital amaurosis and retinitis pigmentosa with Coats-like exudative vasculopathy are associated with mutations in the crumbs homologue 1 (CRB1) gene. Am J Hum Genet. 2001 Jul;69(1):198–203.

117. Jacobson SG, Cideciyan A V., Aleman TS, Pianta MJ, Sumaroka A, Schwartz SB, et al. Crumbs homolog 1 (CRB1) mutations result in a thick human retina with abnormal lamination. Hum Mol Genet. 2003;12(9):1073–8.

118. Den Hollander AI, Ghiani M, De Kok YJM, Wijnholds J, Ballabio A, Cremers

FPM, et al. Isolation of Crb1, a mouse homologue of Drosophila crumbs, and analysis of its expression pattern in eye and brain. Mech Dev. 2001;110(1–2):203–7.

119. den Hollander a I, Johnson K, de Kok YJ, Klebes a, Brunner HG, Knust E, et al. CRB1 has a cytoplasmic domain that is functionally conserved between human and Drosophila. Hum Mol Genet. 2001;10(24):2767–73.

120. Pellissier LP, Lundvig DMS, Tanimoto N, Klooster J, Vos RM, Richard F, et al. CRB2 acts as a modifying factor of CRB1-related retinal dystrophies in mice. Hum Mol Genet. 2014;23(14):3759–71.

121. van de Pavert SA. Crumbs homologue 1 is required for maintenance of photoreceptor cell polarization and adhesion during light exposure. J Cell Sci. 2004;117(18):4169–77.

122. van Rossum AGSH, Aartsen WM, Meuleman J, Klooster J, Malysheva A, Versteeg I, et al. Pals1/Mpp5 is required for correct localization of Crb1 at the subapical region in polarized Müller glia cells. Hum Mol Genet. 2006;15(18):2659–72.

123. Pellikka M, Tanentzapf M, Pinto M, Smith C, McGlade CJ, Ready DF, et al. Crumbs, the Drosophlia homologue of human CRB1/RP12, is essential for photoreceptor morhogenesis. Nature. 2002;416.

124. Slavotinek AM. The Family of Crumbs Genes and Human Disease. Mol Syndromol. 2016 Oct;7(5):274–81.

125. Quinn PM, Pellissier LP, Wijnholds J. The CRB1 complex: Following the trail of crumbs to a feasible gene therapy strategy. Front Neurosci. 2017;11(APR).

126. Alves CH, Sanz sanz A, Park B, Pellissier LP, Tanimoto N, Beck SC, et al. Loss of CRB2 in the mouse retina mimics human retinitis pigmentosa due to mutations in the CRB1 gene. Hum Mol Genet. 2013;22(1):35–50.

127. Pellissier LP, Quinn PM, Henrique Alves C, Vos RM, Klooster J, Flannery JG, et al. Gene therapy into photoreceptors and Mueller glial cells restores retinal structure and function in CRB1 retinitis pigmentosa mouse models. Hum Mol

Genet. 2014;24(11):3104–18.

128. Richard M, Roepman R, Aartsen WM, van Rossum AGSH, den Hollander AI, Knust E, et al. Towards understanding CRUMBS function in retinal dystrophies. Hum Mol Genet. 2006;15(SUPPL. 2):235–43.

129. Kim JY, Song JY, Karnam S, Park JY, Lee JJH, Kim S, et al. Common and distinctive localization patterns of Crumbs polarity complex proteins in the mammalian eye. Gene Expr Patterns. 2015;17(1):31–7.

130. Wang Q, Hurd TW, Margolis B. Tight junction protein Par6 interacts with an evolutionarily conserved region in the amino terminus of PALS1/stardust. J Biol Chem. 2004 Jul 16;279(29):30715–21.

131. Alves CH, Pellissier LP, Wijnholds J. The CRB1 and adherens junction complex proteins in retinal development and maintenance. Prog Retin Eye Res. 2014 May 1;40:35–52.

132. Thompson BJ, Pichaud F, Röper K. Sticking together the Crumbs-an unexpected function for an old friend. Nat Rev Mol Cell Biol. 2013;14(5):307–14.

133. Tepass U, Theres C, Knust E. crumbs encodes an EGF-like protein expressed on apical membranes of Drosophila epithelial cells and required for organization of epithelia. Cell. 1990 Jun 1;61(5):787–99.

134. Wodarz A, Grawe F, Knust E. CRUMBS is involved in the control of apical protein targeting during Drosophila epithelial development. Mech Dev. 1993 Dec;44(2–3):175–87.

135. Suzuki A, Ohno S. The PAR-aPKC system: lessons in polarity. J Cell Sci. 2006 Feb 21;119(6):979–87.

136. Mehalow AK, Kameya S, Smith RS, Hawes NL, Denegre JM, Young JA, et al. CRB1 is essential for external limiting membrane integrity and photoreceptor morphogenesis in the mammalian retina. Hum Mol Genet. 2003;12(17):2179–89.

137. Lad EM, Cheshier SH, Kalani MYS. Wnt-Signaling in Retinal Development and Disease. Stem Cells Dev. 2009 Jan 11;18(1):7–16.

138. Van Raay TJ, Moore KB, Iordanova I, Steele M, Jamrich M, Harris WA, et al. Frizzled 5 Signaling Governs the Neural Potential of Progenitors in the Developing Xenopus Retina. Neuron. 2005 Apr 7;46(1):23–36.

139. Fuhrmann S. Wnt signaling in eye organogenesis. Organogenesis. 2008 Apr;4(2):60–7.

140. Fu X, Sun H, Klein WH, Mu X. β-catenin is essential for lamination but not neurogenesis in mouse retinal development. Dev Biol. 2006 Nov 15;299(2):424–37.

141. Liu C, Bakeri H, Li T, Swaroop A. Regulation of retinal progenitor expansion by Frizzled receptors: implications for microphthalmia and retinal coloboma. Hum Mol Genet. 2012 Apr 15;21(8):1848–60.

142. Bulgakova NA, Knust E. The Crumbs complex: from epithelial-cell polarity to retinal degeneration. J Cell Sci. 2009;122(15):2587–96.

143. Pellissier LP, Alves CH, Quinn PM, Vos RM, Tanimoto N, Lundvig DMS, et al. Targeted Ablation of Crb1 and Crb2 in Retinal Progenitor Cells Mimics Leber Congenital Amaurosis. PLoS Genet. 2013;9(12).

144. Bray SJ. Notch signalling: a simple pathway becomes complex. Nat Rev Mol Cell Biol. 2006 Sep 1;7(9):678–89.

145. Jadhav AP. Notch 1 inhibits photoreceptor production in the developing mammalian retina. Development. 2006;133(5):913–23.

146. Jadhav AP, Cho S-H, Cepko CL. Notch activity permits retinal cells to progress through multiple progenitor states and acquire a stem cell property. Proc Natl Acad Sci U S A. 2006 Dec 12;103(50):18998–9003.

147. Rocha SF, Lopes SS, Gossler A, Henrique D. Dll1 and Dll4 function sequentially in the retina and pV2 domain of the spinal cord to regulate neurogenesis and create cell diversity. Dev Biol. 2009 Apr 1;328(1):54–65.

148. Mitsuishi Y, Hasegawa H, Matsuo A, Araki W, Suzuki T, Tagami S, et al. Human CRB2 inhibits γ-secretase cleavage of amyloid precursor protein by binding to the presenilin complex. J Biol Chem. 2010;285(20):14920–31.

149. Herranz H, Stamataki E, Feiguin F, Milán M. Self-refinement of notch activity through the transmembrane protein crumbs: Modulation of γ-secretase activity. EMBO Rep. 2006;7(3):297–302.

150. Ohata S, Aoki R, Kinoshita S, Yamaguchi M, Tsuruoka-Kinoshita S, Tanaka H, et al. Dual roles of notch in regulation of apically restricted mitosis and apicobasal polarity of neuroepithelial cells. Neuron. 2011;69(2):215–30.

151. Richardson ECN, Pichaud F. Crumbs is required to achieve proper organ size control during Drosophila head development. Development. 2010;137(4):641–50.

152. Tremblay AM, Camargo FD. Hippo signaling in mammalian stem cells. Semin Cell Dev Biol. 2012 Sep 1;23(7):818–26.

153. Chen C-L, Gajewski KM, Hamaratoglu F, Bossuyt W, Sansores-Garcia L, Tao C, et al. The apical-basal cell polarity determinant Crumbs regulates Hippo signaling in Drosophila. Proc Natl Acad Sci U S A. 2010 Sep 7;107(36):15810–5.

154. Varelas X, Samavarchi-Tehrani P, Narimatsu M, Weiss A, Cockburn K, Larsen BG, et al. The Crumbs Complex Couples Cell Density Sensing to Hippo-Dependent Control of the TGF-β-SMAD Pathway. Dev Cell. 2010 Dec 14;19(6):831–44.

155. Laplante M, Sabatini DM. mTOR Signaling in Growth Control and Disease. Cell. 2012 Apr 13;149(2):274–93.

156. Massey-Harroche D, Delgrossi M-H, Lane-Guermonprez L, Arsanto J-P, Borg J-P, Billaud M, et al. Evidence for a molecular link between the tuberous sclerosis complex and the Crumbs complex. Hum Mol Genet. 2007 Mar 1;16(5):529–36.

157. Zhao C, Yasumura D, Li X, Matthes M, Lloyd M, Nielsen G, et al. mTOR-mediated dedifferentiation of the retinal pigment epithelium initiates photoreceptor degeneration in mice. J Clin Invest. 2011 Jan 4;121(1):369–83.

158. Xiao Z, Patrakka J, Nukui M, Chi L, Niu D, Betsholtz C, et al. Deficiency in crumbs homolog 2 (Crb2) affects gastrulation and results in embryonic lethality in mice.

Dev Dyn. 2011;240(12):2646–56.

159. Takahashi K, Yamanaka S. Induction of Pluripotent Stem Cells from Mouse Embryonic and Adult Fibroblast Cultures by Defined Factors. Cell. 2006;126(4):663–76.

160. Linta L, Stockmann M, Kleinhans KN, Böckers A, Storch A, Zaehres H, et al. Rat Embryonic Fibroblasts Improve Reprogramming of Human Keratinocytes into Induced Pluripotent Stem Cells. Stem Cells Dev. 2012;21(6):965–76.

161. Aasen T, Raya A, Barrero MJ, Garreta E, Consiglio A, Gonzalez F, et al. Efficient and rapid generation of induced pluripotent stem cells from human keratinocytes. Nat Biotechnol. 2008 Nov 17;26(11):1276–84.

162. Kim JB, Zaehres H, Wu G, Gentile L, Ko K, Sebastiano V, et al. Pluripotent stem cells induced from adult neural stem cells by reprogramming with two factors. Nature. 2008 Jul 31;454(7204):646–50.

163. Loh Y-H, Agarwal S, Park I-H, Urbach A, Huo H, Heffner GC, et al. Generation of induced pluripotent stem cells from human blood. Blood. 2009 May 28;113(22):5476–9.

164. Sommer CA, Stadtfeld M, Murphy GJ, Hochedlinger K, Kotton DN, Mostoslavsky G. Induced Pluripotent Stem Cell Generation Using a Single Lentiviral Stem Cell Cassette. Stem Cells. 2009 Mar;27(3):543–9.

165. Yu J, Hu K, Smuga-Otto K, Tian S, Stewart R, Slukvin II, et al. Human Induced Pluripotent Stem Cells Free of Vector and Transgene Sequences. Science (80-). 2009 May 8;324(5928):797–801.

166. Warren L, Manos PD, Ahfeldt T, Loh Y-H, Li H, Lau F, et al. Highly Efficient Reprogramming to Pluripotency and Directed Differentiation of Human Cells with Synthetic Modified mRNA. Cell Stem Cell. 2010 Nov;7(5):618–30.

167. Hay DC, Zhao D, Fletcher J, Hewitt ZA, McLean D, Urruticoechea-Uriguen A, et al. Efficient Differentiation of Hepatocytes from Human Embryonic Stem Cells Exhibiting Markers Recapitulating Liver Development In Vivo. Stem Cells. 2008 Apr;26(4):894–902.

168. Yang L, Soonpaa MH, Adler ED, Roepke TK, Kattman SJ, Kennedy M, et al. Human cardiovascular progenitor cells develop from a KDR+ embryonic-stem-cell-derived population. Nature. 2008 May 22;453(7194):524–8.

169. Müller M, Stockmann M, Malan D, Wolheim A, Tischendorf M, Linta L, et al. Ca2+ activated K channels-new tools to induce cardiac commitment from pluripotent stem cells in mice and men. Stem Cell Rev. 2012 Sep 26;8(3):720–40.

170. Zhang X-Q, Zhang S-C. Differentiation of Neural Precursors and Dopaminergic Neurons from Human Embryonic Stem Cells. In: Methods in molecular biology (Clifton, NJ). 2009. p. 355–66.

171. Schulz TC, Palmarini GM, Noggle SA, Weiler DA, Mitalipova MM, Condie BG. Directed neuronal differentiation of human embryonic stem cells. BMC Neurosci. 2003 Oct 22;4:27.

172. Hu B-Y, Du Z-W, Zhang S-C. Differentiation of human oligodendrocytes from pluripotent stem cells. Nat Protoc. 2009 Nov 15;4(11):1614–22.

173. Lancaster MA, Renner M, Martin CA, Wenzel D, Bicknell LS, Hurles ME, et al. Cerebral organoids model human brain development and microcephaly. Nature. 2013;501(7467):373–9.

174. Evans MJ, Kaufman MH. Establishment in culture of pluripotential cells from mouse embryos. Nature. 1981;292:154.

175. Martin GR. Isolation of a pluripotent cell line from early mouse embryos cultured in medium conditioned by teratocarcinoma stem cells. Proc Natl Acad Sci U S A. 1981 Dec;78(12):7634–8.

176. Thomson JA, Itskovitz-Eldor J, Shapiro SS, Waknitz MA, Swiergiel JJ, Marshall VS, et al. Embryonic stem cell lines derived from human blastocysts. Science. 1998 Nov 6;282(5391):1145–7.

177. Osakada F, Ikeda H, Mandai M, Wataya T, Watanabe K, Yoshimura N, et al. Toward the generation of rod and cone photoreceptors from mouse, monkey and human embryonic stem cells. Nat Biotechnol. 2008;26(2):215–24.

178. Osakada F, Jin ZB, Hirami Y, Ikeda H, Danjyo T, Watanabe K, et al. In vitro

differentiation of retinal cells from human pluripotent stem cells by small-molecule induction. J Cell Sci. 2009/08/13. 2009;122(Pt 17):3169–79.

179. Lamba DA, Karl MO, Ware CB, Reh TA. Efficient generation of retinal progenitor cells from human embryonic stem cells. Proc Natl Acad Sci U S A. 2006/08/16. 2006;103(34):12769–74.

180. Ikeda H, Osakada F, Watanabe K, Mizuseki K, Haraguchi T, Miyoshi H, et al. Generation of Rx+/Pax6+ neural retinal precursors from embryonic stem cells. Proc Natl Acad Sci U S A. 2005/08/04. 2005;102(32):11331–6.

181. Buchholz DE, Hikita ST, Rowland TJ, Friedrich AM, Hinman CR, Johnson L V, et al. Derivation of functional retinal pigmented epithelium from induced pluripotent stem cells. Stem Cells. 2009/08/07. 2009;27(10):2427–34.

182. Eiraku M, Takata N, Ishibashi H, Kawada M, Sakakura E, Okuda S, et al. Self-organizing optic-cup morphogenesis in three-dimensional culture. Nature. 2011;472(7341):51–6.

183. Nakano T, Ando S, Takata N, Kawada M, Muguruma K, Sekiguchi K, et al. Self-formation of optic cups and storable stratified neural retina from human ESCs. Cell Stem Cell. 2012 Jun 14;10(6):771–85.

184. Zhong X, Gutierrez C, Xue T, Hampton C, Vergara MN, Cao LH, et al. Generation of three-dimensional retinal tissue with functional photoreceptors from human iPSCs. Nat Commun. 2014/06/11. 2014;5:4047.

185. Wahlin KJ, Maruotti JA, Sripathi SR, Ball J, Angueyra JM, Kim C, et al. Photoreceptor Outer Segment-like Structures in Long-Term 3D Retinas from Human Pluripotent Stem Cells. Sci Rep. 2017/04/12. 2017;7(1):766.

186. Huh D, Matthews BD, Mammoto A, Montoya-Zavala M, Hsin HY, Ingber DE. Reconstituting Organ-Level Lung Functions on a Chip. Science (80-). 2010 Jun 25;328(5986):1662–8.

187. Bhise NS, Manoharan V, Massa S, Tamayol A, Ghaderi M, Miscuglio M, et al. A liver-on-a-chip platform with bioprinted hepatic spheroids. Biofabrication. 2016;8(1):014101.

188. Wilmer MJ, Ng CP, Lanz HL, Vulto P, Suter-Dick L, Masereeuw R. Kidney-on-a-Chip Technology for Drug-Induced Nephrotoxicity Screening. Trends Biotechnol. 2016;34(2):156–70.

189. Warlich E, Kuehle J, Cantz T, Brugman MH, Maetzig T, Galla M, et al. Lentiviral Vector Design and Imaging Approaches to Visualize the Early Stages of Cellular Reprogramming. Mol Ther. 2011 Apr;19(4):782–9.

190. Klingenstein M, Raab S, Achberger K, Kleger A, Liebau S, Linta L. TBX3 Knockdown Decreases Reprogramming Efficiency of Human Cells. Stem Cells Int. 2016 Nov 30;2016:1–7.

191. van de Pavert SA, Sanz AS, Aartsen WM, Vos RM, Versteeg I, Beck SC, et al. Crb1 is a determinant of retinal apical Müller glia cell features. Glia. 2007 Nov 1;55(14):1486–97.

192. Shichida Y, Morizumi T. Mechanism of G-protein Activation by Rhodopsin. Photochem Photobiol. 2006;83(1):70–5.

193. Hendrickson A. Development of Retinal Layers in Prenatal Human Retina. Am J Ophthalmol. 2016 Jan;161:29–35.e1.

194. Raff MC, Barres BA, Burne JF, Coles HS, Ishizaki Y, Jacobson MD. Programmed cell death and the control of cell survival: lessons from the nervous system. Science. 1993 Oct 29;262(5134):695–700.

195. Nijhawan D, Honarpour N, Wang X. Apoptosis in Neural Development and Disease. Annu Rev Neurosci. 2000 Mar 28;23(1):73–87.

196. Cepko CL, Austin CP, Yang X, Alexiades M, Ezzeddine D. Cell fate determination in the vertebrate retina. Proc Natl Acad Sci. 1996;93(2).

197. Haverkamp S, Haeseleer F, Hendrickson A. A comparison of immunocytochemical markers to identify bipolar cell types in human and monkey retina. 2018;

198. Voinescu PE, Emanuela P, Kay JN, Sanes JR. Birthdays of retinal amacrine cell subtypes are systematically related to their molecular identity and soma position. J Comp Neurol. 2009 Dec 10;517(5):737–50.

199. Boije H, Shirazi Fard S, Edqvist P-H, Hallböök F. Horizontal Cells, the Odd Ones Out in the Retina, Give Insights into Development and Disease. Front Neuroanat. 2016;10:77.

200. Bassett EA, Korol A, Deschamps PA, Buettner R, Wallace VA, Williams T, et al. Overlapping expression patterns and redundant roles for AP-2 transcription factors in the developing mammalian retina. Dev Dyn. 2012 Apr;241(4):814–29.

201. Nag TC, Wadhwa S. Calbindin and parvalbumin immunoreactivity in the developing and adult human retina. Dev Brain Res. 1996;93:23–32.

202. Xue Y, Shen SQ, Jui J, Rupp AC, Byrne LC, Hattar S, et al. CRALBP supports the mammalian retinal visual cycle and cone vision. J Clin Invest. 2015 Feb;125(2):727–38.

203. de Souza CF, Nivison-Smith L, Christie DL, Polkinghorne P, McGhee C, Kalloniatis M, et al. Macromolecular markers in normal human retina and applications to human retinal disease. Exp Eye Res. 2016 Sep 1;150:135–48.

204. Sarthy P V, Fu M, Huang J. Developmental expression of the glial fibrillary acidic protein (GFAP) gene in the mouse retina. Cell Mol Neurobiol. 1991 Dec;11(6):623–37.

205. Curcio CA, Medeiros NE, Millican CL. Photoreceptor loss in age-related macular degeneration. Invest Ophthalmol Vis Sci. 1996 Jun;37(7):1236–49.

206. Craft CM, Whitmore DH, Wiechmannll AF. Cone Arrestin Identified by Targeting Expression of a Functional Family. 1994;269(6):4613–9.

207. Kwok MCM, Holopainen JM, Molday LL, Foster LJ, Molday RS. Proteomics of Photoreceptor Outer Segments Identifies a Subset of SNARE and Rab Proteins Implicated in Membrane Vesicle Trafficking and Fusion. Mol Cell Proteomics. 2008;7(6):1053–66.

208. Bascom RA, Manara S, Collins L, Molday RS, Kalnins VI, McInnes RR. Cloning of the CDNA for a novel photoreceptor membrane protein (rom-1) identifies a disk rim protein family implicated in human retinopathies. Neuron. 1992 Jun 1;8(6):1171–84.

209. Busskamp V, Krol J, Nelidova D, Daum J, Szikra T, Tsuda B, et al. miRNAs 182 and 183 are necessary to maintain adult cone photoreceptor outer segments and visual function. Neuron. 2014;83(3):586–600.

210. Ishikawa M, Sawada Y, Yoshitomi T. Structure and function of the interphotoreceptor matrix surrounding retinal photoreceptor cells. Exp Eye Res. 2015;133:3–18.

211. Sparrow JR, Hicks D, Hamel CP. The retinal pigment epithelium in health and disease. Curr Mol Med. 2010 Dec;10(9):802–23.

212. Mellough CB, Collin J, Khazim M, White K, Sernagor E, Steel DH, et al. IGF-1 Signaling Plays an Important Role in the Formation of Three-Dimensional Laminated Neural Retina and Other Ocular Structures From Human Embryonic Stem Cells. Stem Cells. 2015;33(8):2416–30.

213. Chen T-J, Gehler S, Shaw AE, Bamburg JR, Letourneau PC. Cdc42 participates in the regulation of ADF/cofilin and retinal growth cone filopodia by brain derived neurotrophic factor. J Neurobiol. 2006 Feb 5;66(2):103–14.

214. Melendez J, Grogg M, Zheng Y. Signaling role of Cdc42 in regulating mammalian physiology. J Biol Chem. 2011;286(4):2375–81.

215. Genova JL, Jong S, Camp JT, Fehon RG. Functional Analysis of Cdc42 in Actin Filament Assembly, Epithelial Morphogenesis, and Cell Signaling during Drosophila Development. Dev Biol. 2000 May 1;221(1):181–94.

216. Heynen SR, Meneau I, Caprara C, Samardzija M, Imsand C, Levine EM, et al. CDC42 Is Required for Tissue Lamination and Cell Survival in the Mouse Retina. Karl MO, editor. PLoS One. 2013 Jan 23;8(1):e53806.

217. Heynen SR, Tanimoto N, Joly S, Seeliger MW, Samardzija M, Grimm C. Retinal degeneration modulates intracellular localization of CDC42 in photoreceptors. Mol Vis. 2011;17(November):2934–46.

218. van de Pavert SA, Meuleman J, Malysheva A, Aartsen WM, Versteeg I, Tonagel F, et al. A Single Amino Acid Substitution (Cys249Trp) in Crb1 Causes Retinal Degeneration and Deregulates Expression of Pituitary Tumor Transforming

Gene Pttg1. J Neurosci. 2007;27(3):564–73.

219. MacDonald BT, Tamai K, He X. Wnt/beta-catenin signaling: components, mechanisms, and diseases. Dev Cell. 2009 Jul;17(1):9–26.

220. Clevers H, Nusse R. Wnt/β-catenin signaling and disease. Cell. 2012 Jun 8;149(6):1192–205.

221. Yi H, Hu J, Qian J, Hackam AS. Expression of brain-derived neurotrophic factor is regulated by the Wnt signaling pathway. Neuroreport. 2012 Feb 15;23(3):189–94.

222. Hackam AS. The Wnt signaling pathway in retinal degenerations. IUBMB Life. 2005;57(6):381–8.

223. Hackam AS, Strom R, Liu D, Qian J, Wang C, Otteson D, et al. Identification of Gene Expression Changes Associated with the Progression of Retinal Degeneration in the *rd1* Mouse. Investig Opthalmology Vis Sci. 2004 Sep 1;45(9):2929.

224. Fan B, Li F-Q, Song J-Y, Chen X, Li G-Y. Inhibition of mTOR signaling protects photoreceptor cells against serum deprivation by reducing oxidative stress and inducing G2/M cell cycle arrest. Mol Med Rep. 2016 May;13(5):3771–8.

225. Ma S, Venkatesh A, Langellotto F, Le YZ, Hall MN, Rüegg MA, et al. Loss of mTOR signaling affects cone function, cone structure and expression of cone specific proteins without affecting cone survival. Exp Eye Res. 2015 Jun 1;135:1–13.

226. Venkatesh A, Ma S, Le YZ, Hall MN, Rüegg MA, Punzo C. Activated mTORC1 promotes long-term cone survival in retinitis pigmentosa mice. J Clin Invest. 2015 Apr 1;125(4):1446–58.

227. Zhou Y, Mehta KR, Choi AP, Scolavino S, Zhang X. DNA Damage-induced Inhibition of Securin Expression Is Mediated by p53. J Biol Chem. 2003 Jan 3;278(1):462–70.

228. Hamid T, Kakar SS. PTTG/securin activates expression of p53 and modulates its function. Mol Cancer. 2004;3:1–13.

229. Krizaj D, Copenhagen DR. Calcium regulation in photoreceptors. Front Biosci. 2002;7(4):d2023–44.

230. Krigel A, Berdugo M, Picard E, Levy-Boukris R, Jaadane I, Jonet L, et al. Light-induced retinal damage using different light sources, protocols and rat strains reveals LED phototoxicity. Neuroscience. 2016 Dec 17;339:296–307.

231. Johnson K, Grawe F, Grzeschik N, Knust E. Drosophila crumbs is required to inhibit light-induced photoreceptor degeneration. Curr Biol. 2002 Oct 1;12(19):1675–80.

232. Ito SI, Onishi A, Takahashi M. Chemically-induced photoreceptor degeneration and protection in mouse iPSC-derived three-dimensional retinal organoids. Stem Cell Res. 2017/09/09. 2017;24:94–101.

233. Bhutto I, Lutty G. Understanding age-related macular degeneration (AMD): relationships between the photoreceptor/retinal pigment epithelium/Bruch's membrane/choriocapillaris complex. Mol Aspects Med. 2012 Aug;33(4):295–317.

234. Heckenlively JR. Preserved para-arteriole retinal pigment epithelium (PPRPE) in retinitis pigmentosa. Br J Ophthalmol. 1982 Jan;66(1):26–30.

235. Beryozkin A, Zelinger L, Bandah-Rozenfeld D, Harel A, Strom TA, Merin S, et al. Mutations in *CRB1* are a Relatively Common Cause of Autosomal Recessive Early-Onset Retinal Degeneration in the Israeli and Palestinian Populations. Investig Opthalmology Vis Sci. 2013 Mar 27;54(3):2068.

236. Hollyfield JG. Hyaluronan and the functional organization of the interphotoreceptor matrix. Investig Ophthalmol Vis Sci. 1999;40(12):2767–9.

237. O'Brien KB. Development of the Foveal Specialization. Vis Transduct Non-Visual Light Percept. 2008;17–33.

9. Table of Figures

9.1. Figures

9.2. Tables